FREE RADICAL-MEDIATED REACTIVE EXTRUSION OF COMMODITY POLYMERS

by

Praphulla

A thesis submitted to the Department of Chemical Engineering

In conformity with the requirements for

the degree of Doctor of Philosophy

Queen's University

Kingston, Ontario, Canada

(January, 2018)

Abstract

The objective of this thesis is to improve the melt and solid-state properties of poly (propylene) (PP) and poly(lactide) (PLA) by reactive extrusion. Peroxide-mediated melt-state reactive extrusion in the presence of mesate and acrylate-based coagents was implemented to introduce branching and enhance the strain hardening, crystallization kinetics and solid state properties of these commodity polymers, to make them conducive to more high-value applications. The coagent modified PP possessed bimodal molecular weight and branching distributions, whose population varied with coagent structure. Besides changing polymer chain architecture, chemical modification generated a small amount of well-dispersed, coagent-derived nanoparticles. When compared with the parent material and PP samples treated with peroxide alone, coagent-modified materials demonstrated significantly higher crystallization temperatures and crystallization rates, as well as a finer spherulitic structure. Crystallization studies showed that whereas branching had a moderate effect on crystallization kinetics, heterogeneous nucleation effects dominated the crystallization of coagent-modified PP materials. Coagent modified PP specimens prepared by injection molding retained the modulus and tensile strength of the parent PP, in spite of their lower molar mass and viscosities, whereas their elongation at break and the impact strength were improved. This was attributed to the finer spherulitic structure of these materials, and to the disappearance of the skin-core layer that typically forms during the injection molding process.

In the second part of this thesis, structure-property relations of PLA, branched by peroxide-mediated reactive extrusion in the presence various coagents was carried out. The coagent modified PLA, consisted of mixtures of linear, and long chain branched (LCB) PLA chains. A trifunctional coagent (triallyl trimesate, TAM) was extremely effective in producing LCB structures, which promoted substantial increases in viscosity, elasticity, as well as strain hardening characteristics. The reactively-modified injection molded branched PLA formulations had improved Izod impact strength, while maintaining their capacity to degrade hydrolytically were maintained. Furthermore, these materials developed high amounts of crystallinity, when cooled under controlled conditions, revealing a nucleating effect. The improvements in strain hardening resulted in microcellular foams with very high cell densities and sub-micron sized cell size, when these formulations were foamed at temperatures close to the crystallization temperature of the polymer.

Co-Authorship

This thesis contains chapters that present results that have been published in the form of original journal articles as well as material that is in preparation for submission. The complete citations for the published papers and the chapters in which they appear are provided below:

Chapter 2: Zhang, Y., Tiwary, P., Gui, H., Kontopoulou, M., Parent, J.S., "Crystallization of coagent-modified polypropylene: Effect of polymer architecture and cross-linked nanoparticles" *Industrial & Engineering Chemistry Research*, **2014**, 53 (41), 15923-15931.

Chapter 3: Zhang, Y., Tiwary, P., Parent, J.S., Kontopoulou, M., Park C.B., "Crystallization and foaming of coagent-modified polypropylene: Nucleation effects of cross-linked nanoparticles", *Polymer*, **2013**, 54 (18), 4814-4819.

Chapter 4: Tiwary, P., Gui, H., Ferreira, P.L., Kontopoulou, M., "Coagent Modified Polypropylene Prepared by Reactive Extrusion: A New Look into the Structure-Property Relations of Injection Molded Parts" *International Polymer Processing*, **2016**, 31 (4), 433-441.

Chapter 5: Tiwary, P. Kontopoulou, M., "Rheological Characterization of Long-Chain Branched Poly(lactide) prepared by reactive extrusion in the presence of allylic and acrylic coagents" In preparation for submission to *Rheologica Acta*.

Chapter 6: Tiwary, P., Kontopoulou, M., "Tuning the rheological, thermal and solid-state properties of branched PLA by free-radical-mediated reactive extrusion" *ACS Sustainable Chemistry & Engineering*, **2017**, Accepted, In print (DOI: 10.1021/acssuschemeng.7b03617).

Chapter 7: Tiwary, P., Park, C.B., Kontopoulou, M., "Transition from microcellular to nanocellular PLA foams by controlling viscosity, branching and crystallization" *European Polymer Journal*, **2017**, 91, 283-296.

The large majority of the experimental work, analysis and writing have been conducted by the author, or under the author's direct direction. All the papers and manuscripts were co-authored and reviewed prior to publication by the thesis supervisor Prof. Marianna Kontopoulou. The second and third chapter was co-

authored by Dr. Ying Zhang. In these chapters I was responsible for conducting all the crystallization experiments and analysis by differential scanning calorimetry (DSC) and hot stage microscopy, X-ray diffraction (XRD) measurement and analysis, and imaging experiments (Transmission electron microscopy (TEM); scanning electron microscopy (SEM); hot stage microscopy). I was also responsible for writing the final version of the respective manuscripts. The fourth chapter was co-authored by Dr. Gui (visiting researcher) and Mr. Ferreira (summer undergraduate student) who assisted the author with injection molding and mechanical property characterization. The second and third chapter was co-authored and reviewed prior to publication by Prof. J. Scott Parent. The third and seventh paper was co-authored and reviewed prior to publication by Prof. Chul B. Park of the Department of Mechanical and Industrial Engineering, University of Toronto.

---

* The author will like to emphasize that his name in the published articles is Praphulla Tiwary or Tiwary,P.

Acknowledgements

This thesis would not have seen the light of the day without the inspirational mentorship of my supervisor, Dr. Marianna Kontopoulou. Her positive attitude and professionalism towards work is deeply imprinted on myself. I thank her for the enlightening insight into the topic of reactive extrusion and foaming. Dr. Park is gratefully acknowledged for his help and support during numerous visits to his group. I would like to thank Dr. Parent for his inputs on the coagent modification of polymers.

Financial support in the form of scholarships from the National Science and Engineering Research Council (NSERC), and Queen's University (Queen's Graduate Award) is gratefully acknowledged. Funding from the Auto 21 Network of Centres of Excellence and the Innovative Plastic Materials and Manufacturing Processes (NIPMMP) NSERC strategic network are greatly appreciated. Materials were supplied by NatureWorks and Lyondell Basell.

I am grateful to the following people for the technical assistance they provided over the course of this research project: Mr. Charlie Cooney and Mrs. Agatha Dobosz for SEM apparatus, Dr. Xiaohu Yan for TEM apparatus. I would like to thank technical staff: Kelly Sedore, Steve Hodgson, Ying Zhang, and Brooke Belfall for numerous technical discussions.

I would like to thank Chemical Engineering Graduate Association (CEGSA) for keeping me sane with their gatherings and social events. Special thanks to my lab mates: Karolina, Heather, and Yuki for help and discussions. My journey would not have been this adventurous without my friends: Fahim, Prashant, Andrew, Manuel, Ahmed, Haley, Kevin, Jan, Calista, Eric Peterson, and Neil.

Special gratitude goes to the maternal side of my family for instilling belief in myself from a young age. To my sister, Kavya Tiwary and my brother, Prateek Tiwary, thank you for your understanding and support. Last but not the least, my final gratitude goes to my parents; without their influence in my early years I could not have seen this day!

Table of Contents

List of Figures

List of Tables

Nomenclature

a	Mark-Houwink constant
A	Area (m^2)
d	Cell diameter (μm)
d_n	Number average diameter (μm)
d_v	Volume average diameter (μm)
E_H	Horizontal activation energy of the flow (kJ/mol)
G*	Complex modulus (Pa)
G'	Elastic or Storage modulus (Pa)
G"	Viscous or loss modulus (Pa)
K	Mark-Houwink constant (dL/g)
n	Shear thinning constant
S	Strain hardening coefficient
T	Temperature (°C)
t	Time (s)
Tc	Temperature of crystallization (°C)

Greek Symbols

ΔH_f	Heat of fusion
[η]	Intrinsic viscosity (dL/g)
3η+	Linear viscoelastic envelope in uniaxial extension (Pa.s)
δ	Phase degree (°)
$\dot{\varepsilon}$	Henky strain rate (s^{-1})
η*	Complex Viscosity (Pa.s)
η_0	Zero shear viscosity (Pa.s)
η_E^+	Tensile stress growth coefficient (Pa.s)
λ	Relaxation time (s)
ρf	Bulk density of the foam sample (g/cm_3)
ω	Angular frequency (rad/s)

Abbreviations

ASTM	American Society for Testing Materials
DCP	Dicumyl Peroxide
DSC	Differential Scanning Calorimetry
LCB	Long-chain Branching
LDPE	Low Density Polyethylene
LLDPE	Linear Low Density Polyethylene
L-PP	Linear Polypropylene homopolymer
LVE	Linear Viscoelastic
MFI	Melt Flow Index
MFR	Melt Flow Rate
MW	Molecular Weight
PE	Polyethylene
PETA	Pentaerythritol Triacrylate

phr	Parts per Hundred
PLA	Poly (lactic acid)
PP	Polypropylene
SAOS	Small Amplitude Oscillatory Shear
TAM	Triallyl trimesate
TEM	Transmission Electron Microscopy
TMPTMA	Trimethylolpropane trimethacrylate
TSE	Twin-screw Extruder
VER	Volume Expansion Ratio
N_2	Nitrogen
CM-PP	Coagent Modified Polypropylene
MWD	Molecular Weight Distribution
TCB	1,2,4-Trichlorobenzene
GPC	Gel Permeation Chromatography
LS	Light Scattering

Chapter 1

Introduction-Literature Review

Commodity and biobased/biodegradable thermoplastics

Plastics are among the most common synthetic materials available nowadays, with a cumulative annual growth rate of 8.6% [1]. Based on cost and mechanical property considerations, thermoplastics can be divided into two major categories: commodity plastics and engineering plastics. Generally commodity plastics such as poly(ethylene) (PE), poly (propylene) (PP), poly (vinylchloride) (PVC), poly(styrene) (PS) etc. have low cost and provide a range of mechanical properties, depending upon their structure [2–5]. On the other hand engineering plastics possess exceptional mechanical properties, including excellent balance of rigidity and toughness. Due to the higher cost of engineering plastics compared to commodity plastics, they are selectively used in applications requiring high mechanical strength and heat stability[2–6].

The extensive use of plastics during the last century has led to severe accumulation of plastic waste in landfills and the natural environment [7,8]; this is exacerbated by their non-biodegradable character. One of the larger markets for plastics is packaging, whose growth has accelerated by the shift from reusable to single use containers [9]. This has resulted in an increase the share of plastics in municipal solid waste [9]. The available means to deal with plastic waste disposal are: i) combustion, ii) recycling, and iii) landfilling [9,10]. Though thermal means such as pyrolysis or combustion can permanently eliminate the plastic waste , the economics of such disposal means is not profitable [9,10]. Recycling of thermoplastics is practiced by many municipalities and is an effective means of waste diversion, however the diversion rates remain inconsistent within the various jurisdictions [2]. On the other hand the disposal of plastic via land filling is problematic because of high cost of disposal and issues related to ground water pollution [2,7,8,11] .
In addition to the concerns about disposal, the accumulation of plastics in the environment, which results in contamination of terrestrial habitats and the marine environment, is posing serious challenge to the health of various ecosystems [8,11,12]. These environmental and disposal concerns, together with the move to reduce over-reliance on fossil-fuel derived products has boosted interest in bio-based and biodegradable plastics.

Plastics are classified as biobased and /or biodegradable when the monomers used to produce them are derived from bio-resources and/ or have the capability to degrade under various conditions

[2,3,5]. The bioplastics are classified, depending upon the feedstock and ability to degrade, into various sub-sections as shown in Figure 1.1[5]:

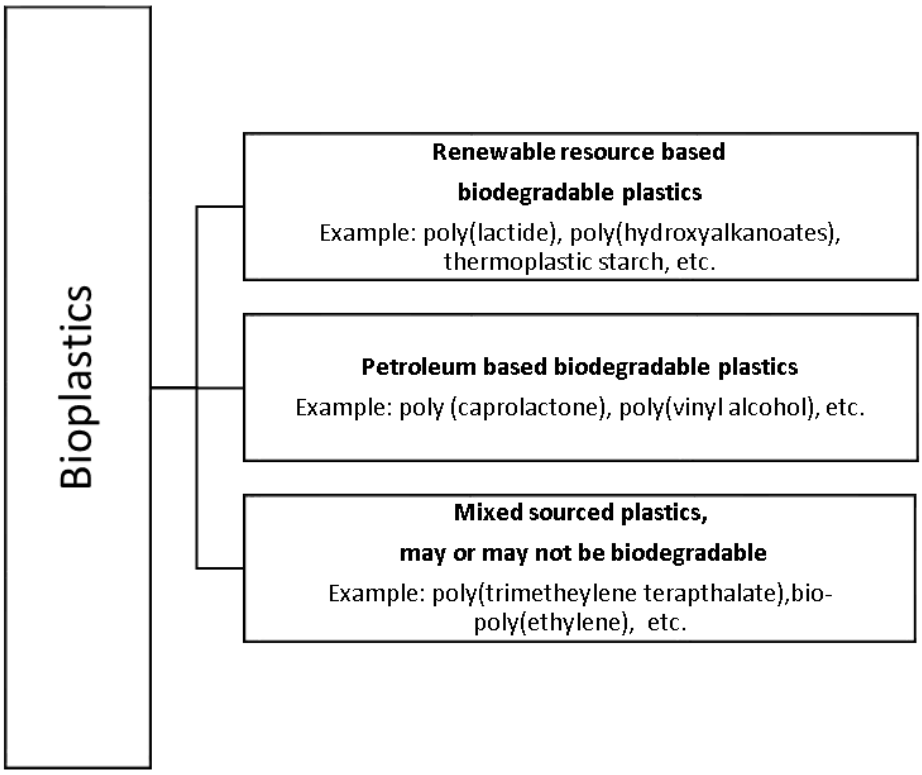

Figure 1.1 Classification of bioplastics with examples [5].

Bio-based and biodegradable plastics support the concept of carbon neutrality. The monomers that are used to synthesize bio-based and biodegradable polymers maybe derived from sustainable resources and at the end of life cycle of the articles, the polymers are degraded in suitable disposal conditions (compost, etc.). Thus the carbon is returned back to nature and the whole cycle can be repeated again [2,3,5]. Greater emphasis has been put on growth of biobased and / or biodegradable polymer with a forecasted growth in global production of 7.8 million tonnes in 2019 from 1.7 million tonnes in 2014 [4,5].

However many inherent challenges have limited the growth of bioplastics in various sectors. Biopolymers generally compete with petroleum based polymers and hence cost is an important criterion for the wide spread market acceptance [2,4]. In addition to their higher cost the mechanical and thermo-mechanical properties have to be matched with the petroleum based polymers to replace them in certain applications. End-of-life issues such as lack of composting facilities and policy development have also limited the acceptance of bioplastics [2,4–6].

Effect of branching on processing of thermoplastics

Whether biobased/bioderived or conventional, the conversion of thermoplastics to finished products is governed by the same polymer processing principles. Successful production of polymeric products requires a specific set of properties, which include suitable melt-state characteristics, crystalline structure, and mechanical properties. For example articles fabricated by injection molding generally require good melt flow properties, fast crystallization and solidification in the mold, while products produced through extrusion blow-molding, film blowing/casting or foaming require sufficient melt strength. Furthermore production rates during extrusion are largely dictated by the degree of shear thinning, which promotes lower viscosities during extrusion conditions. These properties largely depend upon the chain architecture of the polymers, which is further dictated by their method of synthesis. Thus the structure-property relations must be carefully understood.

In addition to the well-known effects of short-chain branching and long-chain branching on the rheology of polyethylenes [13–18], various types of specialty branched chain topographies, including stars, comb-like and hyperbranched (branch-on-branch), have been researched to promote shear thinning and improve extensional strain hardening (melt strength). The degree, length, and structure of branching affect profoundly the rheological properties [18,19]. Model polymers such as stars or combs (**Figure 1.2**) have been synthesized, to study the structure – property relationships [19–21].

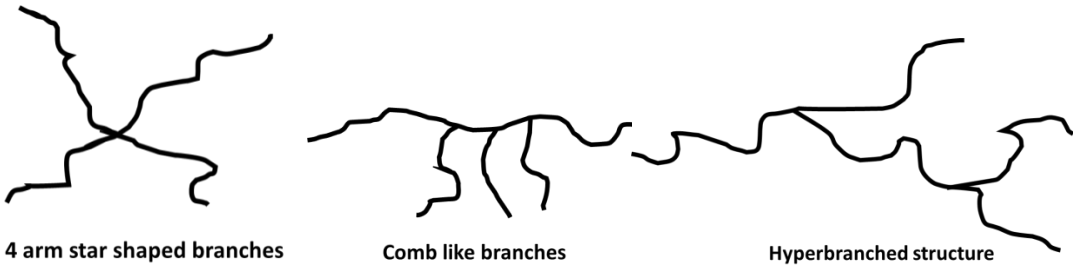

Figure 1.2 Examples of branched architectures in polymers.

The presence of branched architectures changes the linear viscoelastic (LVE) properties of linear polymers. The branched polymers have higher zero-shear viscosities and exhibit intensified shear thinning when compared to linear polymers (Figure 1.3a) [19]. The effect of branch length is prominent on shear thinning behaviour, owing to chain disentanglement [13–15,20,21].

The branches also have significant effect on extensional viscosity (Figure 3b). Linear polymers follow a Trouton-type stress-growth pattern, while the branched polymers, depending on the branch

architecture, show strain hardening which has been attributed to the reduced rate of chain disentanglements because of the presence of branches [13–15,19–24].

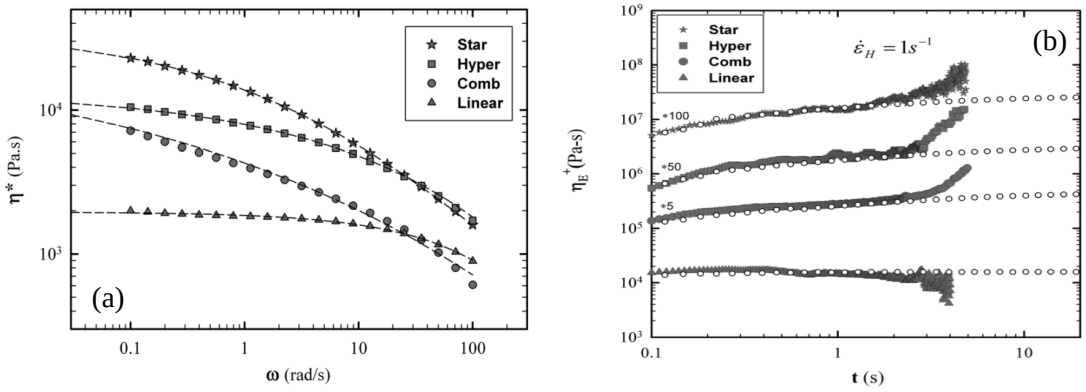

Figure 1.3 (a) Complex viscosity as a function of frequency and (b) extensional viscosity at Hencky strain of $1s^{-1}$ for various chain architectures of PLA [19].

Chain branching can be introduced during synthesis of the polymer; however this is not always possible without costly changes in the manufacturing method/polymerization conditions or expensive catalyst systems [25]. Grafting in the solvent or melt state is frequently used to modify the chain architecture of the polymers[26], post-synthesis. Solvent-state grafting involves dissolution of the polymer in a suitable solvent and then reacting the polymer with certain chemical species to incorporate branching [26]. The solvent state grafting requires costly removal of solvents, and the residual solvent may exclude the application of modified polymers in certain sectors such as biomedical, food contact etc. Melt-state grafting, accomplished by reactive extrusion, is a straightforward method to introduce chain branching and thus manipulate the rheological properties of linear polymers, such as PP and PLA.

Reactive extrusion is a continuous or semi-continuous process which involves reaction of the molten plastic with reactive chemical species. This is accomplished within an extruder, which essentially acts as a chemical reactor. The advantages of reactive extrusion are that it is generally solvent free, it involves short reaction time, and it is a continuous process that can be implemented industrially. Melt state grafting is the most commonly used post-reactor modification of polyolefins, such as PP, and polyesters, such as PLA to introduce long chain branching (LCB)[27–30] . Branching can be accomplished by introducing chain extenders, silane grafting, grafting of multifunctional monomers, and through various peroxide-mediated mechanisms.

Zhang et al. [31] used a mediating agent viz N,N-dimethyldithiocarbamate, ZDMC along with multifunctional monomer (1,6 –hexanediol diacrylate; HDDA) and dicumyl peroxide, to promote

the long chain branching in PP. The presence of LCB improved melt strength, resulting in foams having high cell density of $2.53x10^{12}$ cells/cm^3 as well as better expansion ratios.

PP grafted with glycidyl methacrylate (PP-GMA) was modified by using poly (hexamethylendiamine-guanidine hydrochloride), PHGH in a static mixer [32]. Branched PP showed high melt strength and enhanced elastic response at low frequencies under dynamic oscillatory studies, compared with linear PP. The foams produced by extrusion of branched PP with CO_2 as blowing agent, exhibited expansion ratio of 40 with cell density of $2.7x10^7$ cells/cm^3, whereas the linear PP showed poor expansion ratio of 3 with cell density of $1.8x10^3$ cells/cm^3.

Reactive extrusion of PP has also been performed with silanes, such as ethenyl unsaturated silane, as crosslinking agent [33] and in the presence of a peroxides, and multifunctional monomers [34]. These techniques result in increased melt viscosity, and extensional strain hardening characteristics. Instead of using peroxides, branching and/or crosslinking reactions can also be initiated by exposing PP mixed with multifunctional monomer, to high energy radiation.

Reactive extrusion of PLA in the presence of chain extenders (1, 4 butanediol and 1, 4 butane diisocynate), and a catalyst tin(II) 2-ethylhexanoate, led to enhanced melt viscosity, molecular weight, and elasticity [35] and improved foaming characteristics. Researchers have accomplished chain extension with the help of a multifunctional epoxide, Joncryl® 4368, via reactive extrusion in the melt state using a twin screw extruder[36–38]. Increase in viscosity and molecular weight of modified PLA was observed owing to chain branching and crosslinking reactions. The foams made of branched PLA had higher expansion ratio due to better melt strength.

Mihai et al. used multifunctional styrene-acrylic-epoxy copolymer to introduce branching in PLA [39]. Foaming and reactive extrusion were performed in one step extrusion process with CO_2 as a blowing agent. Typical strain hardening characteristics were observed with branched PLA and also, the shear viscosity was found to increase with the reactive extrusion. The authors observed a decrease in foam density, by nearly half, with reactively modified PLA. Crystallization and chain branching played critical role in obtaining low density foam at low CO_2 concentration of 5 wt.%. This thesis will specifically focus on peroxide-mediated mechanisms, which are described in more detail below:

Peroxide-mediated reactive extrusion:

Polymers, such as polyolefins, can be branched, or cross-linked through peroxide-mediated reactions in the melt state. **Scheme 1.1** shows the dominant pathways of peroxide modification. In a typical melt state modification in the presence of peroxides, hydrogen is abstracted to produce

macroradicals. These macroradicals are unstable and have a tendency to degrade through β-scission pathways [40–42] or to recombine to form C-C crosslinks.

Peroxide thermolysis

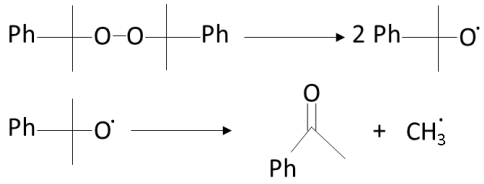

Hydrogen atom abstraction

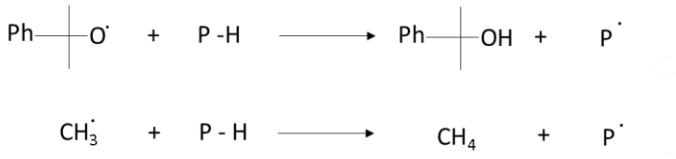

Recombination reaction

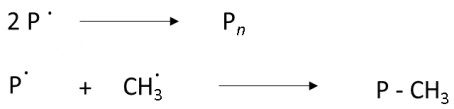

Fragmentation / Degradation reaction- Disproportionation reaction

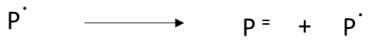

Scheme 1.1: Mechanism for free radical mediated systems [42–44].

The balance of chain scission and cross-linking reactions control the product's branching distributions and molecular weights. PE is known to cross-link[45–48], whereas PP has been shown to degrade in the presence of peroxides [49,50].

In systems that are prone to degradation, such as PP, it is common practice to use multifunctional coagents, in an effort to counteract chain scission and introduce branching (Scheme 1.2) [51–53]

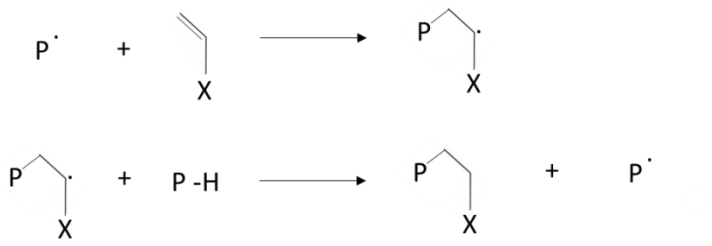

Scheme 1.2: Peroxide-mediated reaction in presence of a multi-functional coagent [49].

There is a vast amount of literature on coagent modification of PP, much of it targeting melt strength improvements to stabilize cell growth during foaming, and therefore to produce good quality foams. Rheological studies of coagent-modified PP [49,54,55] under steady shear [56,57], oscillatory shear [54,56] and extensional deformation [34,49] have demonstrated enhanced melt elasticity and extensional strain hardening behavior, owing to the presence of a hyper-branched chain population in the chemically-modified material [58].

In addition to affecting melt-state rheological properties, coagent-modification has been reported to increase the crystallization temperature and degree of crystallinity of PP [34,59–61], while also affecting isothermal and non-isothermal crystallization kinetics [61–63]. Most accounts of these phenomena focus on branched chains residing in the high molecular weight portion of the molecular weight distribution [61–64], with some researchers proposing that the material's gel fraction provides a "nucleating" effect on crystallization dynamics [65–67]. However these phenomena have not been explained unambiguously, and their consequences on the mechanical properties of PP parts produced by injection molding are not understood.

Coagent modification of PLA is not as widespread. PLA can be branched through free-radical mediated mechanisms, through reactive extrusion in the presence of organic peroxides [68,69] and multifunctional coagents, such as pentaertythritol triacrylate (PETA) and triallyl isocyanurate (TAIC) [70–73]. Recent work in our group showed that in addition to substantial improvements in the strain hardening characteristics of PLA solvent-free, peroxide-initiated grafting of the multi-functional co-agent triallyl-trimesate (TAM) [43,44] results in faster crystallization rates, both under isothermal and non-isothermal conditions.

The structure of PLA branched by reactive extrusion has attracted considerable interest. However the structure-mechanical property relations of these coagent-modified PLAs have not been studied adequately. Given the importance of both melt-state properties, and crystallization kinetics on PLA processing, these coagent modified PLAs emerge as ideal candidate materials for new applications.

1.1 Thesis objectives

Reactive modification of polyolefins is a mature subject. However, in spite of the vast amounts of literature on the topic, the effects of these modifications on the crystallization characteristics and resulting mechanical properties have received sparse attention. The first objective of this thesis is to conduct an in-depth study of the crystallization properties of coagent-modified PP, and to investigate the structure-property relations of these materials. This knowledge will allow the implementation of a single step reactive extrusion process, which will allow tailoring of both the chain architecture and the crystallization properties of the polymers, to achieve substantial improvements in the properties of injection molded and foamed parts.

PLA is a bio-derived and biodegradable/compostable biopolymer, with great potential to replace conventional thermoplastics in many applications, including packaging, consumer goods, as well as specialty applications, such as biomedical, tissue engineering and 3D printing. Like most biopolyesters, PLA suffers from drawbacks, including low melt strength, due to its linear structure and slow crystallization kinetics. In order for biopolyesters such as PLA to become economically viable and succeed in replacing conventional thermoplastics, their processability and properties must be improved, to meet the requirements of the manufacturing sector.

The second objective of this research is therefore to upgrade the melt-state and crystallization properties of PLA by reactive extrusion. This will be accomplished by studying in detail the reaction parameters, including coagent type and amount on the molecular weight and rheological properties of the polymers, and by establishing rigorous relations between the structure and properties of injection molded parts and foams.

1.2 Thesis organization

This thesis consists of eight chapters. Chapter 1 gives introduction and deals with literature review. Chapter 2 investigates the effect of reactive extrusion in the presence of multi-functional coagents and foaming of PP. Chapter 3 examines the origins of these enhancements. Chapter 4 establishes relations between the thermal mechanical properties of coagent-modified PP. Foams prepared from these coagent modified PP are examined in Appendix A. Chapter 5 describes the effects of various multi-functional coagents (allylic vs acrylic) on the rheological properties of reactively modified PLA and uses this information to infer the type of branching. Chapter 6 examines the evolution of molecular weight, branching, thermorheological, and mechanical properties of PLA, prepared by reactive extrusion using various amounts of peroxide and coagent. Chapter 7 exploits the changes in the rheological and crystallization to produce foams of uniform

cell structure and controlled cell sizes. Chapter 8 serves as a summary of the entire work, where conclusions are drawn and recommendations on future work are made.

1.3 References

[1] Consultic Marketing & Industrieberatung GmbH, World Plastics Materials Demand 2015 by Types, Plast. Mark. Res. Gr. / Consult. Mark. Ind. GmbH. (2015) 3. https://committee.iso.org/files/live/sites/tc61/files/The Plastic Industry Berlin Aug 2016 - Copy.pdf (accessed October 1, 2017).

[2] J.H. Song, R.J. Murphy, R. Narayan, G.B.H. Davies, Biodegradable and compostable alternatives to conventional plastics, Philos. Trans. R. Soc. B Biol. Sci. 364 (2009) 2127–2139. doi:10.1098/rstb.2008.0289.

[3] R.P. Babu, K. O'Connor, R. Seeram, Current progress on bio-based polymers and their future trends, Prog. Biomater. 2 (2013) 8. doi:10.1186/2194-0517-2-8.

[4] M. Lettner, J.P. Schöggl, T. Stern, Factors influencing the market diffusion of bio-based plastics: Results of four comparative scenario analyses, J. Clean. Prod. 157 (2017) 289–298. doi:10.1016/j.jclepro.2017.04.077.

[5] M. Lackner, Bioplastics, Kirk-Othmer Encycl. Chem. Technol. (2015) 1–41. doi:10.1002/0471238961.koe00006.

[6] S. Brockhaus, M. Petersen, W. Kersten, A crossroads for bioplastics: exploring product developers' challenges to move beyond petroleum-based plastics, J. Clean. Prod. 127 (2016) 84–95. doi:10.1016/j.jclepro.2016.04.003.

[7] D.K.A. Barnes, F. Galgani, R.C. Thompson, M. Barlaz, Accumulation and fragmentation of plastic debris in global environments, Philos. Trans. R. Soc. B Biol. Sci. 364 (2009) 1985–1998. doi:10.1098/rstb.2008.0205.

[8] M. Wagner, C. Scherer, D. Alvarez-Muñoz, N. Brennholt, X. Bourrain, S. Buchinger, et al., Microplastics in freshwater ecosystems: what we know and what we need to know, Environ. Sci. Eur. 26 (2014) 12. doi:10.1186/s12302-014-0012-7.

[9] R. Geyer, J.R. Jambeck, K.L. Law, Production, use, and fate of all plastics ever made, Sci. Adv. 3 (2017) e1700782. doi:10.1126/sciadv.1700782.

[10] R.S. Stein, Polymer recycling: opportunities and limitations., Proc. Natl. Acad. Sci. U. S. A. 89 (1992) 835–838. doi:10.1073/PNAS.89.3.835.

[11] M.C. Rillig, Microplastic in terrestrial ecosystems and the soil, Environ. Sci. Technol. 46 (2012) 6453–6454. doi:10.1021/es302011r.

[12] K.A. V. Zubris, B.K. Richards, Synthetic fibers as an indicator of land application of sludge, Environ. Pollut. 138 (2005) 201–211. doi:10.1016/j.envpol.2005.04.013.

[13] P. Wood-Adams, S. Costeux, Thermorheological behavior of polyethylene: Effects of microstructure and long chain branching, Macromolecules. 34 (2001) 6281–6290. doi:10.1021/ma0017034.

[14] A.H. Willbourn, Polymethylene and the structure of polyethylene: Study of short-chain branching, its nature and effects, J. Polym. Sci. 34 (1959) 569–597. doi:10.1002/pol.1959.1203412740.

[15] F.A. Bovey, F.C. Schilling, F.L. McCrackin, H.L. Wagner, Short-Chain and Long-Chain Branching in Low-Density Polyethylene, Macromolecules. 9 (1976) 76–80. doi:10.1021/ma60049a014.

[16] S. Costeux, P. Wood-Adams, D. Beigzadeh, Molecular structure of metallocene-catalyzed polyethylene: Rheologically relevant representation of branching architecture in single catalyst and blended systems, Macromolecules. 35 (2002) 2514–2528. doi:10.1021/ma011432c.

[17] P.M. Wood-Adams, J.M. Dealy, Using rheological data to determine the branching level in metallocene polyethylenes, Macromolecules. 33 (2000) 7481–7488. doi:10.1021/ma991534r.

[18] P.M. Wood-Adams, J.M. Dealy, A.W. DeGroot, O.D. Redwine, Effect of molecular structure on the linear viscoelastic behavior of polyethylene, Macromolecules. 33 (2000)

7489–7499. doi:10.1021/ma991533z.
[19] S. Nouri, C. Dubois, P.G. Lafleur, Effect of chemical and physical branching on rheological behavior of polylactide, J. Rheol. 59 (2015) 1045–1063. doi:10.1122/1.4922486.
[20] M. Kapnistos, D. Vlassopoulos, J. Roovers, L.G. Leal, Linear rheology of architecturally complex macromolecules: Comb polymers with linear backbones, Macromolecules. 38 (2005) 7852–7862. doi:10.1021/ma050644x.
[21] M. Kapnistos, G. Koutalas, N. Hadjichristidis, J. Roovers, D.J. Lohse, D. Vlassopoulos, Linear rheology of comb polymers with star-like backbones: Melts and solutions, Rheol. Acta. 46 (2006) 273–286. doi:10.1007/s00397-006-0106-2.
[22] Y. Zhao, Q. Cai, J. Jiang, X. Shuai, J. Bei, C. Chen, et al., Synthesis and thermal properties of novel star-shaped poly (L -lactide) s with starburst PAMAM – OH dendrimer macroinitiator, Polymer . 43 (2002) 5819–5825. doi:10.1016/S0032-3861(02)00529-3.
[23] Liangliang Gu, Star vs long chain branching of poly(lactic acid) with multifunctional aziridine, J. Rheol. 61 (2017) 785–796. doi:10.1122/1.4985344.
[24] J.R. Dorgan, J.S. Williams, D.N. Lewis, Melt rheology of poly(lactic acid): Entanglement and chain architecture effects, J. Rheol. 43 (1999) 1141. doi:10.1122/1.551041.
[25] T. Meyer, Scale-up of polymerization process: A practical example, Org. Process Res. Dev. 7 (2003) 297–302. doi:10.1021/op025605p.
[26] V. Pillay, A. Seedat, Y.E. Choonara, L.C. du Toit, P. Kumar, V.M.K. Ndesendo, A Review of Polymeric Refabrication Techniques to Modify Polymer Properties for Biomedical and Drug Delivery Applications, AAPS PharmSciTech. 14 (2013) 692–711. doi:10.1208/s12249-013-9955-z.
[27] C. Tzoganakis, J. Vlachopoulos, A.E. Hamielec, Production of controlled- rheology polypropylene resins by peroxide promoted degradation during extrusion, Polym. Eng. Sci. 28 (1988) 170–180.
[28] S.H. Ryu, C.G. Gogos, M. Xanthos, Melting behaviour of controlled rheology polypropylene, Polymer 32 (1991) 2449–2455. doi:10.1016/0032-3861(91)90088-Z.
[29] S. Coiai, E. Passaglia, M. Aglietto, F. Ciardelli, Control of degradation reactions during radical functionalization of polypropylene in the melt, Macromolecules. 37 (2004) 8414–8423. doi:10.1021/ma0400315.
[30] E. Passaglia, S. Coiai, S. Augier, Control of macromolecular architecture during the reactive functionalization in the melt of olefin polymers, Prog. Polym. Sci. 34 (2009) 911–947. doi:10.1016/j.progpolymsci.2009.04.008.
[31] W. Zhang, L. Yang, H. Zhang, W. Lin, Y. Wang, Investigation on multifunctional monomer modified polypropylene and its foamability, J. Appl. Polym. Sci. 130 (2013) 1675–1681. doi:10.1002/app.39345.
[32] S. Li, M. Xiao, Y. Guan, D. Wei, H. Xiao, A. Zheng, A novel strategy for the preparation of long chain branching polypropylene and the investigation on foamability and rheology, Eur. Polym. J. 48 (2012) 362–371. doi:10.1016/j.eurpolymj.2011.11.015.
[33] G. Song, S. Yang, C. Yang, X. She, Foaming polypropylene prepared by a novel one-step silane-grafting and crosslinking method, J. Porous Mater. 13 (2006) 297–301. doi:10.1007/s10934-006-8020-7.
[34] G.J. Nam, J.H. Yoo, J.W. Lee, Effect of long-chain branches of polypropylene on rheological properties and foam-extrusion performances, J. Appl. Polym. Sci. 96 (2005) 1793–1800. doi:10.1002/app.21619.
[35] Y. Di, S. Iannace, E. Di Maio, L. Nicolais, Reactively modified poly (lactic acid): Properties and foam processing, Macromol. Mater. Eng. 290 (2005) 1083–1090. doi:10.1002/mame.200500115.
[36] Y. Baimark, P. Srihanam, Influence of chain extender on thermal properties and melt flow index of stereocomplex PLA, Polym. Test. 45 (2015) 52–57.

doi:10.1016/j.polymertesting.2015.04.017.
[37] Q. Meng, M.C. Heuzey, P.J. Carreau, Control of thermal degradation of polylactide/clay nanocomposites during melt processing by chain extension reaction, Polym. Degrad. Stab. 97 (2012) 2010–2020. doi:10.1016/j.polymdegradstab.2012.01.030.
[38] Q.K. Meng, M.C. Heuzey, P.J. Carreau, Effects of a Multifunctional Polymeric Chain Extender on the Properties of Polylactide and Polylactide/Clay Nanocomposites, Int. Polym. Process. 27 (2012) 505–516. doi:10.3139/217.2647.
[39] M. Mihai, M.A. Huneault, B.D. Favis, Rheology and extrusion foaming of chain-branched poly(lactic acid), Polym. Eng. Sci. 50 (2010) 629–642. doi:10.1002/pen.21561.
[40] M.W. Bodley, Functional nitroxyls in polypropylene based thermoplastic vulcanizates, MASc. Thesis, Queen's University at Kingston, Ontario, Canada, 2017.
[41] D.K. Hyslop, Delayed-onset crosslinking using fucntional nitroxyls, MAsc. Thesis, Queen's University at Kingston, Ontario, Canada, 2012.
[42] B. Molloy, Functionalized-Nitroxyls for Use in Peroxide-Initiated Modifications of Polymers, MASc. thesis, Queen's University at Kingston, Ontario, Canada, 2014. http://qspace.library.queensu.ca/handle/1974/12463.
[43] M. Nerkar, J.A. Ramsay, B.A. Ramsay, A.A. Vasileiou, M. Kontopoulou, Improvements in the melt and solid-state properties of poly(lactic acid), poly-3-hydroxyoctanoate and their blends through reactive modification, Polymer. 64 (2015) 51–61. doi:10.1016/j.polymer.2015.03.015.
[44] M. Nerkar, J.A. Ramsay, B.A. Ramsay, M. Kontopoulou, Dramatic Improvements in Strain Hardening and Crystallization Kinetics of PLA by Simple Reactive Modification in the Melt State, Macromol. Mater. Eng. (2014) 1419–1424. doi:10.1002/mame.201400078.
[45] T. Bremner, A. Rudin, Peroxide modification of linear low- density polyethylene: A comparison of dialkyl peroxides, J. Appl. Polym. Sci. 49 (1993) 785–798. doi:10.1002/app.1993.070490504.
[46] G. Hulse, R. Kerstring, D. Warfel, Chemistry of dicumyl peroxide induced crosslinking of linear polyethylene, J. Polym. Sci. Polym. Chem. Ed. 19 (1981) 655–667. http://onlinelibrary.wiley.com/doi/10.1002/pol.1981.170190305/full.
[47] E.M. Kampouris, A.G. Andreopoulos, Benzoyl peroxide as a crosslinking agent for polyethylene, J. Appl. Polym. Sci. 34 (1987) 1209–1216. doi:10.1002/app.1987.070340328.
[48] H.A. Khonakdar, J. Morshedian, U. Wagenknecht, S.H. Jafari, An investigation of chemical crosslinking effect on properties of high-density polyethylene, Polymer (Guildf). 44 (2003) 4301–4309. doi:10.1016/S0032-3861(03)00363-X.
[49] J.S. Parent, A. Bodsworth, S.S. Sengupta, M. Kontopoulou, B.I. Chaudhary, D. Poche, et al., Structure–rheology relationships of long-chain branched polypropylene: Comparative analysis of acrylic and allylic coagent chemistry, Polymer. 50 (2009) 85–94. doi:10.1016/j.polymer.2008.11.014.
[50] Y. Zhang, J.S. Parent, M. Kontopoulou, C.B. Park, Foaming of reactively modified polypropylene: Effects of rheology and coagent type, J. Cell. Plast. 51 (2015) 505–522. doi:10.1177/0021955X14566209.
[51] J. Cailloux, O.O. Santana, E. Franco-Urquiza, J.J. Bou, F. Carrasco, J. Gámez-Pérez, et al., Sheets of branched poly(lactic acid) obtained by one step reactive extrusion calendering process: Melt rheology analysis, Express Polym. Lett. 7 (2012) 304–318. doi:10.3144/expresspolymlett.2013.27.
[52] K. El Mabrouk, J.S. Parent, B.I. Chaudhary, R. Cong, Chemical modification of PP architecture: Strategies for introducing long-chain branching, Polymer. 50 (2009) 5390–5397. doi:10.1016/j.polymer.2009.09.066.
[53] M.J. Krell, A. Brandolin, E.M. Vallés, Controlled Rheology Polypropylenes. An Improved

Model with Experimental Validation for the Single Screw Extruder Process, Polym. React. Eng. 2 (1994) 389–408. doi:10.1080/10543414.1994.10744461.
[54] E. Borsig, M. van Duin, a. D. Gotsis, F. Picchioni, Long chain branching on linear polypropylene by solid state reactions, Eur. Polym. J. 44 (2008) 200–212. doi:10.1016/j.eurpolymj.2007.10.008.
[55] W. Zhao, Y. Huang, X. Liao, Q. Yang, The molecular structure characteristics of long chain branched polypropylene and its effects on non-isothermal crystallization and mechanical properties, Polymer. 54 (2013) 1455–1462. doi:10.1016/j.polymer.2012.12.073.
[56] B.K. Kim, K.J. Kim, Cross-linking of polypropylene by peroxide and multifunctional monomer during reactive extrusion, Adv. Polym. Technol. 12 (1993) 263–269. doi:10.1002/adv.1993.060120304.
[57] X. Wang, C. Tzoganakis, G.L. Rempel, Chemical modification of polypropylene with peroxide/pentaerythritol triacrylate by reactive extrusion, J. Appl. Polym. Sci. 61 (1996) 1395–1404. doi:10.1002/(SICI)1097-4628(19960822)61:8<1395::AID-APP21>3.0.CO;2-X.
[58] A.D. Gotsis, B.L.F. Zeevenhoven, A.H. Hogt, The effect of long chain branching on the processability of polypropylene in thermoforming, Polym. Eng. Sci. 44 (2004) 973–982. doi:10.1002/pen.20089.
[59] Ä. Supe, D. Graebling, Synthesis of branched polypropylene by a reactive extrusion process, Macromolecules. 35 (2002) 4602–4610. doi:10.1021/ma0109469.
[60] S.A. Mousavi-Saghandikolaei, M. Frounchi, S. Dadbin, S. Augier, E. Passaglia, F. Ciardelli, Modification of isotactic polypropylene by the free-radical grafting of 1,1,1-trimethylolpropane trimethacrylate, J. Appl. Polym. Sci. 104 (2007) 950–958. doi:10.1002/app.25796.
[61] J. Tian, W. Yu, C. Zhou, Crystallization behaviors of linear and long chain branched polypropylene, J. Appl. Polym. Sci. 104 (2007) 3592–3600. doi:10.1002/app.26024.
[62] P.K. Agarwal, R.H. Somani, W. Weng, A. Mehta, L. Yang, S. Ran, et al., Shear-induced crystallization in novel long chain branched polypropylenes by in situ rheo-SAXS and -WAXD, Macromolecules. 36 (2003) 5226–5235. doi:10.1021/ma034154l.
[63] J. Tian, W. Yu, C. Zhou, Crystallization kinetics of linear and long-chain branched polypropylene, J. Macromol. Sci. Part B Phys. 45 B (2006) 969–985. doi:10.1080/00222340600870507.
[64] F. Yu, H. Zhang, R. Liao, H. Zheng, W. Yu, C. Zhou, Flow induced crystallization of long chain branched polypropylenes under weak shear flow, Eur. Polym. J. 45 (2009) 2110–2118. doi:10.1016/j.eurpolymj.2009.03.011.
[65] Z. Zhang, D. Wan, H. Xing, Z. Zhang, H. Tan, L. Wang, et al., A new grafting monomer for synthesizing long chain branched polypropylene through melt radical reaction, Polymer . 53 (2012) 121–129. doi:10.1016/j.polymer.2011.11.033.
[66] D. Wan, L. Ma, H. Xing, L. Wang, Z. Zhang, J. Qiu, et al., Preparation and characterization of long chain branched polypropylene mediated by different heteroaromatic ring derivatives, Polymer. 54 (2013) 639–651. doi:10.1016/j.polymer.2012.12.014.
[67] J.Y. Kim, E.S. Seo, D.S. Park, K.M. Park, S.W. Kang, C.H. Lee, et al., Chemical modification of isotactic polypropylene by melt blending, Fibers Polym. 4 (2003) 107–113. doi:10.1007/BF02875456.
[68] M. Takamura, T. Nakamura, S. Kawaguchi, T. Takahashi, K. Koyama, Molecular characterization and crystallization behavior of peroxide-induced slightly crosslinked poly(L-lactide) during extrusion, Polym. J. 42 (2010) 600–608. doi:10.1038/pj.2010.42.
[69] M. Takamura, T. Nakamura, T. Takahashi, K. Koyama, Effect of type of peroxide on cross-linking of poly(l-lactide), Polym. Degrad. Stab. 93 (2008) 1909–1916. doi:10.1016/j.polymdegradstab.2008.07.001.

[70] T.M. Quynh, H. Mitomo, N. Nagasawa, Y. Wada, F. Yoshii, M. Tamada, Properties of crosslinked polylactides (PLLA & PDLA) by radiation and its biodegradability, Eur. Polym. J. 43 (2007) 1779–1785. doi:10.1016/j.eurpolymj.2007.03.007.
[71] S. lin Yang, Z.H. Wu, W. Yang, M.B. Yang, Thermal and mechanical properties of chemical crosslinked polylactide (PLA), Polym. Test. 27 (2008) 957–963. doi:10.1016/j.polymertesting.2008.08.009.
[72] J. You, L. Lou, W. Yu, C. Zhou, The preparation and crystallization of long chain branching polylactide made by melt radicals reaction, J. Appl. Polym. Sci. 129 (2013) 1959–1970. doi:10.1002/app.38912.
[73] C.Q. Chen, D.M. Ke, T.T. Zheng, G.J. He, X.W. Cao, X. Liao, An Ultraviolet-Induced Reactive Extrusion to Control Chain Scission and Long-Chain Branching Reactions of Polylactide, Ind. Eng. Chem. Res. 55 (2016) 597–605. doi:10.1021/acs.iecr.5b04094.

Chapter 2

Crystallization of coagent-modified polypropylene: Effect of polymer architecture and cross-linked nanoparticles*

2.1 Introduction

Linear isotactic polypropylene (L-PP) is valued for its chemical resistance, high strength and stiffness, but its low melt strength limits its utility for processes that involve extensional flow, such as thermoforming, film extrusion, and foaming [1]. Significant improvements can be gained by peroxide-initiated graft-modification of L-PP with multifunctional coagents [2, 3] to yield long chain branched (LCB) derivatives. Rheological studies of coagent-modified PP [4-6] under steady shear [7, 8], oscillatory shear [5, 7] and extensional deformation [4, 9] have demonstrated enhanced melt elasticity and extensional strain hardening behavior, owing to the presence of a hyper-branched chain population in the chemically-modified material [10].

In addition to affecting melt-state rheological properties, coagent-modification has been reported to increase the crystallization temperature (T_c) and degree of crystallinity of PP [3, 9, 11, 12], while also affecting isothermal and non-isothermal crystallization kinetics [12-14]. Most accounts of these phenomena focus on branched chains residing in the high molecular weight portion of the molecular weight distribution [12-15], with some researchers proposing that the material's gel fraction provides a "nucleating" effect on crystallization dynamics [16-18]. It should be noted, however, that branched materials prepared by alternate technologies, including LCB-PP prepared by metallocene polymerization [19], electron beam irradiation [20] and silane crosslinking [21], do not show significant shifts in T_c. Therefore, crystallization of coagent-modified LCB-PP materials has not been explained unambiguously. Recent studies of the products derived from coagent-based processes have shed light on the architecture and morphology of these LCB-PP materials. Parent and co-workers have shown that graft modification with triallyl trimesate (TAM) involves simultaneous chain scission and crosslinking to generate bimodal molecular weight and branching distributions.

---

*A version of this chapter has been published: Ying Zhang, **Praphulla Tiwary**, Hua Gui, Marianna Kontopoulou, JS Parent, *Industrial & Engineering Chemistry Research*, **2014**, 53 (41), 15923-15931.

These distributions are typically comprised of a linear PP matrix whose molecular weight is significantly lower than that of the parent material, and a small population of highly branched chains [4]. Furthermore, these materials can contain a small amount of well-dispersed, rigid nanoparticles derived from coagent oligomerization [22, 23].

The present report clarifies and differentiates the effects on crystallization kinetics of cross-linked particles dispersed throughout LCB-PP materials from those generated by the polymer's long chain branch population. Four classes of PP samples with different architectures and nanoparticle content are prepared, including peroxide degraded PP, coagent-modified LCB-PP prepared from TAM and TMPTMA, and particle-free LCB-PP synthesized by silane grafting and moisture curing chemistry. These are further characterized by differential scanning calorimetry (DSC) and optical microscopy studies of their phase transition temperatures and crystallization kinetics.

2.2 Experimental

2.2.1 Materials

Triallyl trimesate (TAM, 98%, Monomer Polymer Inc.), trimethylolpropanetrimethacrylate (TMPTMA, 98%), vinyltriethoxysilane (VTES, 97%), and dicumyl peroxide (DCP, 98%) were used as received from Sigma-Aldrich. Dibutyltindilaurate (DBTDL, 98%) was used as received from Alfa Aesar. ESCORENE™ PP 1042, an isotactic linear polypropylene homopolymer (PP) (MFR = 1.9 g/10 min), with a number average molecular weight (M_n) of 96 kg/mol and a weight average molecular weight (M_w), of 460 kg/mol, as determined by triple detector gel permeation chromatography (GPC), was obtained from ExxonMobil.

2.2.2 PP-g-TAM and PP-g-TMPTMA preparation

Peroxide-degraded PP (PP-DCP) was prepared by coating ground PP powder with an acetone solution containing DCP, according to the formulations shown in Table 2.1, and allowing the solvent to evaporate. The resulting mixture was charged to a Haake Polylab R600 internal batch mixer at 180°C at 60 rpm for 10 min, yielding DCP-PP. Coagent-modified PP samples were prepared as described for PP-DCP from mixtures of PP, DCP and TMPTMA or TAM to yield PP-g-TMPTMA and PP-g-TAM respectively, according to the formulations shown in **Table 2.1**. PP was processed under identical conditions, to ensure a consistent thermal history.

Table 2.1 Formulations and molecular weights of PP and its derivatives

Sample Designation	DCP (phr*)	TAM (phr)	TMPTMA (phr)	M_n (kg/mol)	M_w (kg/mol)	M_w/M_n
PP	0	0	0	96.2	458	4.8
PP-DCP 0.1	0.1	0	0	60.9	211	3.5
PP-DCP 0.3	0.3	0	0	51.6	126	2.4
PP-g-TAM	0.3	6	0	95.2	266	2.8
PP-g-TMPTMA	0.3	0	6	69.1	183	2.6

*part per hundred resin

2.2.3 PP-g-VTES- XL preparation

PP powder (40 g) was tumble-mixed with a solution of DCP (0.04 g, 0.1 wt.%) in VTES (1.2 g, 3 wt.%). The resulting mixture was charged to a HaakePolylab R600 internal batch mixer maintained at 180°C and screw speed of 60 rpm. After a reaction time of 7 min, Irganox B225 (500 ppm) and DBTDL (0.2 ml) was added and mixing was continued for a further 3 min, yielding PP-g-VTES. This material was compressed into thin films, immersed in boiling water for 15h, and dried under vacuum at 60 ℃ to give cross-linked PP-g-VTES-XL.

2.2.4 Gel Permeation Chromatography (GPC)

Molecular weight distributions were measured using a triple detector GPC (GPCIR by PolymerChar) at 145°C, employing 1,2,4-trichlorobenzene (TCB) as the mobile phase. Polymer samples were dissolved in TCB at a concentration of 1 mg mL^{-1} and held at 150 °C for 60 min. Samples with an injection volume of 200 µL were eluted through three linear Polymer Laboratories columns at a flow rate of 1 ml min^{-1}. The light scattering (LS) detector at 15° from the incident beam was used for molecular weight determinations.

2.2.5 Gel content analysis

Gel content analysis was conducted by extraction into boiling xylenes from a 120 mesh stainless steel sieve for 6 hours, according to ASTM D 2765. The residual polymer was dried to constant weight, with gel contents reported as a weight percentage of unextracted material.

In addition, polymer samples were subjected to hot xylenes extraction from Soxhlet cellulose thimbles to capture insoluble particles that could not be isolated using the ASTM method described

above. Solvent was replaced every 3 hours, and after 10 hours no residual polymer could be recovered from the extraction solution by precipitation from acetone. The thimble was cut into pieces, soaked in acetone and sonicated. The resulting dispersion was deposited onto glass slides, acetone was removed by evaporation, and the sample coated with gold for characterization with a JEOL JSM-840 Scanning Electron Microscope (SEM) instrument. Image analysis of the isolated particles was done using SigmaScan Pro® 5.0 (SPSS Inc.).

2.2.6 Rheological Characterization

Compression moulded discs of 20 mm in diameter were prepared for dynamic shear rheology measurements. A controlled stress rheometer, ViscoTech by Reologica, equipped with parallel plate fixtures was operated with a 1 mm gap at180 °C under a continuous nitrogen purge. Stress sweeps were performed to ensure that all data were acquired within the linear viscoelastic regime.

Samples were further characterized in simple uniaxial extension using an SER-2 universal testing platform from Xpansion Instruments hosted on the MCR-301 Anton Paar rheometer. Measurements were conducted at 170 °C at Hencky extension rates ranging between 0.01 and $10s^{-1}$. Specimens were prepared by compression molding material into 1mm thick plaques between polyester films, from which 6.8 mm wide test strips were cut. Linear viscoelastic (LVE) oscillatory measurements obtained at 170 °C were used to calculate the LVE stress growth curve and check the consistency of the extensional measurements.

2.2.7 Thermal Analysis

Crystallization temperature (T_c), heat of fusion (ΔH_f) and melting temperature (T_m) were determined using a TA Instruments DSC Q 100. Weighed samples were sealed in aluminum hermetic pans and analyzed between -30 and 210 °C at a heating/cooling rate of 5 °C/min. After the first heating, each sample was held isothermally at 210 °C for 3 minutes before cooling, followed by a second heating step. The data from the second heating were used for the determination of Tm and ΔH_f. Percent crystallinity was determined by using 209 J/g as the enthalpy of fusion of 100% crystalline PP [24].

Isothermal studies involved heating the sample to 220 °C at 20°C/min (isothermal for 5 min), followed by cooling at 20°C/min to 136°C. The relative crystallinity as a function of time was expressed as

$$X_c = \frac{\int_0^t (dH_c/dt)dt}{\int_0^\infty (dH_c/dt)dt} \qquad (1)$$

where dH_c denotes the enthalpy of crystallization during an infinitesimal time interval, dt.

The Avrami equation [25] was used to fit the data obtained isothermally. The time-dependent relative volumetric crystallinity X(t) for an isothermal crystallization process was expressed as [26]

$$X_c(t) = 1- exp[-(Kt)^n] \quad (2)$$

where n is the Avrami constant, whose value depends on the form and mechanism of crystal growth and K is the rate constant, containing the nucleation and growth parameters [14].

Data obtained from the cooling scans were used for the non-isothermal crystallization kinetics analysis. The actual crystallization times were calculated from the crystallization temperature T_c, the onset temperature T_o where crystallization began, and the cooling rate α, according to equation

$$t = (T_o- T_c)/ \alpha \quad (3)$$

2.2.8 Hot stage Microscopy

Isothermal crystallization experiments were performed using a Linkam CSS 450 hot stage mounted on an Olympus BX51 optical microscope. Thin films were first heated to 200 °C at a rate of 30 °C /min and held for 10 minutes to eliminate their heat history. The melt was then cooled to 140 °C at 30 °C/min and the temperature was kept constant for 1 hour. Images of the sample undergoing crystallization were acquired using a Sony ExwaveHAD 3 CCD digital recorder.

2.2.9 Transmission Electron Microscopy (TEM)

Compression molded samples were cryosectioned at -90°C and 90nm thickness on a Leica Ultracut UCT equipped with a Leica EMFCS cryo-system. The sections were placed on 400 mesh copper grids coated with a carbon film and viewed on a FEI Tecnai 20 TEM operated at 200kV. Images were captured on an AMT 16000 camera.

2.2.10 X-Ray diffraction

X-ray diffraction analysis of compression molded discs (1.25 mm thick, 15 mm dia) was conducted with a Philips X'pert pro diffractometer using Cu kα radiation (λ=1.5406Å). Measurements were performed at 45 kV and 40 mA, with data recorded in reflection mode in the range of 2θ = 10 - 30°.

2.3 Results and Discussion

2.3.1 Material Characterization

Linear PP materials

Our starting material was a commercial grade of linear PP homopolymer that had a M_n of 96.2 kg/mol and dispersity of 4.8. Its unimodal molecular weight distribution is revealed by the light scattering detector plot of **Figure 2.1a**, while its linear architecture is demonstrated by the intrinsic viscosity data plotted in **Figure 2.1b**, which abided by a standard Mark-Houwink relationship to molar mass.

Reaction of L-PP with different amounts of dicumyl peroxide (DCP) at 180°C provided two derivatives, PP-DCP-0.1 and PP-DCP-0.3. GPC confirmed that the extent of molecular weight degradation scaled with peroxide loading (**Table 2.1**), and that the samples retained a linear chain architecture (**Figure 2.1b**). Melt-state dynamic rheological analysis of PP-DCP-0.1 and PP-DCP-0.3 confirmed these conclusions regarding molecular architecture, as both samples demonstrated reduced complex viscosity throughout the entire frequency range, and a pronounced Newtonian plateau (**Figure 2.2a**). Terminal slopes of 2 in the elastic modulus vs. frequency curves (**Figure2.2b**) provided further evidence of a linear polymer structure [18]. The van-Gurp Palmen plots **(Figure 2.2c)** also confirm the linear architecture as the terminal angle tends to 90°.

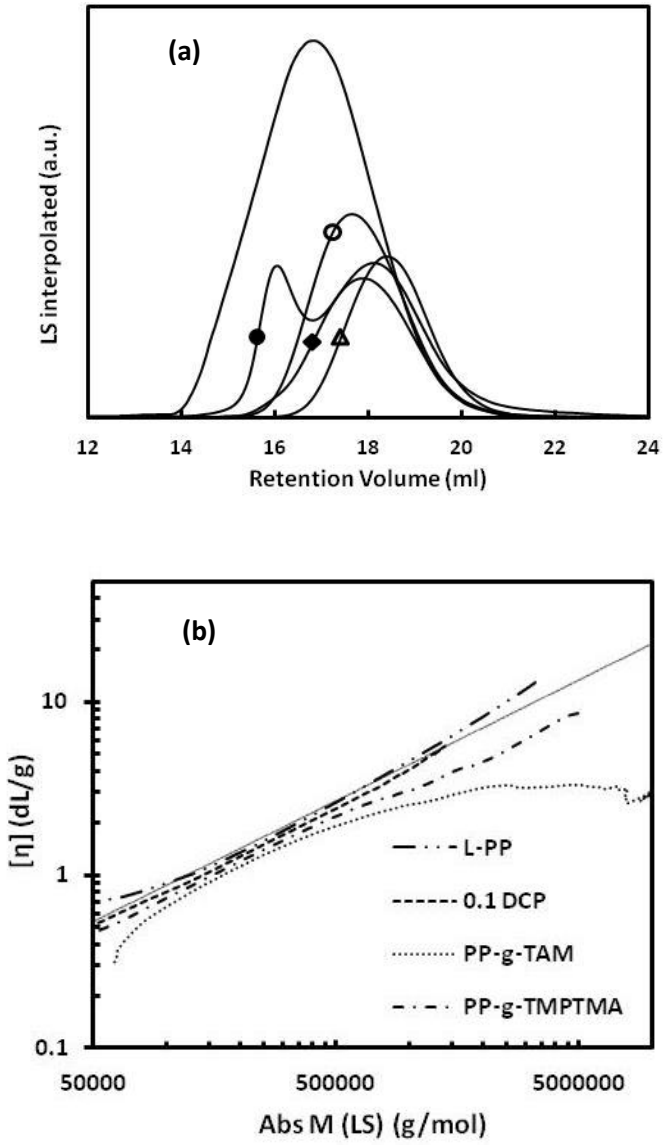

Figure 2.1 (a)Light scattering intensity as a function of retention volume; - L-PP (M_n = 96.2 kg/mol, M_w/M_n = 4.8), ○ PP-DCP 0.1 (M_n = 60.9 kg/mol, M_w/M_n = 3.5), Δ PP-DCP 0.3 (M_n=51.6 kg/mol, M_w/M_n=2.4), ◊ PP-g- TMPTMA (M_w=183 kg/mol, M_w/M_n=2.6) and ● PP-g-TAM (M_w=266 kg/mol, M_w/M_n=2.8); Figure 2b Intrinsic viscosity as a function of molecular weight; The solid line represents the Mark-Houwink relation $[\eta] = KM^a$.

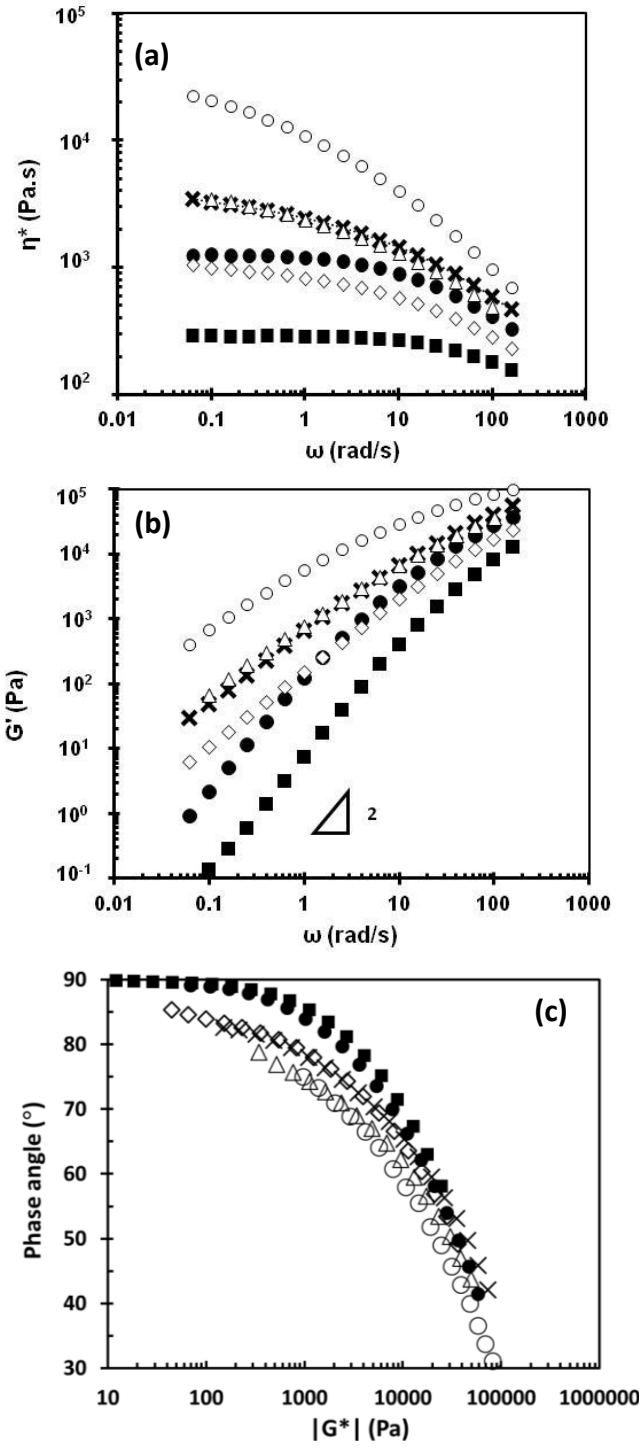

Figure 2.2 (a) Complex viscosity and (b) storage modulus as a function of angular frequency , and (c) van-Gurp Palmen plots at 180 °C. ○ PP, × PP-g-TMPTMA, ◇ PP-g-TAM, △ PP-VTES-XL, ● PP-DCP 0.1, and ■ PP-DCP 0.3.

Coagent modified LCB-PP

Chemical modification of PP using 0.3 phr DCP and 6.0 phr of TAM or TMPTMA produced coagent-modified derivatives, PP-g-TAM and PP-g-TMPTMA, respectively. Both materials possessed M_w and zero shear viscosities that were lower than those of their parent material (**Table 2.1**), indicating that chain scission was dominant over polymer cross-linking in both cases. However, M_n values were greater than those observed when PP was treated with peroxide alone. This is the expected result, since radical addition and hydrogen transfer reactions involving a coagent decrease the population of PP backbone macroradicals, thereby suppressing β-scission of tertiary alkyl radical intermediates [22].

The graft modification of PP with TAM has been well described in the literature, and proceeds efficiently to yield a hyper-branched chain population that can progress beyond the gel point. The resulting products have bimodal molecular weight and branch distribution. The light scattering data plotted for PP-g-TAM demonstrate a strong response at high molar mass (**Figure 2.1a**), while the intrinsic viscosity data provide evidence of the hyper-branched character of this chain population in the form of a deviation from the Mark-Houwink relation [10, 22] (**Figure 2.1b**). In contrast, GPC analysis of the soluble component of PP-g-TMPTMA revealed molecular weight and branching distributions resembling those of PP-DCP-0.1. That is, the methacrylate-based coagent did not produce a hyper-branched chain population that could be detected by either light-scattering or intrinsic viscosity analysis (**Figure 2.1a,b**). Given that allylic hydrogen atom abstraction is known to reduce the efficiency of methacrylate grafting to polyolefins, the relative inefficiency of LCB creation by TMPTMA relative to TAM is predictable [27,28].

Dynamic oscillatory and extensional rheometry studies of the coagent-modified samples confirmed conclusions drawn from GPC analysis. PP-g-TAM exhibited greater shear thinning character and a deviation from terminal flow behavior when compared to its peroxide-degraded analogue, PP-DCP-0.1 (**Figure 2.2a,b**); this is attributed to the presence of LCB [10,29,30]. Moreover, PP-g-TAM demonstrated pronounced strain hardening under extensional deformation (**Figure 2.3**). In contrast, strain hardening was absent for PP-g-TMPTMA due to its lack of a significant LCB chain population.

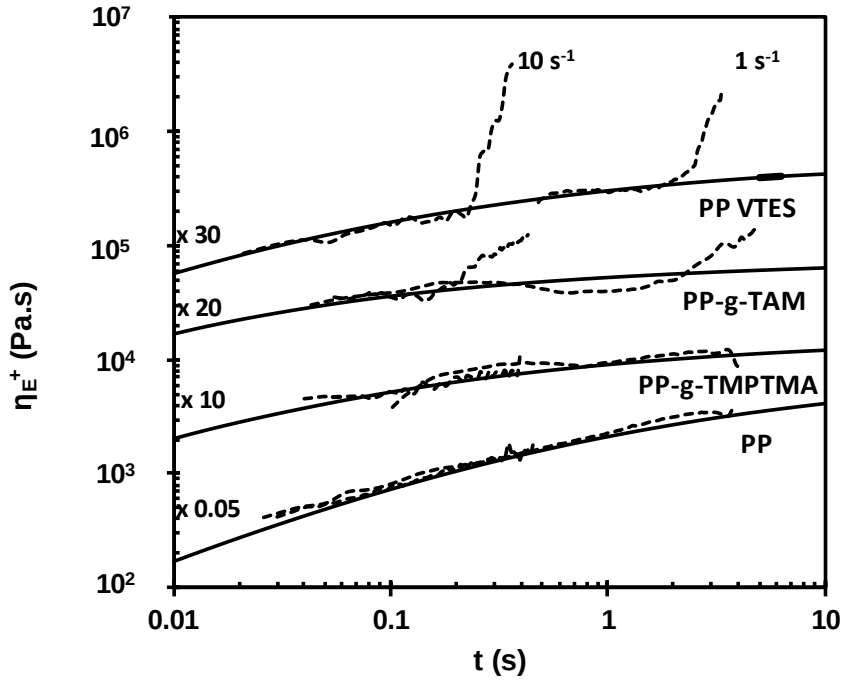

Figure 2.3 Tensile stress growth coefficient (η_E^+) as a function of time at Hencky strain rates of 1 and 10s^{-1}. Curves are shifted by an arbitrary factor for the sake of clarity. Solid lines represent the LVE envelope.

Although TAM and TMPTMA differ in terms of their ability to produce LCB, both coagents produced a population of cross-linked nanoparticles within their PP derivatives. This is easily recognized by the unaided eye from the creamy appearance of PP-g-TAM and PP-g-TMPTMA in their melt state, which results from scattering of light by a dispersed particle phase [23]. SEM images of particles isolated by extraction from a Soxhlet thimble (**Figures 2.4a,b**) and TEM images of microtomed PP-g-TMPTMA (**Figure 2.4c**) showed the dimension of these particles to be on the nanometer scale. The pronounced tendency of oligomerization of TMPTMA is revealed by the relatively higher amount of coagent-derived particles generated within the PP-g-TMPTMA material.

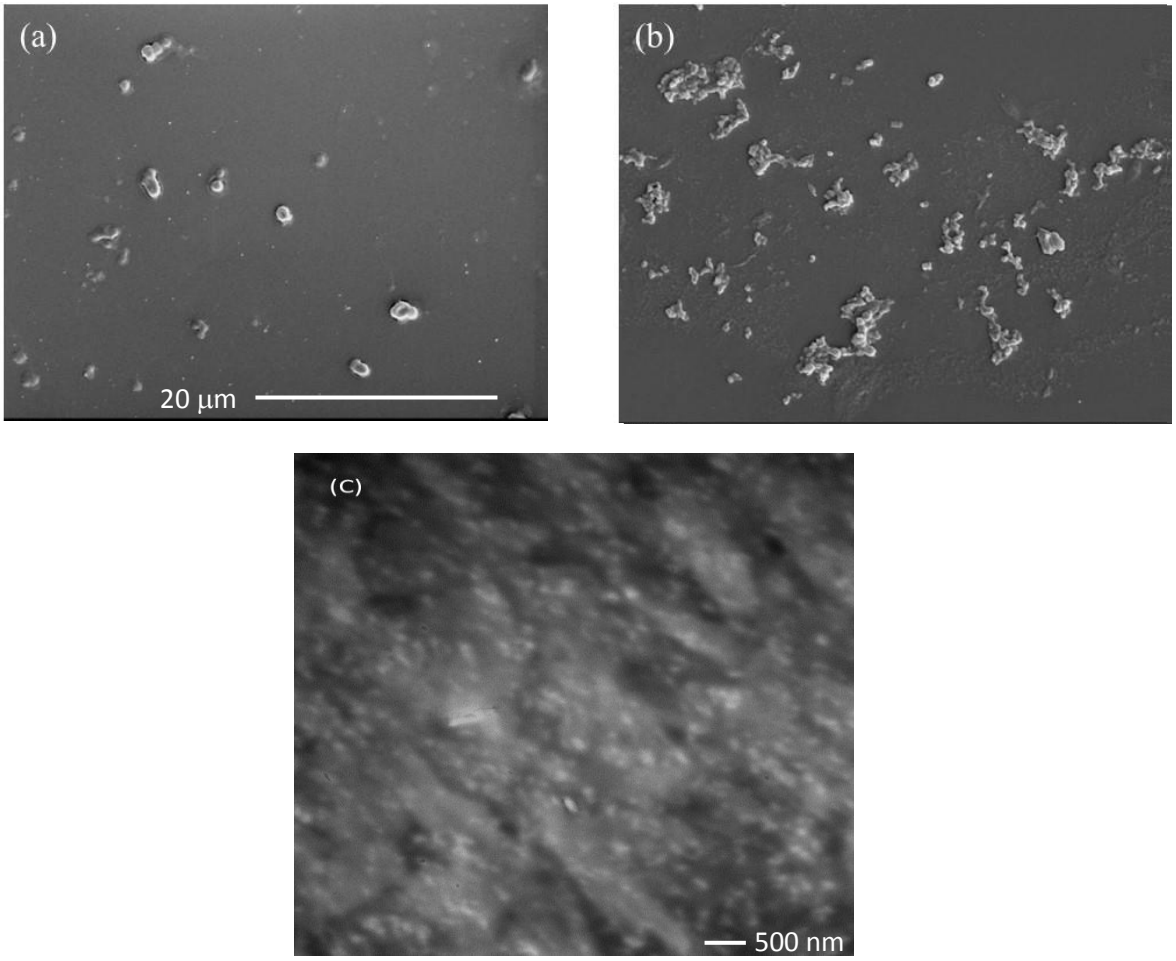

Figure 2.4 SEM images of particles isolated from (a) PP-g-TAM and (b) PP-g-TMPTMA; (c) TEM image showing particles generated in situ in PP-g-TMPTMA samples

Silane-modified LCB-PP

An alternate approach to the preparation of long chain branched materials involves the radical addition of a vinyltrialkoxysilane monomer to PP, followed by moisture-curing of pendant silane groups. This two-step process produces a more uniform branching distribution than coagent-based processes, and does not yield a dispersed particle phase [31]. As such, the PP-g-VTES-XL sample prepared and analyzed in this work served as a control material that contained no particles, but a substantial LCB content. The latter is evident from the enhanced shear thinning and elasticity (**Figure 2.2**), as well as extensive strain hardening characteristics (**Figure 2.3**) demonstrated by this reference material.

2.3.2 Crystallization Kinetics

The three classes of materials described above (linear, branched with particles, branched without particles) provide an opportunity to determine why LCB-PP materials demonstrate such a wide range of crystallization behaviour. **Table 2.2** provides a summary of phase transition data measured by non-isothermal crystallization studies of all six PP samples. Our peroxide treated materials, PP-DCP-0.1 and PP-DCP-0.3, responded in a manner that is consistent with literature reports on degraded PP, as they exhibited a double melting peak, lowered crystallization temperature, and depressed degree of crystallinity [17,32]. This is generally attributed to an increase in the number of chain ends, causing the formation of crystals with different levels of imperfections and structural defects.

Table 2.2 Melting points (T_m), crystallization points (T_c) and % crystallinity and crystallization half-times, recorded during non-isothermal crystallization experiments at a cooling a rate of 5°C.min^{-1}.

Sample	T_m (°C)	T_c onset (°C)	T_c peak (°C)	% Crystallinity	$t_{1/2}$ (min)
PP	163	121	118	47	2.3
PP-DCP-0.1	158/164	119	113	43	1.9
PP-DCP 0.3	154/163	118	113	43	1.9
PP-g-TAM	163	132	130	45	1.8
PP-g-TMPTMA	164	131	130	45	2.2
PP-g-VTES-XL	162	123	118	45	2.3

Both coagent-modified samples responded differently, with onset and peak crystallization temperatures exceeding those of the unmodified PP by 12°C, and those of the degraded PPs by 17°C (**Table 2.2** and **Figure 2.5**). The behaviour of PP-g-TMPTMA is particularly interesting, since it displayed a substantial enhancement in T_c while containing little, if any, long chain branching. On the other hand, the T_c of the highly branched sample, PP-g-VTES-XL, was not different from that of the linear PP parent material. This indicates that long chain branching alone cannot account for the unique crystallization dynamics generated by coagent-modified PP.

Shifts in the crystallization temperature in coagent modified PPs have been extensively reported in the literature [12, 14], but these reports may have potentially overlooked the formation of secondary, insoluble phases, such as gels, in coagent modified PPs. Kim et al.,[16] and more

recently Wan et al. and Zhang et al., [17, 18] alluded to the potential effects of gels, or other by-products stemming from the grafting reaction of the coagent. In the present work, in spite of the absence of gel, both PP-g-TAM and PP-g-TMPTMA contained a small population of cross-linked nanoparticles (**Figure 2.5**) whose dimensions are comparable to those of common nucleating agents [33,34] Given their nature, these particles may influence PP crystallization through heterogeneous nucleation that is independent of long chain branching effects. We suggest that the pronounced shifts in crystallization temperature for coagent modified PPs, which are often attributed to polymer branching, are actually due to heterogeneous nucleation by the cross-linked particle phase.

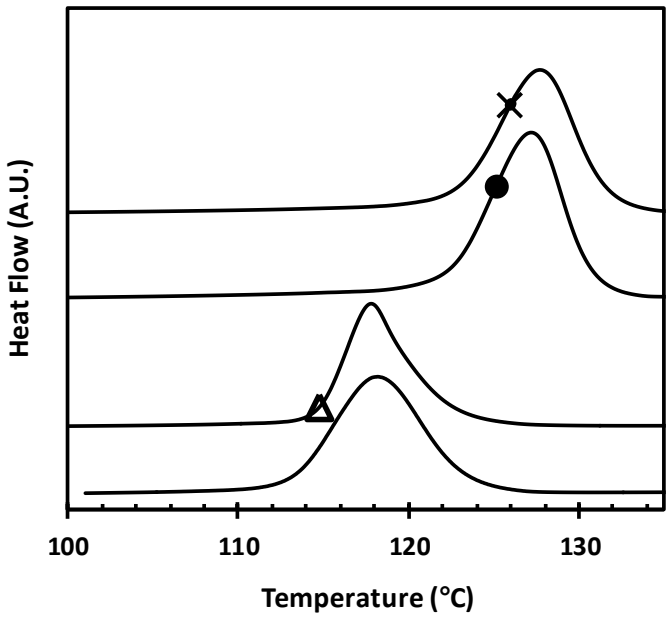

Figure 2.5 DSC exotherms for – L-PP; × PP-g-TMPTMA; ● PP-g-TAM and Δ PP-g-VTES-XL.

In spite of the significant difference in the onset temperature of crystallization, the crystallization half-times ($t_{1/2}$), defined as the time needed for the materials to reach relative crystallinity of 50%, remained relatively unaffected in non-isothermal kinetics experiments (**Table 2.2** and **Figure 2.6**).

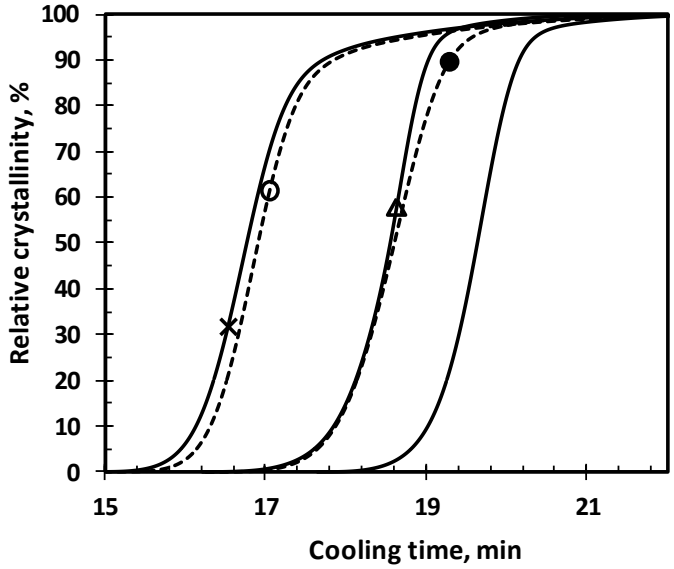

Figure 2.6 Relative crystallinity as a function of cooling time (time recorded from the start of the cooling cycle) obtained from non-isothermal studies at cooling rate of 5°C/min; ● PP, ×PP-g-TMPTMA, ○ PP-g-TAM, △ PP-g-VTES-XL and – PP-DCP 0.1. For comparison purposes, the x-axis depicts the time elapsed after the beginning of the cooling cycle.

Further insight into crystallization dynamics was gained from isothermal crystallization experiments. Plots of relative crystallinity as a function of time at 136°C revealed three distinct patterns (**Figure 2.7**). PP and its degraded derivative had a crystallization half-time on the order of 100 min. At this temperature, excessive chain mobility of linear PP inhibits the formation of stable nuclei, thereby resulting in a slow crystal growth rate.

The half-time of PP-g-TAM and PP-g-TMPTMA was an order of magnitude smaller, at 2.5 min (**Table 2.3**), consistent with the heterogeneous nucleation effects described above. It is interesting to note that PP-g-VTES-XL lied in between, at 54 min. The enhancement observed for this material is consistent with previous literature reports on the isothermal crystallization kinetics of branched polypropylene [12], and may be attributed to the presence of branching that restricts movement of the chains in the melt, thus generating a higher number of more stable nucleation sites. According to Wang et al.[35] the presence of long chain branching in polyolefins may affect the crystallization kinetics in opposing ways. Generally, longer branches and low levels of LCB tend to promote nucleation, whereas higher amounts of LCB result in entanglements, slowing down the rearrangement of chains and therefore the crystallization rate.

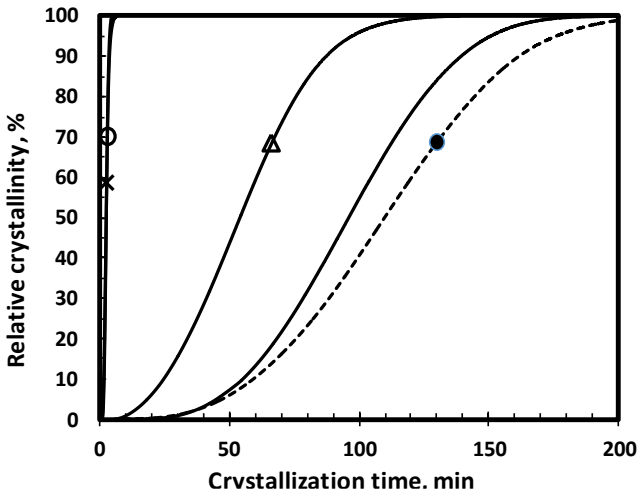

Figure 2.7 Evolution of relative crystallinity as a function of time obtained from isothermal crystallization experiments at 136°C, in which • PP, ×PP-g-TMPTMA, ○ PP-g-TAM, Δ PP-g-VTES-XL and – PP-DCP 0.1.

Pronounced differences in isothermal crystallization kinetics are also evident in the Avrami plots provided in **Figures 2.8a** and **b**. A linear region can be clearly identified for PP, PP-DCP 0.1 and PP-g-VTES-XL (**Figure 2.8a**), providing Avrami exponent values in the range of 3-3.5 for PP and PP-DCP 0.1 (**Table 2.3**). These are indicative of sporadic spherulitic crystal growth. The presence of extensive branching within PP-g-VTES-XL may have limited somewhat the direction of crystal growth, as suggested by the lower Avrami exponent recorded for this sample (**Table 2.3**).

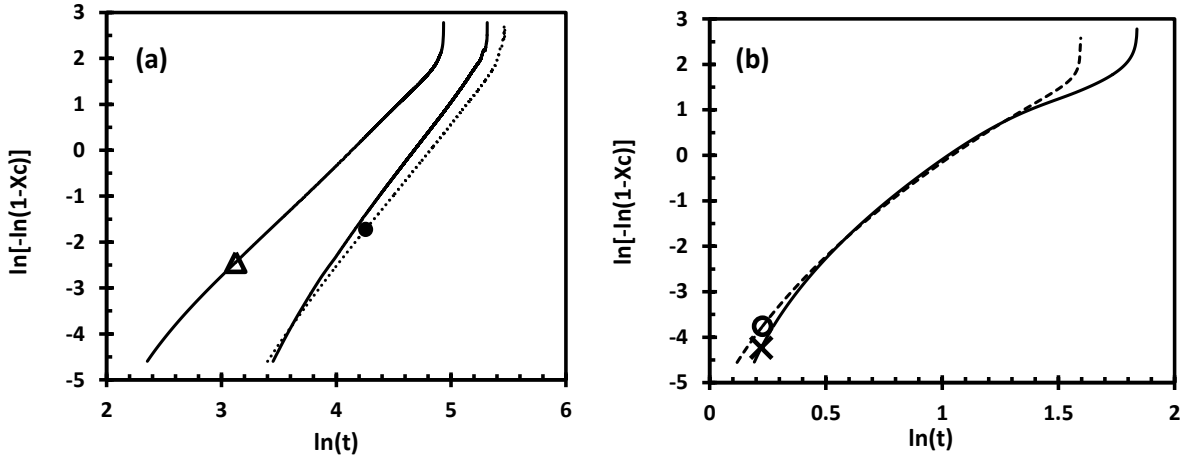

Figure 2.8 Avrami plots of isothermal crystallization at 136°C, (a) • PP, – PP-DCP 0.1, Δ PP-VTES ; (b) × PP-g-TMPTMA and ○- PP-g-TAM.

In contrast, a linear region could not be identified in the Avrami plots generated for coagent-modified PPs (**Figure 2.8b**). Non linearity in the Avrami plots, combined with exponents higher than 4, is consistent with transient nucleation [36] whose crystallization parameters are time-dependent [37]. This can occur when nucleation consists of instantaneous and spontaneous modes, as well as in composite systems [38] and suggests a complex crystallization pattern and different spherulitic development in the coagent-modified PPs. Furthermore, the values of the crystallization rate parameter, K, were much higher than those of the linear PPs, in the range of 0.35-0.39, depending on the region of the plot, for both coagent modified PPs, reflecting the much faster rate of nucleation and growth at this temperature.

Table 2.3 Avrami parameters and crystallization half-time for isothermal crystallization at 136°C of PP derivatives.

	PP	**PP-DCP 0.1**	**PP-g-TAM**	**PP-g-TMPTMA**	**PP-g-VTES-XL**
n	3.6	3.3	3.2-4.8	2.8-5	2.5
K, min^{-1}	0.009	0.009	0.35-0.38	0.35-0.39	0.016
$t_{1/2}$, min*	110	96	2.6	2.5	54

* $t_{1/2}$ has been calculated experimentally from isothermal experiments.

Direct evidence of differences in spherulitic development was gained by optical microscopy studies of isothermal crystallization (**Figure 2.9**). Linear PP materials displayed spherulitic structure that is typical of isotactic PP (**Figure 2.9a and b**). The PP-g-VTES-XL sample produced a similar pattern, with more nuclei formed slightly earlier, and a higher amount of spherulites forming within the time-frame of the experiment (**Figure 2.9e**).

The images presented in **Figure 2.9** (c and d) show that PP-g-TAM and PP-g-TMPTMA produced higher nucleation rates when compared to all the PP materials examined in this study. Moreover, the coagent-modified samples demonstrated entirely different crystal growth habits, as evidenced by repeated rapid branching along the axis of crystal formation. Because of the formation of a large quantity of nucleating sites, spherulite growth was restricted, eventually leading to smaller sizes and a grainy spherulitic structure. This type of spherulitic structure is likely responsible for improvements reported in the impact strength of coagent modified materials [6].

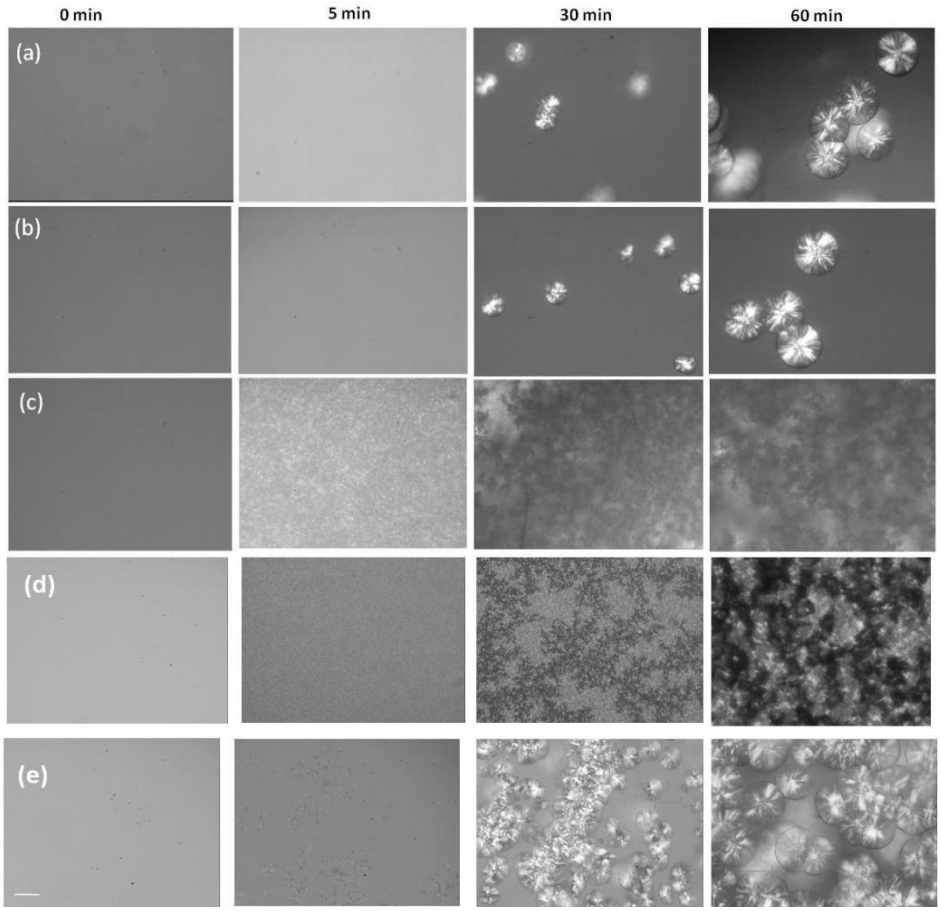

Figure 2.9 Hot stage microscopy of a) L-PP, b) PP DCP-0.1, c) PP-g-TMPTMA, d) PP-g-TAM, e) PP-g-VTES-XL at 140°C; the scale bar represents 60 microns.

Despite the clear differences in crystallization kinetics and spherulite size, the XRD patterns plotted in **Figure 2.10** show that all of our PP materials contained primarily monoclinic form α-crystals ((110), (040), (130), (111) and (131) planes, located at 2θ of 14.1, 16.9, 18.6, 21.1, 21.8 and 25.3° respectively) and small amounts of pseudohexagonal, β-crystals ((300) plane at 16.12°) [14,39,40].

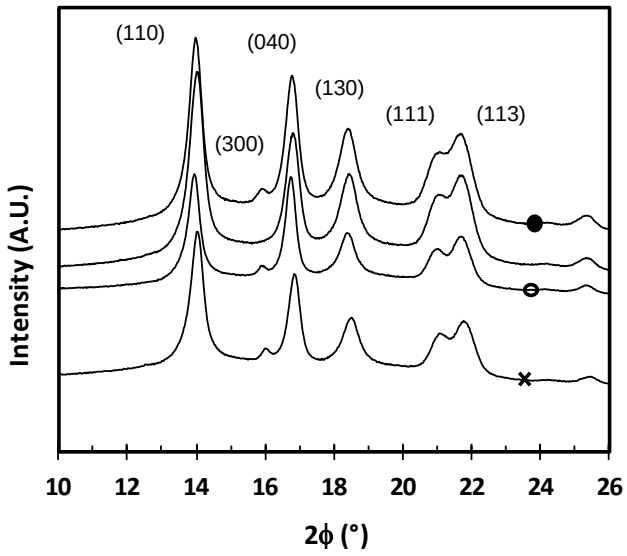

Figure 2.10 XRD patterns for PP and its derivatives. -•- PP, – PP-DCP 0.1, × PP-g-TMPTMA, ○ PP-g-TAM

Therefore, differences in crystallization between linear, branched and coagent-modified PPs lie in their crystallization peak temperature, crystallization kinetics and spherulitic structure, whereas the ultimate degree of crystallinity and crystalline structure remained similar. Improvements in the crystallization kinetics, and finer spherulitic structure are attributes typically associated with the addition of common nucleating agents [33,34,40,41].

These results suggest that even though these coagent modifications are typically used to improve melt strength, the enhancement in crystallization kinetics may be exploited in applications such as injection molding. Whereas controlled rheology polypropylenes generated by peroxide degradation are commonly used in injection molding processes, *in-situ* generation of the nucleating nanoparticles by peroxide-initiated coagent modification may provide the desired melt rheology as well as crystallization rates, without need for the addition of nucleating agents.

2.4 Conclusions

Four classes of PP samples with different architectures were prepared using a linear PP as the starting material. These included unmodified linear PP, peroxide degraded PP, coagent-modified LCB-PP prepared from TAM and TMPTMA, and LCB-PP synthesized by silane grafting and moisture curing chemistry. In addition to changing polymer chain architecture, these chemical modifications generated a small amount of well-dispersed, coagent-derived nanoparticles. When compared with the parent material and with PP samples treated with peroxide alone, coagent-modified materials demonstrated significantly higher crystallization temperatures. Furthermore it

was demonstrated that the cross-linked nanoparticle phase formed within coagent-modified PP is as efficient nucleating agent for crystallization, resulting in significantly higher onset crystallization temperatures, faster crystallization kinetics and a finer spherulitic structure. The influence of LCB on the crystallization behavior of polypropylene, while significant, is considerably weaker than the heterogeneous nucleation mechanism.

The next chapter of this thesis examines and differentiates the effects on crystallization kinetics of cross-linked particles dispersed throughout the PP material from those generated by LCB population. Also, the effect of coagent modification on foaming behavior of PP is thoroughly dealt with.

2.5 References

(1) Burt, J. G. The Elements of Expansion of Thermoplastics Part II. *J. Cell. Plast.* **1978**, *6*, 341-345.

(2) Passaglia, E.; Coiai, S.; Augier, S. Control of macromolecular architecture during the reactive functionalization in the melt of olefin polymers. *Prog. Polym. Sci.* **2009**, *9*, 911-947.

(3) Graebling, D. Synthesis of Branched Polypropylene by a Reactive Extrusion Process. *Macromolecules* **2002**, 35, 4602-4610.

(4) Parent, J. S.; Bodsworth, A.; Sengupta, S. S.; Kontopoulou, M.; Chaudhary, B. I.; Poche, D.; Cousteaux, S. Structure–rheology relationships of long-chain branched polypropylene: Comparative analysis of acrylic and allylic coagent chemistry. *Polymer* **2009**, *1*, 85-94.

(5) Borsig, E.; Van Duin, M.; Gotsis, A. D.; Picchioni, F. Long chain branching on linear polypropylene by solid state reactions. *Eur. Polym. J.* **2008**, *1*, 200-212.

(6) Zhao, W.; Huang, Y.; Liao, X.; Yang, Q. The molecular structure characteristics of long chain branched polypropylene and its effects on non-isothermal crystallization and mechanical properties. *Polymer* **2013**, *4*, 1455-1462.

(7) Kim,B.K.; Kim,K.J. Cross-Linking of polypropylene by peroxide and multifunctional monomer during reactive extrusion. *Adv. Polym. Tech.* **2003**, 12, 263-269.

(8) Wang,X.; Tzoganakis,C.; Rempel,G.L. Chemical Modification of Polypropylene with Peroxide/ Pentaerythritol Triacrylate by Reactive Extrusion. *J. Appl. Polym. Sci.* **1996**, 61, 1395-1404.

(9) Nam,G.J.; Yoo,J.H.; Lee,J.W. Effect of long-chain branches of polypropylene on rheological properties and foam-extrusion performances. *J. Appl. Polym. Sci.* **2005**, 96, 1793-1800.

(10) Gotsis, A. D.; Zeevenhoven, B. L. F.; Hogt, A. H. The effect of long chain branching on the processability of polypropylene in thermoforming. *Polym. Eng. Sci.*, **2004**, 44, 973-982.

(11) Mousavi-Saghandikolaei,S.A.; Frounchi,M.; Dadbin,S.; Augier,S.; Passaglia,E.; Ciardelli,F Modification of Isotactic Polypropylene by the Free-Radical Grafting of 1,1,1-Trimethylolpropane Trimethacrylate. *J. Appl. Polym. Sci.* **2006**, 2, 950-958.

(12) Tian,J.; Yu,W.; Zhou,C Crystallization behaviors of linear and long chain branched polypropylene. *J. Appl. Polym. Sci.* **2007**, *6*, 3592-3600.

(13) Agarwal, P. K.; Somani, R. H.; Weng, W.; Mehta, A.; Yang, L.; Ran, S.; Liu, L.; Hsiao, B. S. Shear-Induced Crystallization in Novel Long Chain Branched Polypropylenes by in Situ Rheo-SAXS and WAXD. *Macromolecules* **2003**, *14*, 5226-5235.

(14) Tian, J.; Yu, W.; Zhou, C. Crystallization Kinetics of Linear and Long-Chain Branched Polypropylene. *J. Macromol. Sci., Phys.* **2006**, *5*, 969-985.

(15) Yu, F.; Zhang, H.; Liao, R.; Zheng, H.; Yu, W.; Zhou, C. Flow induced crystallization of long chain branched polypropylenes under weak shear flow. *Eur. Polym. J.* **2009**, *7*, 2110-2118.
(16) Kim, J.; Seo, E.; Park, D.; Park, K.; Kang, S.; Lee, C.; Kim, S. Chemical modification of isotactic polypropylene by melt blending. *Fiber Polym* **2003**, *3*, 107-113.
(17) Wan, D.; Ma, L.; Xing, H.; Wang, L.; Zhang, Z.; Qiu, J.; Zhang, G.; Tang, T. Preparation and characterization of long chain branched polypropylene mediated by different heteroaromatic ring derivatives. *Polymer* **2013**, *2*, 639-651.
(18) Zhang, Z.; Wan, D.; Xing, H.; Zhang, Z.; Tan, H.; Wang, L.; Zheng, J.; An, Y.; Tang, T. A new grafting monomer for synthesizing long chain branched polypropylene through melt radical reaction. *Polymer* **2012**, *1*, 121-129.
(19) Weng, W.; Hu, W.; Dekmezian, A. H.; Ruff, C. J. Long Chain Branched Isotactic Polypropylene. *Macromolecules* **2002**, *10*, 3838-3843.
(20) Krause, B.; Voigt, D.; Huler, L.; Auhl, D.; Münstedt, H. Characterization of electron beam irradiated polypropylene: Influence of irradiation temperature on molecular and rheological properties. *J Appl Polym Sci* **2006**, *4*, 2770-2780.
(21) Wang, Z.; Wu, X.; Gui, Z.; Hu, Y.; Fan, W. Thermal and crystallization behavior of silane-crosslinked polypropylene. *Polym. Int.* **2005**, *2*, 442-447.
(22) Parent, J. S.; Sengupta, S. S.; Kaufman, M.; Chaudhary, B. I. Coagent-induced transformations of polypropylene microstructure: Evolution of bimodal architectures and cross-linked nano-particles. *Polymer* **2008**, *18*, 3884-3891.
(23) Wu, W.; Parent, J. S.; Sengupta, S. S.; Chaudhary, B. I. Preparation of Crosslinked Microspheres and Porous Solids from Hydrocarbon Solutions: A New Variation of Precipitation Polymerization Chemistry. *J Polym Sci A1* **2009**, *23*, 6561-6570.
(24) Ning, N.; Yin, Q.; Luo, F.; Zhang, Q.; Du, R.; Fu, Q. Crystallization behavior and mechanical properties of polypropylene/halloysite composites. *Polymer* **2007**, *25*, 7374-7384.
(25) Avrami, M. Kinetics of Phase Change. I General Theory. *J Chem Phys* **1979**, 7, 1103.
(26) Long, Y.; Shanks, R. A.; Stachurski, Z. H. Kinetics of polymer crystallisation. *Prog Polym Sci* **1995**, *4*, 651-701.
(27) Russell, K. E. Free radical graft polymerization and copolymerization at higher temperatures. *Prog Polym Sci* **2002**, *6*, 1007-1038.
(28) Moad, G. The synthesis of polyolefin graft copolymers by reactive extrusion. *Prog Polym Sci* **1999**, *1*, 81-142.

(29) Auhl, D.; Stange, J.; Münstedt, H.; Krause, B.; Voigt, D.; Lederer, A.; Lappan, U.; Lunkwitz, K. Long-chain branched polypropylenes by electron beam irradiation and their rheological properties. *Macromolecules* **2004**, *25*, 9465-9472.

(30) Tsenoglou, C.; Gotsis, A. Rheological characterization of long chain branching in a melt of evolving molecular architecture. *Macromolecules* **2001**, *14*, 4685-4687.

(31) El Mabrouk, K.; Parent, J. S.; Chaudhary, B. I.; Cong, R. Chemical modification of PP architecture: Strategies for introducing long-chain branching. *Polymer* **2009**, *23*, 5390-5397.

(32) Ryu, S. H.; Gogos, C. G.; Xanthos, M. Melting behaviour of controlled rheology polypropylene. *Polymer* **1991**, *13*, 2449-2455.

(33) Ferrage, E.; Martin, F.; Boudet, A.; Petit, S.; Fourty, G.; Jouffret, F.; Micoud, P.; De Parseval, P.; Salvi, S.; Bourgerette, C.; Ferret, J.; Saint-Gerard, Y.; Buratto, S.; Fortune, J. P. Talc as nucleating agent of polypropylene: morphology induced by lamellar particles addition and interface mineral-matrix modelization. *J. Mater. Sci.* **2002**, *8*, 1561-1573.

(34) Jang, G.; Cho, W.; Ha, C. Crystallization behavior of polypropylene with or without sodium benzoate as a nucleating agent. *J. Polym. Sci. B Polym. Phys.* **2001**, *10*, 1001-1016.

(35) Wang, L.; Wan, D.; Zhang, Z.; Liu, F.; Xing, H.; Wang, Y.; Tang, T. Synthesis and Structure–Property Relationships of Polypropylene-g-poly(ethylene-co-1-butene) Graft Copolymers with Well-Defined Long Chain Branched Molecular Structures. *Macromolecules* **2011**, *11*, 4167-4179.

(36) Sinha, I.; Mandal, R. K. Avrami exponent under transient and heterogeneous nucleation transformation conditions. *J. Non Cryst. Solids* **2011**, *3*, 919-925.

(37) Sajkiewicz, P. Transient and athermal effects in the crystallization of polymers. I. Isothermal crystallization. *J. Polym. Sci. B Polym. Phys.* **2002**, *17*, 1835-1849.

(38) Piorkowska, E.; Galeski, A.; Haudin, J. Critical assessment of overall crystallization kinetics theories and predictions. *Prog Polym Sci* **2006**, *6*, 549-575.

(39) Chen, J.; Tsai, F.; Nien, Y.; Yeh, P. Isothermal crystallization of isotactic polypropylene blended with low molecular weight atactic polypropylene. Part I. Thermal properties and morphology development. *Polymer* **2005**, *15*, 5680-5688.

(40) Kalaitzidou, K.; Fukushima, H.; Askeland, P.; Drzal, L. The nucleating effect of exfoliated graphite nanoplatelets and their influence on the crystal structure and electrical conductivity of polypropylene nanocomposites. *J. Mater. Sci.* **2008**, *8*, 2895-2907.

(41) Papageorgiou, D. G.; Papageorgiou, G. Z.; Bikiaris, D. N.; Chrissafis, K. Crystallization and melting of propylene–ethylene random copolymers. Homogeneous nucleation and β-nucleating agents. *Eur. Polym. J.* **2013**, *6*, 1577-1590.

Chapter 3

Crystallization and foaming of coagent-modified polypropylene: Nucleation effects of cross-linked nanoparticles*

3.1 Introduction

The chemical modification of linear, isotactic PP (L-PP) by peroxide-initiated grafting of coagents can provide long-chain branched derivatives with improved melt elasticity and extensional viscosity [1]. These solvent-free processes involve simultaneous chain scission and cross-linking, the balance of which controls the product's molecular weight and branching distributions [2,3]. In general, products derived from coagents bearing multiple acrylate, allylic or styrenic groups are comprised of a linear chain population of relatively low molecular weight, and a high molecular weight chain population containing a disproportionate amount of long chain branching. The effect of these microstructure changes on melt-state rheological properties are well documented, with several groups reporting losses in complex viscosity as well as enhanced elasticity and strain hardening characteristics [4-7]. However, only recently has the generation of cross-linked particles within coagent modified PP (CM-PP) been identified [8]. These nanoparticles are produced by a precipitation polymerization mechanism wherein coagent oligomerization yields adducts that are insoluble in the polymer melt, leading to the separation of a coagent-rich phase that cross-links to a very high extent [9]. As a result, CM-PP samples prepared by this chemistry can contain small, rigid particles that are well-dispersed throughout the polymer matrix.

A prime motivation for preparing CM-PP is to develop the extensional strain hardening characteristics needed to suppress cell coalescence during melt foaming processes. When compared to L-PP materials, CM-PP derivatives provide higher volume expansion ratios and more uniform cell sizes [4, 10]. These improvements to foam properties have, to date, been attributed to the melt state rheology, while the potential of coagent-rich nano-particles to affect the foaming of CM-PP has been overlooked. Similarly, significant differences in the crystallization behavior of linear and coagent-modified PP samples have been observed [4,11,12].

---

*A version of this chapter has been published: Ying Zhang, **Praphulla Tiwary**, J. Scott Parent, Marianna Kontopoulou, Chul B. Park, *Polymer*, **2013**, 54 (18), 4814-4819

Whereas branching in homogeneous polyethylenes is usually associated with lower crystallization rates and crystallinities [13, 14], CM-PP materials are reported to crystallize at higher temperatures. Knowledge of the origin of these differences is currently incomplete.

The present work involves the comparison of an isotactic L-PP with two of its derivatives: peroxide degraded PP (DCP-PP), and CM-PP modified with trimethylolpropane trimethacrylate (TMPTMA, Scheme 3.1) [11]. These materials are subjected to standard characterization techniques including molecular weight distribution as well as oscillatory shear and extensional rheometry. CM-PP is subjected to further analysis by FT-IR to confirm TMPTMA graft content, as well as SEM studies of the sub-micron particles dispersed throughout the sample. Careful studies of CM-PP crystallization and foaming are presented, with the objective of discerning the effect of coagent-rich nano-particles on phase nucleation phenomena. Further insight is gained through studies of L-PP compounds containing small amounts of independently synthesized coagent nano-particles.

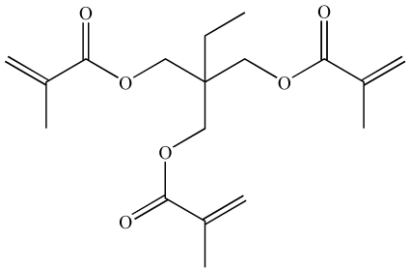

Scheme 3.1 Molecular structure of TMPTMA

3.2 Experimental

3.2.1 Materials and reactive modification

Trimethylolpropane trimethacrylate (TMPTMA, 98%) and dicumyl peroxide (DCP, 98%) were used as received from Sigma-Aldrich. ESCORENE™ PP 1042, an isotactic linear polypropylene homopolymer (L-PP) (MFR = 1.9 g/10 min), with a number average molecular weight (M_n) of 96 kg/mol and a weight average molecular weight (M_w), of 460 kg/mol, as determined by triple detector gel permeation chromatography (GPC), was obtained from ExxonMobil.

Peroxide-degraded PP (DCP-PP) was prepared by coating ground L-PP powder (40 g) with an acetone solution containing DCP (0.08 g, 296 μmole) and allowing the solvent to evaporate. The resulting mixture was charged to a Haake Polylab R600 internal batch mixer at 180°C at 60 rpm for 10 min, yielding DCP-PP with a M_n = 63.1 kg/mol and a M_w= 159 kg/mol. Coagent-modified PP (CM-PP) was synthesized as described for DCP-PP from a mixture of L-PP (40 g), DCP (0.08g, 296μmole) and TMPTMA (2.4g, 7.1mmole). The product had a M_n = 77.5 kg/mol and a M_w= 209

kg/mol. Gel content analysis was conducted by extraction into boiling xylenes from a 120 mesh stainless steel sieve for 6 hours, according to ASTM D 2765. Residual polymer was dried to constant weight, with gel contents reported as a weight percentage of unextracted material.

Isolation of particles from CM-PP was accomplished by hot xylenes extraction of the polymer from Soxhlet cellulose thimbles. Solvent was replaced every 3 hours, and after 10 hours no residual polymer could be recovered by precipitation from acetone. The thimble was cut into pieces, soaked in acetone and sonicated. The resulting dispersion was deposited onto glass slides, and coated with gold after solvent evaporation. A JEOL JSM-840 Scanning Electron Microscope (SEM) instrument was used to view the isolated particles.

Cross-linked particles were prepared according to the method proposed by Wu et al [9]. A homogeneous solution of dodecane (49.3 g, 290.3 mmol), TMPTMA (0.5 g, 1.5 mmol) and DCP (0.05 g, 0.2 mmol) was heated at 170°C for 10 min, cooled to room temperature and left standing for 12 hr to allow particles to settle. Residual liquid was decanted carefully from a minimal volume of suspended solids, a portion of which were deposited on a glass slide and dried under vacuum at 100°C for 12 hr. prior to SEM characterization. The total particle yield was 0.2 g (40% based on TMPTMA).

A L-PP based compound containing 1 wt. % TMPTMA particles was prepared as follows. L-PP (1 g) was dissolved in boiling xylenes (20 mL) before adding to a suspension of particles (0.2 g) in dodecane (10 mL). Residual dodecane and xylene were removed under vacuum at 100°C for 12hr, and the resulting masterbatch mixture (0.2 g) was mixed further with L-PP (2.8 g) using a DSM 5 ml microcompounder, equipped with co-rotating screws, and operating at 230°C and 150 rpm for 5 min.

3.2.2 Characterization

Molecular weight distributions were measured using a triple detector GPC (GPCIR by PolymerChar) at 145°C, employing 1,2,4-trichlorobenzene (TCB) as the mobile phase. Polymer samples were dissolved in TCB at a concentration of 1 mg mL^{-1} and held at 150 °C for 60 min. Samples with an injection volume of 200 µL were eluted through three linear Polymer Laboratories columns which were operated at a flow rate of 1 ml min^{-1}. The light scattering (LS) detector at 15° from the incident beam was used for molecular weight determinations.

FT-IR measurements were carried out in transmittance mode with an Avatar 360 FT-IR ESP spectrometer. Samples were purified by dissolving in boiling xylene and precipitating from acetone prior to drying under vacuum and melt pressing into thin films.

A controlled stress rheometer (ViscoTech by Rheologica) with parallel plate fixtures was used in the oscillatory mode at 180 °C with a gap of 1 mm under a nitrogen purge. Stress sweeps were used to ensure that measurements were made within the linear viscoelasticity region. Samples were further characterized in uniaxial extension using an SER-2 universal testing platform from Xpansion Instruments hosted on an MCR-501 Anton Paar rheometer [15]. Measurements were conducted at 170 °C at extension rates ranging from 0.010 to 10 s^{-1} under nitrogen purge.

Differential scanning calorimetry (DSC) was conducted using a DSC Q 100 by TA Instruments. Samples were scanned between -30 and 210 °C at a heating rate of 5 °C/min. After the first heating, each sample was held isothermally at 210 °C for 3 min before cooling at 5°C/min, to determine the crystallization onset and peak temperatures according to ASTM D3418.

Isothermal crystallization experiments were performed using a Linkam CSS 450 hot stage mounted on an Olympus BX51 optical microscope. Thin films were first heated to 200 °C at a rate of 30 °C /min and held for 10 minutes to eliminate their heat history. The melt was then cooled to 140 °C at 30 °C/min and the temperature was kept constant for 1 hour. The crystallization process was recorded using a Sony ExwaveHAD 3 CCD digital recorder.

3.2.3 Foaming visualization

Foaming visualization experiments, using N_2 as the blowing agent, were conducted using a batch foaming simulation system, consisting of a pressurized chamber equipped with a sapphire glass window, and a high speed camera/imaging system, at 180ºC at 203 MPa of N_2 [16]. Disks (7 mm diameter x 200 μm thickness) were heated to 180ºC at 203 MPa of N_2. The temperature and pressure in the simulation chamber were regulated using a thermostat and a syringe pump, respectively. A program based on Labview® was used to open the solenoid valve and record the pressure decay after the pressure within the chamber had been maintained for 30 minutes of saturation, while simultaneously, a high speed camera recorded the cell growth and collapse phenomena at 500 hundred frames per second. For each sample, at least three separate experiments were run, and the images were extracted using the Sigma Scan Pro Plus 6.0® image analysis software.

3.3 Results and Discussion

3.3.1 Material Characterization

Our investigation examined three materials, unmodified linear PP (L-PP) and two of its chemically modified derivatives, peroxide-degraded PP (DCP-PP), and coagent-modified PP (CM-PP). The parent material, L-PP, had a unimodal molecular weight distribution (**Figure 3.1a**) with

M_w = 460 kg/mole and a polydispersity of 4.8. Its melt-state rheological properties were typical of an unbranched polymer of relatively high molecular weight. Oscillatory shear rheometry demonstrated conventional shear thinning behavior (**Figure 3.1b**), while no evidence of strain hardening was observed when the sample was subjected to an extensional deformation (**Figure 3.1c**).

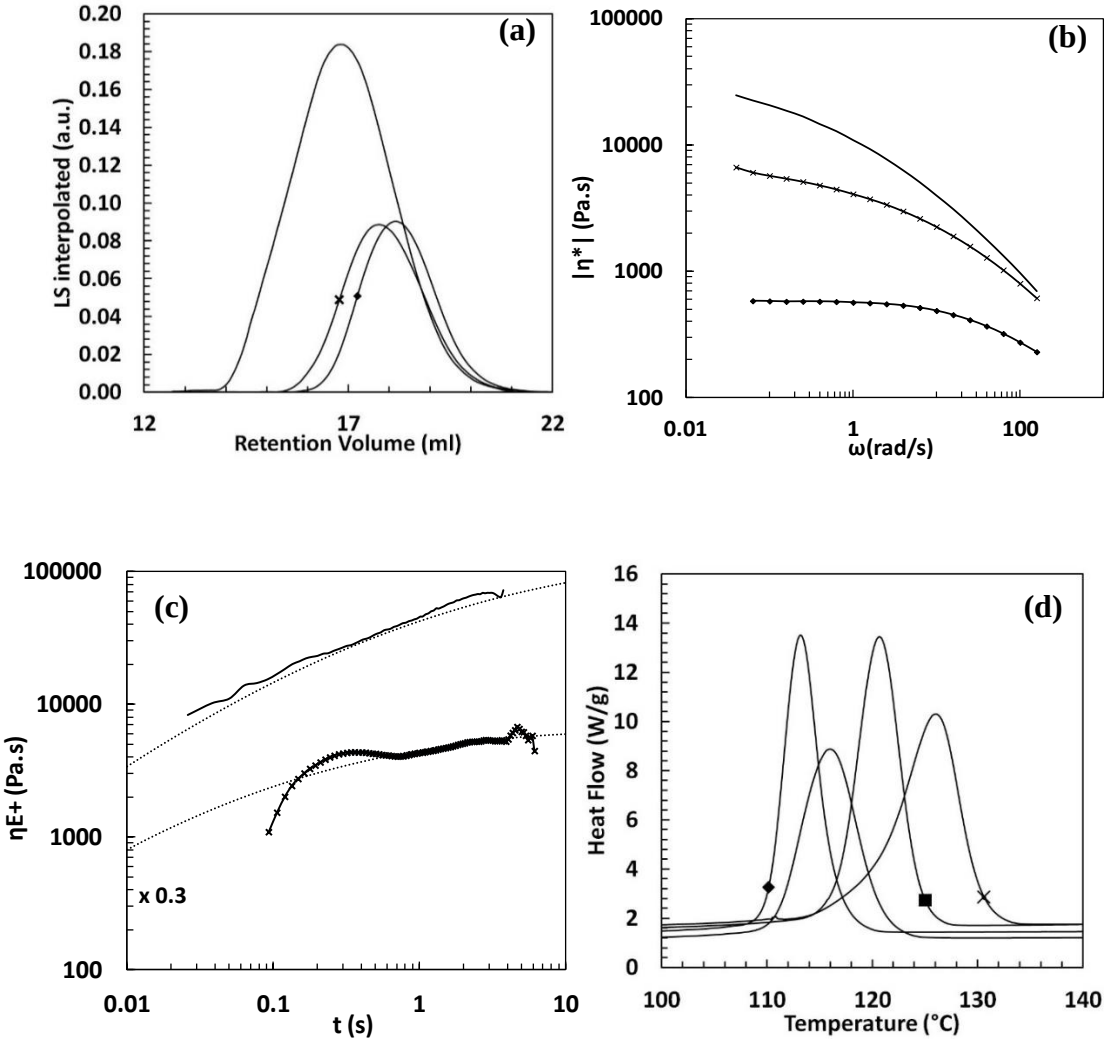

Figure 3.1 (a) GPC light scattering detector response profiles; (b) complex viscosity; (c) tensile stress growth coefficient at 1s-1 (ηE+). The dotted lines indicate the LVE envelope; (d) crystallization exotherms – L-PP; ◆ DCP-PP; ✕ CM-PP; ■ L-PP/ TMPTMA particles.

Treatment of PP with peroxide alone leads to a loss of molecular weight and a narrowing of the molecular weight distribution, as has been well documented for the production of "controlled rheology polypropylene" [17]. In the present case, the thermolysis of 0.2 wt. % of dicumyl peroxide

(DCP) in the starting material at 180 °C gave DCP-PP with M_w = 160 kg/mole and a polydispersity of 2.5. This loss of molecular weight substantially reduced the complex viscosity, while facilitating relaxation to yield a pronounced Newtonian plateau (**Figure 3.1b**). Note that the zero-shear viscosity of 587 Pa·s recorded for DCP-PP is below the threshold needed to support extensional viscosity analysis.

Both L-PP and DCP-PP are control samples for use in evaluating the properties of the coagent-modified derivative, CM-PP. Whereas most PP branching reactions are designed to maximize the extent of long chain branching, we sought a material containing a small branch content, but a significant particle concentration. As such, the influence of dispersed nano-particles could be examined without significant contribution from the rheological effects of a branched polymer chain population. To achieve this sample morphology, a relatively high concentration of trimethacrylate coagent was used. It is well known that acrylate-based coagents require small amounts of peroxide to achieve full C=C conversion, but their cross-linking efficiency is compromised by a pronounced tendency to homopolymerize [1]. The grafting efficiency of methacrylate-based systems is further compromised by allylic hydrogen atom abstraction from the monomer. These effects make TMPTMA a relatively poor choice for L-PP branching, but well-suited for the objectives of this work.

The CM-PP prepared by treating L-PP with 0.2 wt. % DCP and 6 wt. % TMPTMA had a M_w= 210 kg/mole and a polydispersity of 2.7. The light scattering (LS) detector response is a sensitive indicator of the presence of hyperbranched material, which typically generates a bimodal response with an intense peak at low retention volumes [8]. The LS response of our CM-PP (**Figure 3.1a**) showed no evidence of a hyperbranched population. Solvent extraction of the sample according to ASTM D 2765 did not recover a measurable gel fraction, indicating that the entire sample could escape from the 74 micron pores in the stainless steel mesh. FT-IR analysis of purified material revealed a significant carbonyl absorption derived from converted TMPTMA in the product. The higher M_w, coupled with the presence of some long chain branching, resulted in a significantly higher complex viscosity over DCP-PP (**Figure 3.1b**). However, branching within CM-PP was not sufficient to generate strain hardening characteristics under an extensional deformation (**Figure 3.1c**).

Although extraction of CM-PP from wire mesh did not isolate insoluble material, extraction from a Soxhlet thimble was capable of separating particles from most of the polymer matrix. An SEM image of the nano-particles separated by this technique is provided in **Figure 3.2a**. Note that these particles are similar in dimension to those observed previously for atactic-PP modified by DCP and triallyl trimesate, with average diameters on the order of 500 nm [8]. However, unlike

this previous work, particles were coated with insoluble material that could not be removed from the thimble. Therefore, we conclude that CM-PP contained a small amount of gel as well as a significant population of cross-linked particles.

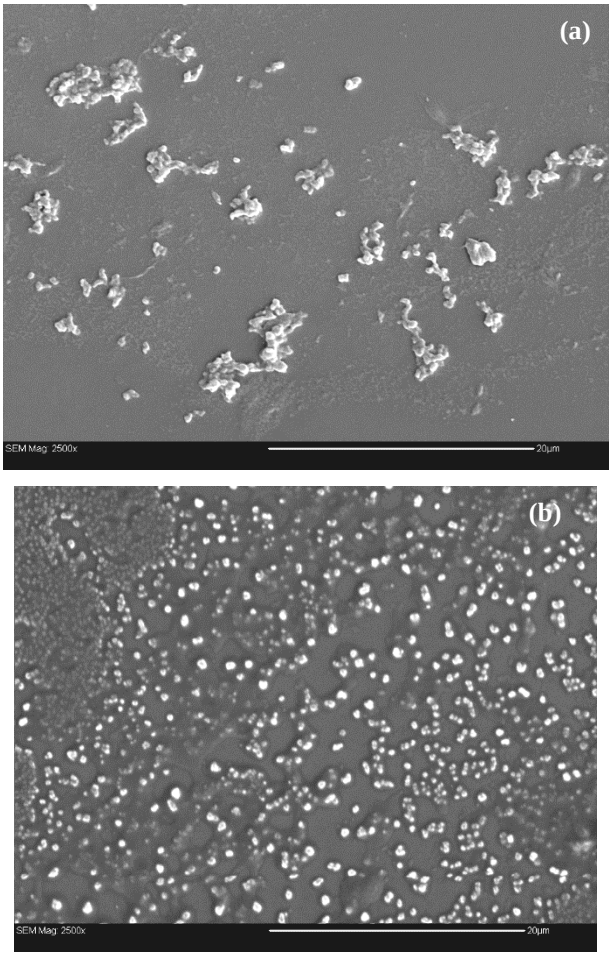

Figure 3.2 SEM image of (a) nanoparticles extracted from CM-PP; (b) TMPTMA particles.

3.3.2. Crystallization Behaviour

The potential for the dispersed solid phase within CM-PP to affect crystallization was examined through DSC studies and optical microscopy analyses. The crystallization exotherms illustrated in **Figure 3.1d** show that the onset of L-PP crystallization was at 122°C (crystallization peak temperature of 116°C), whereas CM-PP crystallization began at 132°C (fully 10°C higher than L-PP), with a peak temperature at 126 °C. Higher crystallization temperatures are not unique to our CM-PP material, as our finding is consistent with reports of other coagent-modified PP formulations [4,11,12]. However, the underlying cause of these shifts in coagent-modified PP crystallization temperatures has not been defined unambiguously.

Insight into the potential for coagent-rich particles to affect PP crystallization was gained by compounding L-PP with solids that were prepared separately. To facilitate the isolation of TMPTMA particles in high yield, they were prepared from dodecane solution as opposed to a PP matrix. Figure 3.2b provides an SEM image of these solids, which demonstrates the similarity of particle size and shape when compared to material isolated from an L-PP modification reaction (**Figure 3.2a**). When compounded into L-PP to give a 1 wt. % composite, these TMPTMA particles increased the onset of crystallization by 4°C, and the peak crystallization temperature of the polymer by 4.5°C compared to L-PP (Figure 3.1d). This suggests that coagent-rich nano-particles influence crystallization of L-PP by creating an enhanced heterogeneous nucleation effect. Their effect is not as dramatic as the shift seen in CM-PP, presumably due to differences in the amount of particles, as well as the different state of dispersion of the TMPTMA particles within L-PP, compared to the nanoparticles that are generated in-situ from a PP matrix during coagent modification.

Further evidence of the enhanced heterogeneous nucleation in CM-PP and in L-PP doped with TMPTMA particles was gained by optical microscopy studies of isothermal crystallization. The images presented in **Figure 3.3** show the advanced rate of spherulite formation in CM-PP and L-PP/ TMPTMA particles (**Figures 3.3(c) and (d)** respectively) relative to L-PP and DCP-PP (**Figures 3.3(a) and 3(b)** respectively), leading to significantly smaller spherulites in the coagent-modified sample (**Figure 3.3(c)**).

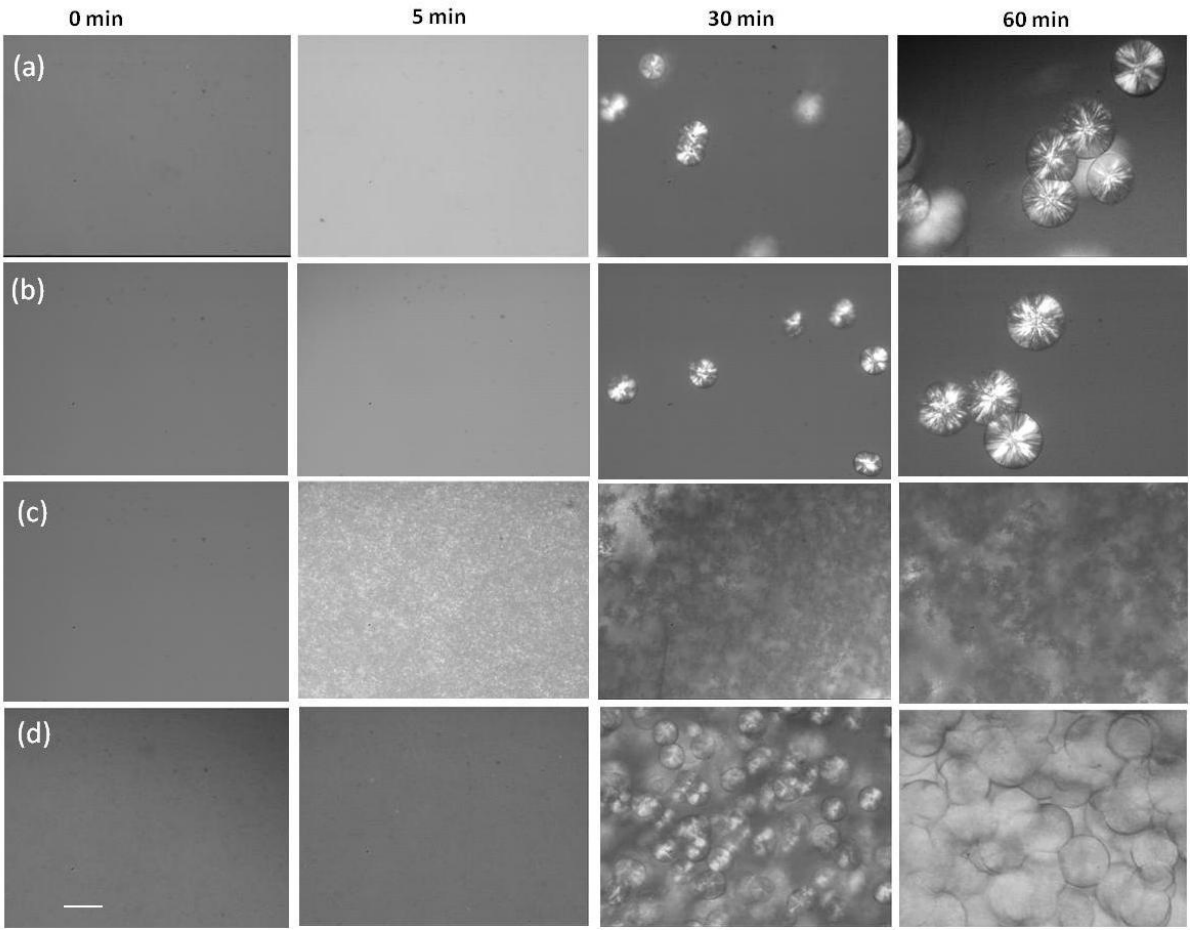

Figure 3.3 Optical microscope images of (a) L-PP; (b) DCP-PP; (c) CM-PP and (d) L-PP/ TMPTMA particles during isothermal crystallization at 140 °C. The scale bar represents 60µm.

We note that increases in crystallization temperature, crystallinity and crystallization rate are commonly observed in formulations containing small amounts (0.1 - 0.3 wt. %) of organic nucleating agents such as carboxylate salts [18] and sorbitol-based clarifiers [19]. Talc and other inorganic fillers provide similar effects, albeit at higher solids loading due to their lower nucleating efficiency [20, 21]. In the present context, the solid phase in our CM-PP material has dimensions that are consistent with common nucleating agents, and a defined interface between the melt-state and the cross-linked particle [21, 22]. The notion that nanoparticles formed during the coagent modification of PP affect crystallite nucleation has significant implications for material processing operations such as injection molding.

3.3.3 Foaming Behaviour

Given the importance of nucleation on foaming dynamics and final properties [23], the performance of CM-PP relative to L-PP and DCP-PP was investigated in a simple batch foaming process. The sequence of images shown in **Figure 3.4** reveals clear evidence of improved nucleation rates and cell densities in the coagent-modified material. Consistent with the enhanced nucleation effect reported in crystallization, we suggest that nanoparticles provide sites for heterogeneous nucleation in foaming, resulting in more efficient initial nucleation, as well as sustained cell nucleation throughout the foaming process, thereby providing foams of higher cell density.

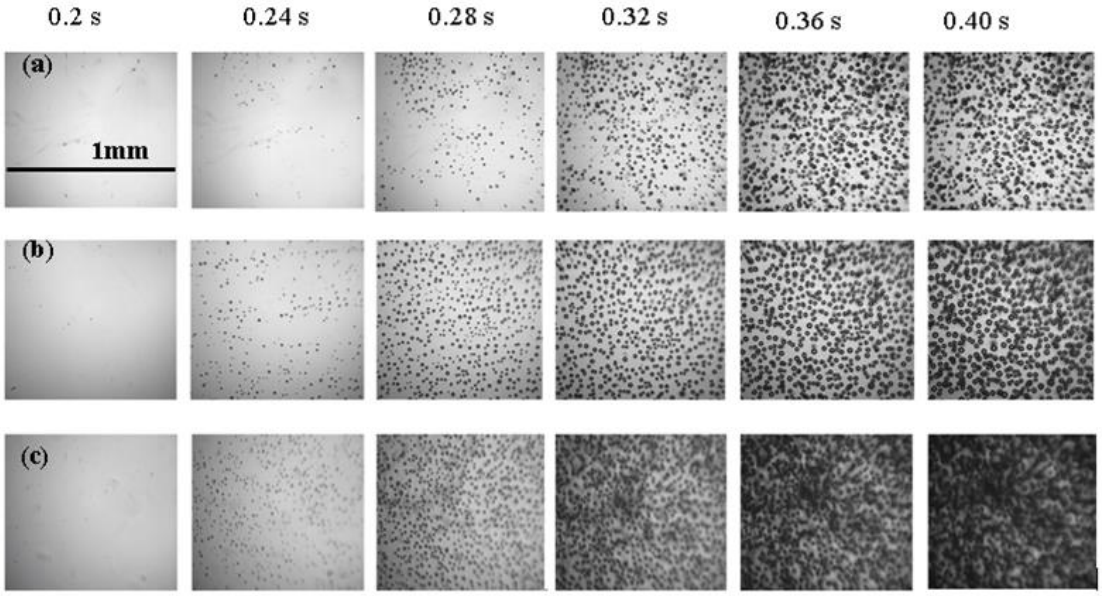

Figure 3.4 Images of cell nucleation sequence of (a) L-PP, (b) DCP-PP and (c) CM-PP.

3.4 Conclusions

Cross-linked nanoparticles generated *in situ* during coagent-modification of PP can serve as heterogeneous nucleation sites for crystallization from the melt, and for gas phase formation during batch foaming. Therefore, the performance of these materials is dictated not only by the rheological properties brought about by chemical modification, but also through the enhanced nucleation generated by the dispersed solid phase.

The findings presented in the chapter is expected to play a significant role in the structure-property characterizations. In the next chapter of the thesis, the detailed characterization of these coagent modified PPs are performed with special focus on thermal and mechanical properties.

3.5 References

[1] J.S. Parent, A. Bodsworth, S.S. Sengupta, M. Kontopoulou, B.I. Chaudhary, D. Poche, et al., Structure–rheology relationships of long-chain branched polypropylene: Comparative analysis of acrylic and allylic coagent chemistry, Polymer. 50 (2009) 85–94. doi:10.1016/j.polymer.2008.11.014.

[2] E. Passaglia, S. Coiai, S. Augier, Control of macromolecular architecture during the reactive functionalization in the melt of olefin polymers, Prog. Polym. Sci. 34 (2009) 911–947. doi:10.1016/j.progpolymsci.2009.04.008.

[3] G. Moad, The synthesis of polyolefin graft copolymers by reactive extrusion, Prog. Polym. Sci. 24 (1999) 81–142. doi:https://doi.org/10.1016/S0079-6700(98)00017-3.

[4] G.J. Nam, J.H. Yoo, J.W. Lee, Effect of long-chain branches of polypropylene on rheological properties and foam-extrusion performances, J. Appl. Polym. Sci. 96 (2005) 1793–1800. doi:10.1002/app.21619.

[5] E. Borsig, M. van Duin, a. D. Gotsis, F. Picchioni, Long chain branching on linear polypropylene by solid state reactions, Eur. Polym. J. 44 (2008) 200–212. doi:10.1016/j.eurpolymj.2007.10.008.

[6] B.K. Kim, K.J. Kim, Cross-linking of polypropylene by peroxide and multifunctional monomer during reactive extrusion, Adv. Polym. Technol. 12 (1993) 263–269. doi:10.1002/adv.1993.060120304.

[7] X. Wang, C. Tzoganakis, G.L. Rempel, Chemical modification of polypropylene with peroxide/pentaerythritol triacrylate by reactive extrusion, J. Appl. Polym. Sci. 61 (1996) 1395–1404. doi:10.1002/(SICI)1097-4628(19960822)61:8<1395::AID-APP21>3.0.CO;2-X.

[8] J.S. Parent, S.S. Sengupta, M. Kaufman, B.I. Chaudhary, Coagent-induced transformations of polypropylene microstructure: Evolution of bimodal architectures and cross-linked nano-particles, Polymer. 49 (2008) 3884–3891. doi:10.1016/j.polymer.2008.07.007.

[9] W. Wu, J.S. Parent, S.S. Sengupta, B.I. Chaudhary, Preparation of crosslinked microspheres and porous solids from hydrocarbon solutions: A new variation of precipitation polymerization chemistry, J. Polym. Sci. Part A Polym. Chem. 47 (2009) 6561–6570. doi:10.1002/pola.23699.

[10] M. Frounchi, a. Sharif-Pakdaman, S. a. Mousavi, S. Dadbin, Polypropylene Foaming in a Reactive Process, J. Cell. Plast. 43 (2007) 445–458. doi:10.1177/0021955X07079368.

[11] S.A. Mousavi-Saghandikolaei, M. Frounchi, S. Dadbin, S. Augier, E. Passaglia, F. Ciardelli, Modification of isotactic polypropylene by the free-radical grafting of 1,1,1-trimethylolpropane trimethacrylate, J. Appl. Polym. Sci. 104 (2007) 950–958. doi:10.1002/app.25796.

[12] J. Tian, W. Yu, C. Zhou, Crystallization behaviors of linear and long chain branched polypropylene, J. Appl. Polym. Sci. 104 (2007) 3592–3600. doi:10.1002/app.26024.

[13] I.S. Kolesov, R. Androsch, H.J. Radusch, Non-isothermal crystallization of polyethylenes as function of cooling rate and concentration of short chain branches, J. Therm. Anal. Calorim. 78 (2004) 885–895. doi:10.1007/s10973-004-0455-y.

[14] B. Yang, M. Yang, W.-J. Wang, S. Zhu, Effect of long chain branching on nonisothermal crystallization behavior of polyethylenes synthesized with constrained geometry catalyst, Polym. Eng. Sci. 52 (2012) 21–34. doi:10.1002/pen.22040.

[15] M. Sentmanat, E.B. Muliawan, S.G. Hatzikiriakos, Fingerprinting the processing behavior of polyethylenes from transient extensional flow and peel experiments in the melt state, Rheol. Acta. 44 (2004) 1–15. doi:10.1007/s00397-004-0398-z.

[16] Q. Guo, J. Wang, C.B. Park, M. Ohshima, A microcellular foaming simulation system with

a high pressure-drop rate, Ind. Eng. Chem. Res. 45 (2006) 6153–6161. doi:10.1021/ie060105w.
[17] C. Tzoganakis, J. Vlachopoulos, A.E. Hamielec, Production of controlled-rheology polypropylene resins by peroxide promoted degradation during extrusion, Polym. Eng. Sci. 28 (1988) 170–180.
[18] M. Blomenhofer, S. Ganzleben, D. Hanft, H.W. Schmidt, M. Kristiansen, P. Smith, et al., "Designer" nucleating agents for polypropylene, Macromolecules. 38 (2005) 3688–3695. doi:10.1021/ma0473317.
[19] K. Hoffmann, G. Huber, D. Mäder, Nucleating and clarifying agents for polyolefins, Macromol. Symp. 176 (2001) 83–92. doi:10.1002/1521-3900(200112)176:1<83::AID-MASY83>3.0.CO;2-N.
[20] D. Libster, A. Aserin, N. Garti, Advanced nucleating agents for polypropylene, Polym. Adv. Technol. 18 (2007) 685–695. doi:10.1002/pat.970.
[21] E. Ferrage, F. Martin, A. Boudet, S. Petit, G. Fourty, F. Jouffret, et al., Talc as nucleating agent of polypropylene: morphology induced by lamellar particles addition and interface mineral-matrix modelization, J. Mater. Sci. 37 (2002) 1561–1573. doi:10.1023/A:1014929121367.
[22] G.-S. Jang, W.-J. Cho, C.-S. Ha, Crystallization behavior of polypropylene with or without sodium benzoate as a nucleating agent, J. Polym. Sci. Part B Polym. Phys. 39 (2001) 1001–1016. doi:10.1002/polb.1077.
[23] J.W.S. Lee, C.B. Park, S.G. Kim, Reducing Material Costs with Microcellular/Fine-celled Foaming, J. Cell. Plast. 43 (2007) 297–312. doi:10.1177/0021955X07077601.

Chapter 4

Coagent Modified Polypropylene Prepared by Reactive Extrusion: A New Look into the Structure-Property Relations of Injection Molded Parts*

4.1 Introduction

Isotactic polypropylene (PP) is valued in engineering and commodity applications for its high stiffness, chemical and thermal resistance and low cost. To make PP more conducive to a wider variety of processing techniques, such as injection molding, thermoforming, film and foam extrusion, a variety of modification techniques are used in industry. Peroxide-assisted reactive extrusion is widely used to prepare controlled-rheology PP [1–4] having low molar mass, narrow molar mass distribution and thus suitable rheological properties for injection molding applications. Nucleating agents, such as sorbitol and sodium benzoate [5,6] are commonly used to improve the crystallization kinetics and to alter the crystalline structure of the polymer. Cheap fillers, such as talc are effective in improving crystallization rate and modulus, while reducing material costs, but may have detrimental effects on ductility and impact strength.

PP homopolymer produced by Ziegler-Natta polymerization typically has a linear architecture. This results in low melt strength, which limits the utility of PP in processes that involve extensional flow, such as foaming, thermoforming and film extrusion [7,8]. Peroxide-initiated graft-modification in the presence of multifunctional coagents [3,9] leads to the introduction of long chain branching (LCB), causing significant improvements in melt strength, as confirmed by various rheological studies [10–15]. In addition to altering the melt-state rheological properties, coagent modification has been reported to increase the crystallization temperature and/or degree of crystallinity of PP [9,14,16,17]. Furthermore, it has been demonstrated that these materials may contain small amounts of well-dispersed, rigid sub-micron sized particles derived from coagent oligomerization [18]. In the previous chapters we have shown that these particles may influence the rheology of these materials, but most importantly they act as nucleating agents and cause significant increases in the crystallization temperature, as well as enhancements in the

---

*A version of this chapter has been published: **Praphulla Tiwary**, Hua Gui, Pedro Luiz Ferreira, Marianna Kontopoulou, International Polymer Processing, 2016, 31 (4), 433-441.

crystallization kinetics of CM-PP. Additionally CM-PP exhibited a finer and denser spherulitic structure. It is well known that molar mass, molar mass distribution, chain branching and crystalline structure affect the macroscopic mechanical properties of PP [19]. It is therefore intuitive that the changes in the architecture, crystalline structure and crystallization kinetics should have a pronounced effect on the mechanical properties of injection molded CM-PP. Even though a great deal of literature exists on the CM-PP, this manuscript examines for the first time the effect of coagent modification on the various physical properties of injection molded specimens, in light of our findings in last two chapters of this thesis that reactive modification of PP not only influences the rheological properties, but also yields a matrix which contains uniformly dispersed in-situ generated coagent-rich nanoparticles, which induce an enhanced nucleation effect.

4.2. Experimental

4.2.1 Materials

Polypropylene, Pro-fax® 6523 (Melt flow rate (MFR) = 4 g/ 10 min @ 230°C, general purpose extrusion grade) was obtained from LyondellBasell. Triallyl trimesate (TAM, 98%) was purchased from Monomer Polymer and Dajac labs Inc. Trimethylolpropane trimethacrylate (TMPTMA, 98%), and dicumyl peroxide (DCP, 98%) were purchased from Sigma-Aldrich. All reagents were used as received.

4.2.2 Reactive extrusion

Reactive extrusion was conducted in a Coperion ZSK 18 ML twin screw co-rotating extruder equipped with a strand die, water cooling bath, and pelletizer, using the screw design shown in Figure 5.1. The temperature profile was 160/180/180/190/200/200/210 °C (feed to die). The extrusion was performed at a feeder RPM of 60 with a screw RPM of 120 (average throughput: 0.54 kg/ hr), and average residence time of 3 min 50 sec, to allow for the complete reaction of PP with various amounts of DCP and coagents. The detailed formulations are shown in Table 4.1.

Figure 4.1 Screw design used in reactive extrusion (left most is the feed port)

Table 4.1 Formulations and rheological properties

	DCP (phr)	TAM (phr)	TMPTMA (phr)	η* (Pa.s)	λ (s)
L-PP	0	0	0	15,900	21.6
0.1DCP	0.1	0	0	350	1.3
0.1/ 1.5 TAM	0.1	1.5	0	700	4.3
0.1/1.5 TMPTMA	0.1	0	1.5	1,050	5.6
0.3/ 6 TAM	0.3	6	0	1,050	12.3
0.3/6 TMPTMA	0.3	0	6	1,700	11.5

phr – Parts per hundred resin, η* – complex viscosity at 0.1 rad s^{-1}, λ - relaxation time at frequency of 0.1 rad s^{-1}, calculated from equation (1).

4.2.3 Gel content analysis and gel permeation chromatography (GPC)

Gel content analysis, conducted by extraction into boiling xylenes from a 120 mesh stainless steel sieve for 6 hours, according to ASTM D 2765 revealed that all the samples were gel free. High temperature gel permeation chromatography (GPC) was performed in an Agilent Cirrus multi-detector GPC at 150°C and solvent flow rate of 1 $ml.min^{-1}$. The samples were dissolved in trichlorobenzene (TCB) at a concentration of 0.1 $mg.ml^{-1}$ and stabilized with 0.0125 % butyrated hydroxytoluene.

4.2.4 Injection molding

Injection molding was done in a Nissei ES 200 ELJECT injection molder with a fixed mold temperature of 25°C and mold cooling time of 30 s. The injection pressure was set to 1000 psi with an injection speed of 30 $mm.min^{-1}$. The temperature of the injection molding machine was kept constant to 190 °C, from hopper to nozzle.

4.2.5 Mechanical testing

Tensile tests were performed in an Instron 3369 universal testing machine equipped with 50 N load cell. Tensile tests were done on injection molded samples according to ASTM D 638 (type IV sample, cross head speed of 50 $mm.min^{-1}$). An impact tester from Satec System Inc. equipped with

a 7 lbs. hammer was used to perform notched Izod test according to ASTM D 256. A Qualitest notch cutter was used to make the notch. All the mechanical tests were done after 48 hours of molding.

4.2.6 Optical microscopy

A Leica microtome was used to prepare 30 μm – thick sections from the injection molded Izod samples. These sections were observed under an Olympus BX51 polarized optical microscope equipped with cross polarizers.

4.2.7 Differential scanning calorimetry (DSC)

Differential scanning calorimetry was conducted using a DSC Q1000 by TA instruments. Thermal cycles were performed between -30 to 210°C, at heating and cooling rates of 5°C.min^{-1}. After the first heating scan, the samples were held isothermally at 210°C for 3 min before cooling at 5°C.min^{-1} to -30°C, to determine the peak crystallization temperatures according to ASTM D3418. The heats of fusion and melting temperatures were determined from the melting endotherm obtained from the first heating scan, to better reflect the thermal history of the samples. Two sets of measurements were performed on thin sections obtained from the skin layer of injection molded specimens, and from the bulk "core" layer.

4.2.8 Rheological characterization

A controlled stress rheometer, ViscoTech by Rheologica, with 20-mm parallel plate fixtures was used in the oscillatory mode with a gap of 1 mm to measure the linear viscoelastic properties at 180°C. Stress sweeps were conducted to ensure that the measurements were within the linear viscoelastic region.

Samples were further characterized in a uniaxial testing platform from Xpansion instruments hosted on a MCR-301 Anton Paar rheometer [20] The measurements were conducted at 170°C at an extension rate of 1 s^{-1}. The linear viscoelastic (LVE) oscillatory measurements obtained at 170 °C were used to calculate the LVE stress growth curve, η^+, and to check the consistency of the extensional measurements. The curve corresponding to $3\eta^+$ represents the LVE envelope in uniaxial extension, according to Trouton's law.

4.3. Results and Discussion

4.3.1 Rheological Characterization

The starting material was a commercial grade linear PP (L-PP) homopolymer with weight-average molar mass (M_w) of 340 kg.mol^{-1} and dispersity (D) of 5, as determined by GPC. Reaction of L-PP with 0.1 phr DCP produced DCP-PP (sample 0.1 DCP) with reduced M_w and narrower dispersity (M_w=170 kg.mol^{-1} and D=3.6), due to degradation attributed to β-scission of tertiary alkyl radical intermediates. This translated to significantly lower viscosity compared to the original L-PP, as shown in Figure 4.2a. The linear architecture of DCP-PP is confirmed by the presence of a pronounced Newtonian plateau (**Figure 4.2a**), the terminal slope of 2 in the elastic modulus vs. frequency curves (**Figure 4.2b**), and the Van Gurp-Palmen plot (**Figure 4.3**), which shows that the phase angle tends to the limit of 90°.

Radical addition and hydrogen transfer reactions involving a coagent decrease the population of PP backbone macroradicals, thereby suppressing β-scission of tertiary alkyl radical intermediates [21]. Therefore all CM-PPs had higher viscosities, compared to DCP-PP (**Figure 4.2(a)**), and longer terminal relaxation times, λ, as calculated by equation (1) [22].

$$\lambda = \frac{G'}{\omega\, G''} \qquad (1)$$

where G′ is storage modulus and G′′ is loss modulus at the given frequency of ω (rad/s). The rheological properties are summarized in **Table 4.1**.

The viscosities of all CM-PPs remained significantly lower than those of the parent L-PP material, indicating that vis-breaking due to β-chain scission was still dominant. The highly modified 0.3/6 TMPTMA had the highest molar mass among the CM-PP samples (M_w=199 kg.mol^{-1}, D=3.3), and consequently the highest viscosity (**Table 4.1** and **Figure 4.1(a)**). It should be noted that in all cases extraction of coagent modified PP from wire mesh did not isolate insoluble material, therefore excluding the presence of gels that would affect these results.

PP modified with the highest amounts of DCP and TAM showed unique behaviour among the CM-PPs. Specifically, the 0.3 DCP/6 TAM sample exhibited a significant upturn in zero shear viscosity, with loss of the Newtonian plateau, pronounced shear thinning, and deviation from terminal flow (**Figures 4.2a and b**). The latter is more obvious in the Van Gurp-Palmen plot, shown in **Figure 4.3**. It should be noted that at high frequencies the values of the complex viscosity of this sample approached those of the 0.1 DCP material, indicative of a highly degraded matrix (having M_n =158 kg.mol^{-1} and D =4), whereas the upturn of the complex viscosity at low frequencies

represents a highly-branched, or hyperbranched fraction [10]. We have demonstrated previously that the graft modification of PP with TAM coagent proceeds efficiently to yield a hyper-branched chain population and that the resulting products have bimodal molecular weight and branch distribution [23].

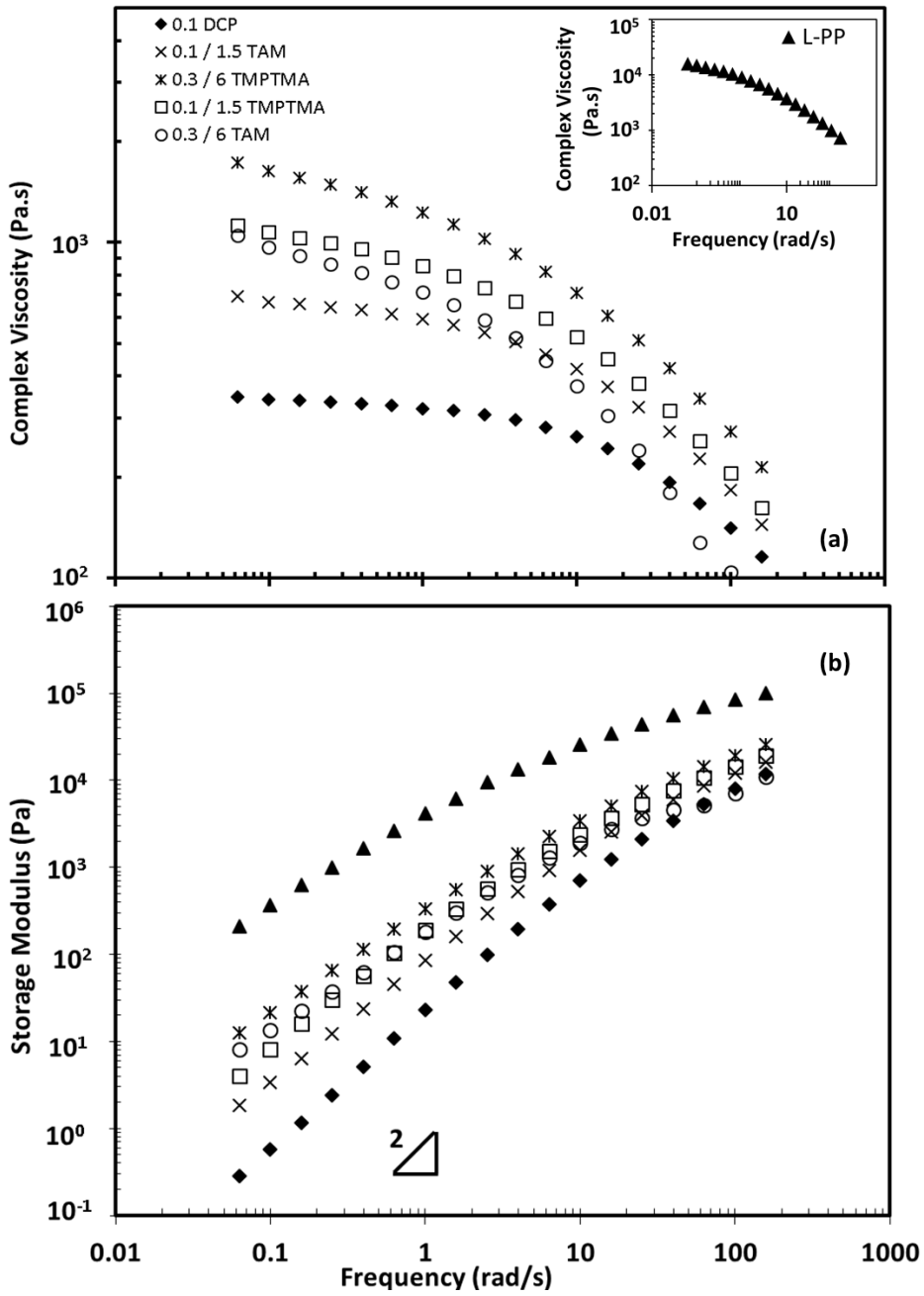

Figure 4.2 (a) Complex viscosity and (b) storage modulus of L-PP, DCP-PP and CM-PPs as a function of angular frequency at 180°C.

The GPC results shown in **Figure 4.4** confirmed the presence of such bimodality in the highly-modified 0.3 DCP/6 TAM only. The presence of strain hardening under extensional deformation provides further evidence of branching in this sample only (**Figure 4.5**).

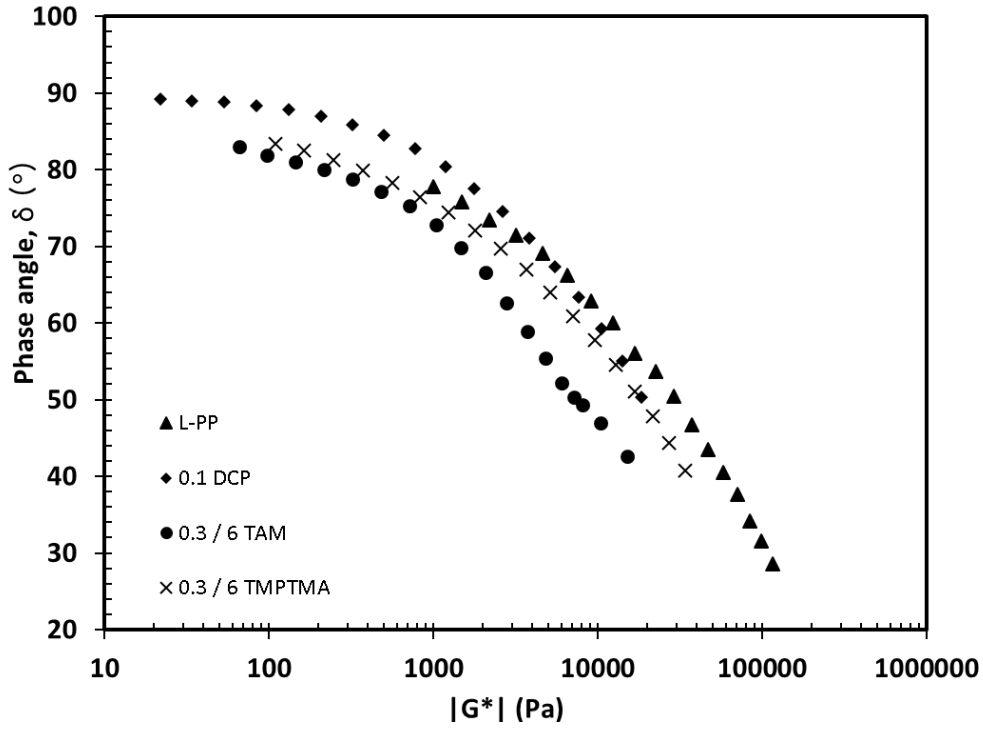

Figure 4.3 Van Gurp-Palmen plot at 180°C L-PP, DCP-PP and selected CM-PPs.

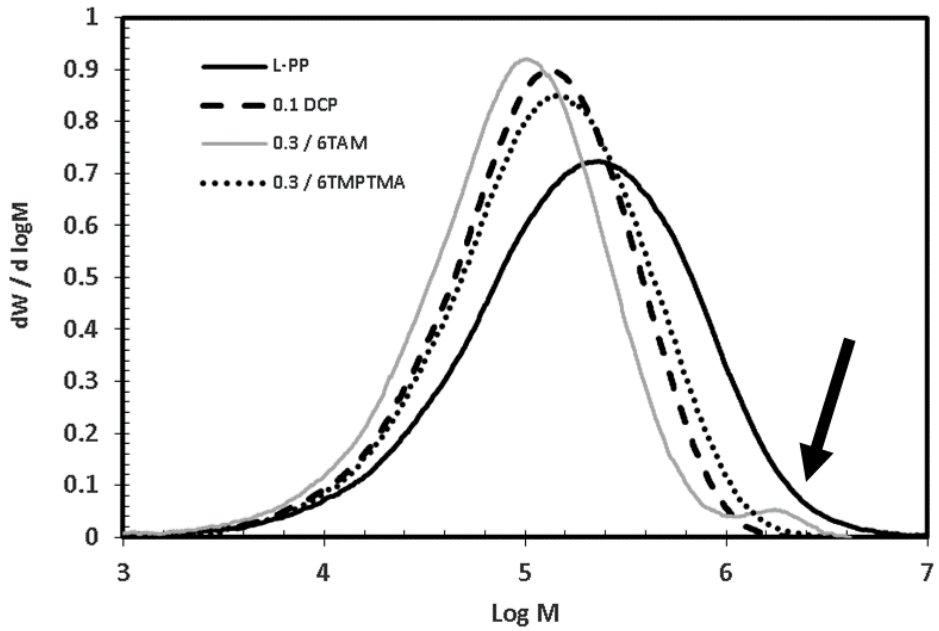

Figure 4.4 Molecular weight distribution of L-PP, DCP-PP and selected CM-PPs.

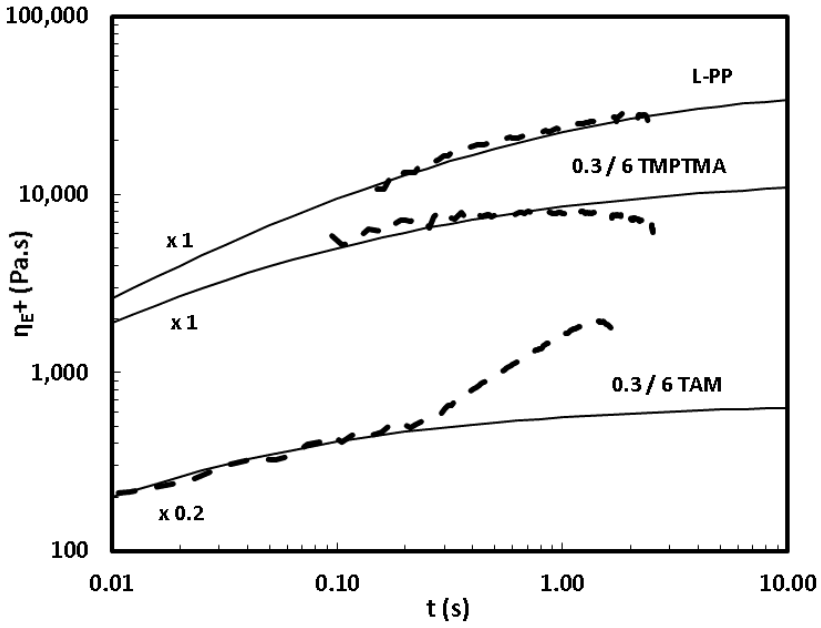

Figure 4.5 Tensile stress growth coefficient (ηE+) of L-PP and CM-PPs as a function of strain rate and time at a Hencky strain rate of 1s-1. Curves are shifted by an arbitrary factor for the sake of clarity. Solid lines represent the LVE envelope at 170°C.

4.3.2. Thermal properties and crystalline structure of the skin and core layers

The existence of temperature gradients inside the injection mold [24], and consequently the differences in cooling and crystallization rates within the thickness of the polymer [25] result in the formation of a skin-core structure in injection molded products [19,26–28]. The presence of skin and core layers with a thick skin layer, approximately 72 μm wide is clearly seen in the injection molded L-PP specimens (**Figure 4.6(a)**). Typical PP spherulitic structure is evident in Figure 4.7(a) obtained from the core layer of these samples. On the contrary the skin, which crystallizes faster because of its proximity to the mold walls, consists of much smaller and denser spherulites.

Examination of the heats of fusion obtained during the first DSC heating scan (**Table 4.2**) confirmed that the heat of fusion of the skin layer was lower, indicative of lower crystallinity compared to the core layer, because of the rapid cooling of the portion of the material that is adjacent to the mold [29]. The width of the skin layer was reduced considerably to about 40 μm in the 0.1 DCP specimen **(Figure 4.6(b)),** consistent with the decrease in viscosity and the narrower molecular weight distribution [30]. The DCP-PP sample maintained large spherulites in the core layer (**Figure 4.6(b)**) and the distinction between skin and core layers is still evident in **Figure 4.6(b)** and **Table 4.2**.

Coagent modification influenced substantially the thermal properties of PP. PP-TAM and PP-TMPTMA exhibited significant increases in crystallization temperature, by 10°C at the highest loadings of peroxide and coagents, whereas the increase was more modest in the lightly modified CM-PPs (**Table 4.2**). Additionally the core of specimens injection molded from the heavily modified CM-PP samples consisted of very small spherulites, and had a denser, grainier structure (**Figures 4.6(e) and (f)**).

These observations are in agreement with our previous reports that irrespective of their efficiency in producing branching, grafting of both types of coagents resulted in increases in the crystallization temperature of PP. Even though CM-PP samples were gel-free, scanning electron and transmission electron microscopy revealed the presence of well-dispersed particles, with sub-micron dimensions, comparable to the dimensions of common nucleating agents (shown in previous chapters). This small population of particles is probably derived from coagent oligomerization [18], and influences the crystallization properties of the polymer, by acting as nucleating agents.

The fact that the shifts are most pronounced at the highest loadings of peroxide and coagents provides further proof that this effect is related to the amount of coagent, which oligomerizes when in excess, thus forming a coagent-rich secondary phase. The formation of a large quantity of

nucleating sites, attributed to the presence of in-situ generated coagent-rich nanoparticles, nucleates a large amount of crystals, and restricts spherulite growth, eventually leading to the grainier spherulitic structure shown in **Figures 4.7(e)** and (f). Such reductions are typical of nucleated PP, wherein the addition of nucleating agents promotes a finer spherulitic structure [5,31].

Moreover, as a result of the enhanced nucleation effect, CM-PPs crystallize faster (shown in previous chapters), and therefore they should not be as sensitive to the different temperature gradients during cooling. Because of the factors described above, the boundaries between the skin and core layers became more diffuse in the samples modified by 0.1 phr DCP and 3 phr coagent (Figures (c) and (e), and disappeared completely in the CM-PPs containing 0.3 phr DCP and 6 phr coagent. (**Figures 4.6 (e) and (f)**). These findings are consistent with literature observations that addition of nucleating agents suppresses the skin-core morphology and causes a uniform distribution of spherulite size along the sample thickness [32,33].

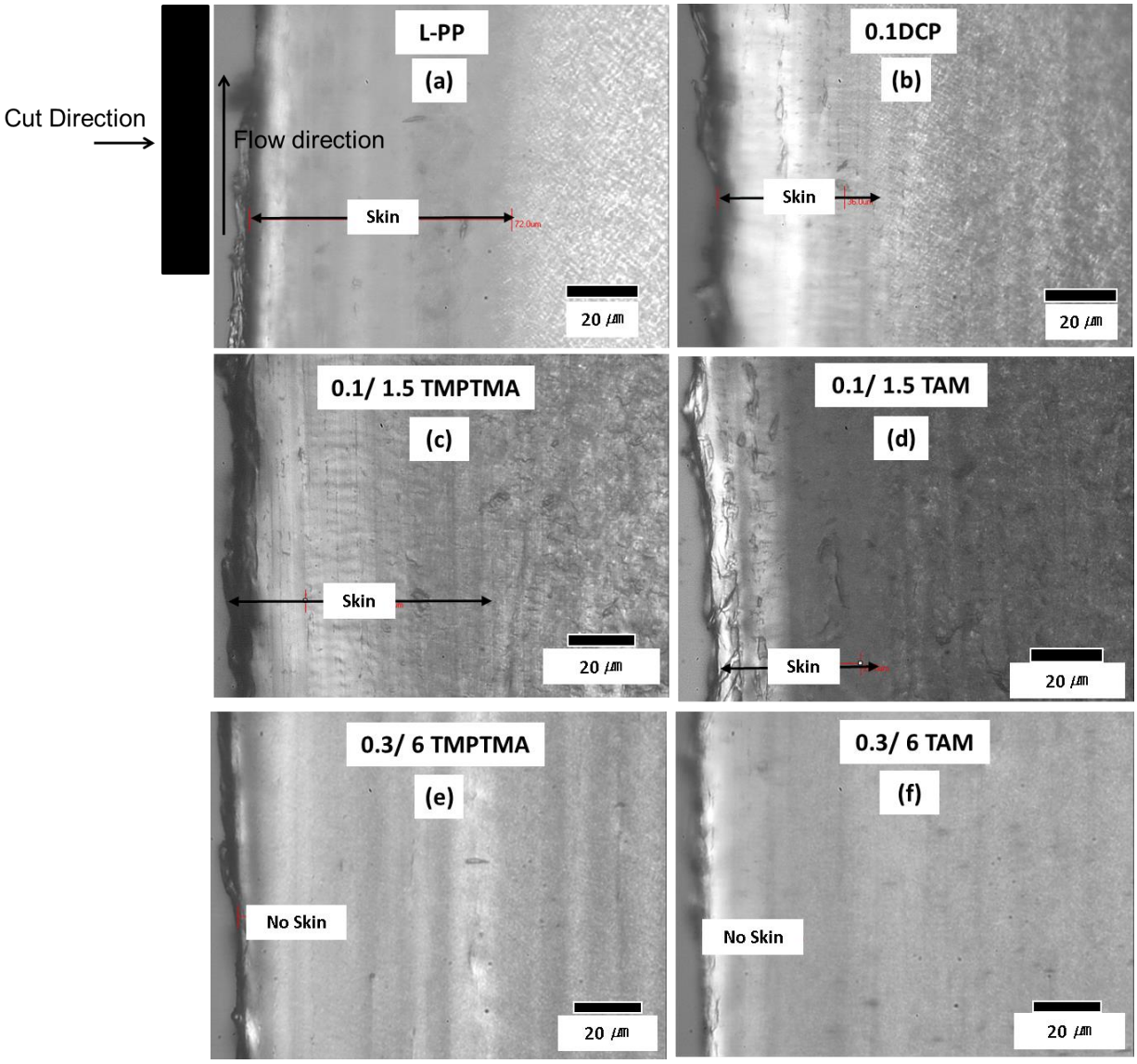

Figure 4.6 Polarized optical microscopy images of skin layer of L-PP, DCP-PP and CM-PP (all samples imaged at same magnification, scale bar represents 20μm). The inset shows the direction of the sectioning.

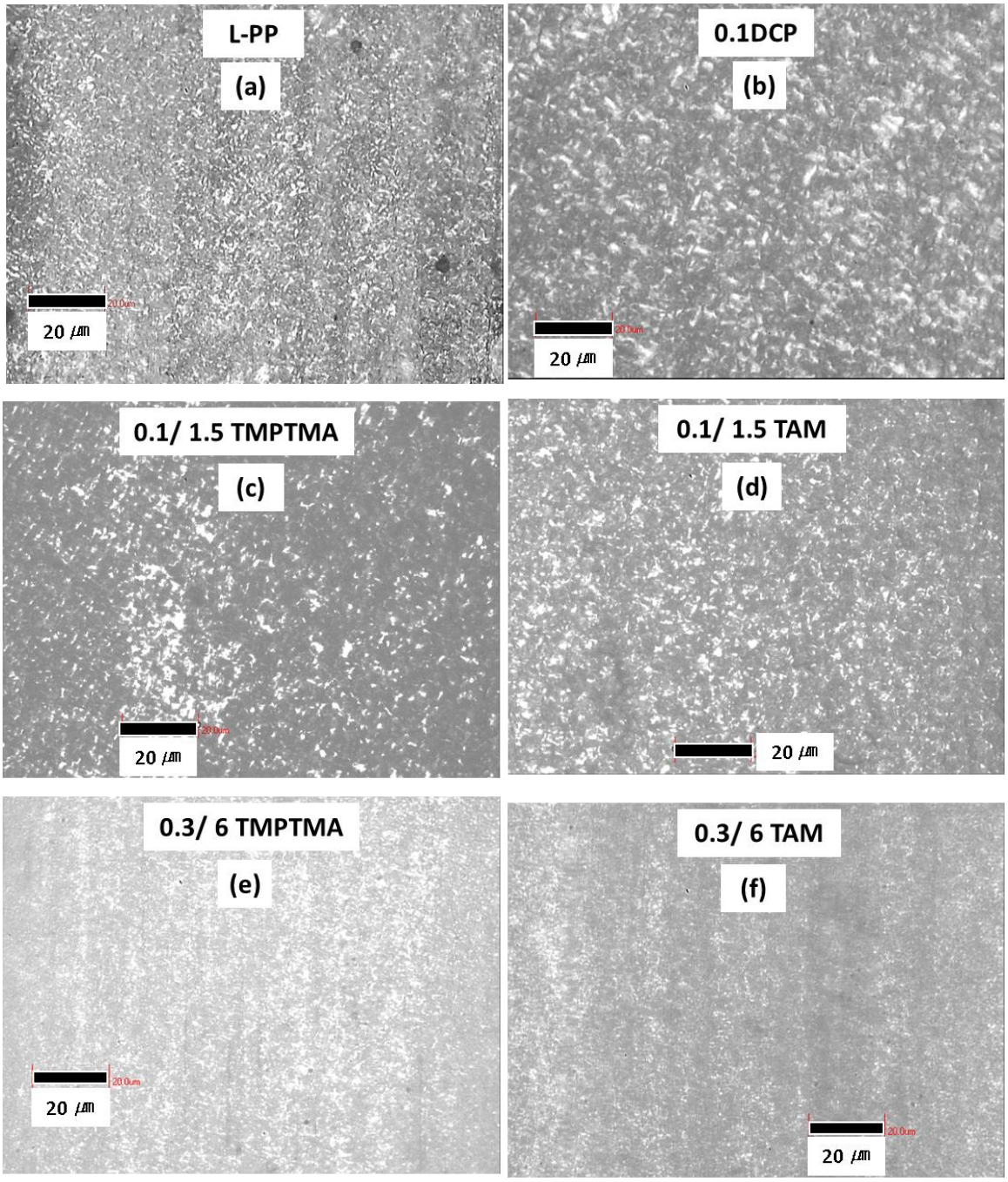

Figure 4.7 Polarized optical microscopy images of core layer of L-PP, DCP-PP and CM-PPs (all samples imaged at same magnification, scale bar represents 20µm)

Table 4.2 Thermal properties of skin and core layer of L-PP, DCP-PP and CM-PPs. The melting temperatures and heats of fusion are obtained from the first heating scan.

	T_c (℃)	T_{m1} (1st scan), ℃	ΔH_{f1} (1st scan), J/g
L-PP Skin	120	165	78
L-PP Core	121	168	85
0.1DCP Skin	121	167	78
0.1DCP Core	121	167	82
0.1/ 1.5 TAM Skin	125	167	80
0.1/ 1.5 TAM Core	125	167	85
0.3/ 6 TAM Skin	131	166	78
0.3/ 6 TAM Core	131	167	81
0.1/1.5 TMPTMA Skin	124	166	79
0.1/1.5 TMPTMA Core	123	166	83
0.3/6 TMPTMA Skin	131	167	82
0.3/6 TMPTMA Core	130	168	80

T_c – crystallization temperature, T_{m1} – melting point peak first heating, ΔH_{f1} – heat of fusion for first heating.

4.3.3 Mechanical Properties

It is well-known that the intricate microstructure of injection-molded parts controls their mechanical properties [26]. The three classes of materials described above (L-PP, DCP-PP, CM-PP modified with two different types of coagents) provide an opportunity to examine and interpret the effects of these modifications on the mechanical properties of injection molded products and to establish structure-property relationships.

Reaction with peroxide only resulted in a drop in the Young's modulus (**Figure 4.8a**) and tensile stress at yield (**Figure 4.8b**), compared to the neat material, consistent with the degradation and decrease in molecular weight of DCP-PP [34]. CM-PPs containing small amounts of peroxide and coagent (0.1 phr DCP/ 1.5 phr coagent) resulted in a minor increase in Young's modulus compared to 0.1 DCP (**Figure 4.8a**). On the other hand both CM-PPs modified by 0.3 phr DCP and 6 phr

coagent exhibited a substantial increase in their Young`s modulus compared to 0.1 DCP (**Figure 4.8a**).

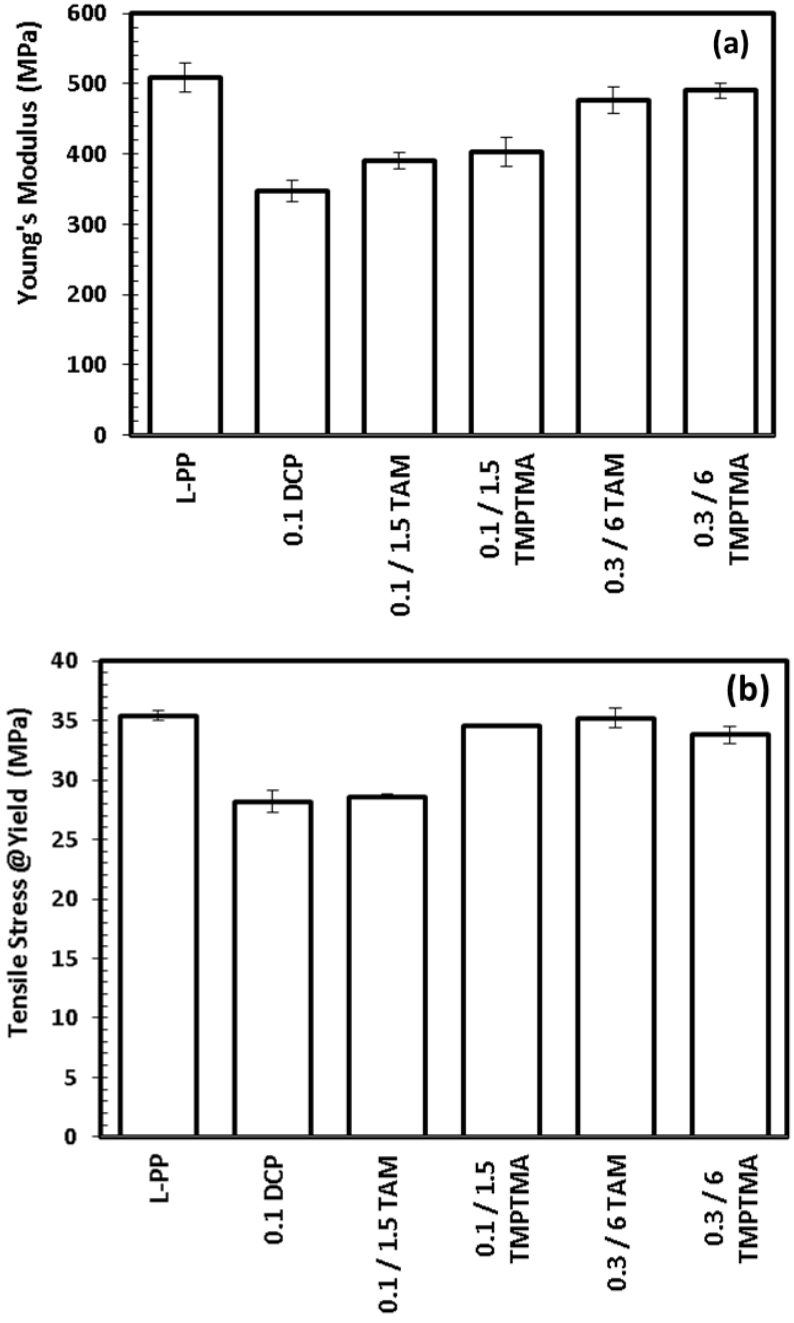

Figure 4.8 (a) Young's modulus and (b) tensile stress at yield of L-PP, DCP-PP and CM-PP.

In fact, the modulus, as well as the tensile strength of these heavily-modified PPs appeared to fully recover to the values of the unmodified L-PP, even though their molecular weight was lower. Such increases in Young's modulus are typically observed in nucleated systems containing sorbitol, talc etc., due to the formation of smaller and more uniform crystals, which contribute to better distribution of applied stresses [35,36]. This is obviously the case in our system, where the improvement observed can be related to the formation of small spherulites in the core layer, attributed to the nucleating effects of the in-situ generated coagent rich nanoparticles, as discussed earlier (**Figure 4.6**).

The elongation at break of the peroxide modified DCP-PP increased, when compared to neat PP (**Figure 4.9**). This may be related to plasticization ability of the smaller molecular weight fractions created by vis-breaking of the PP chains [34]. The elongation at break of all the CM-PPs remained higher than the neat PP; however 0.3/ 6 TAM had decreased ductility compared to the rest of the formulations. This is consistent with previous reports that branched PPs generally have lower elongation at break [37].

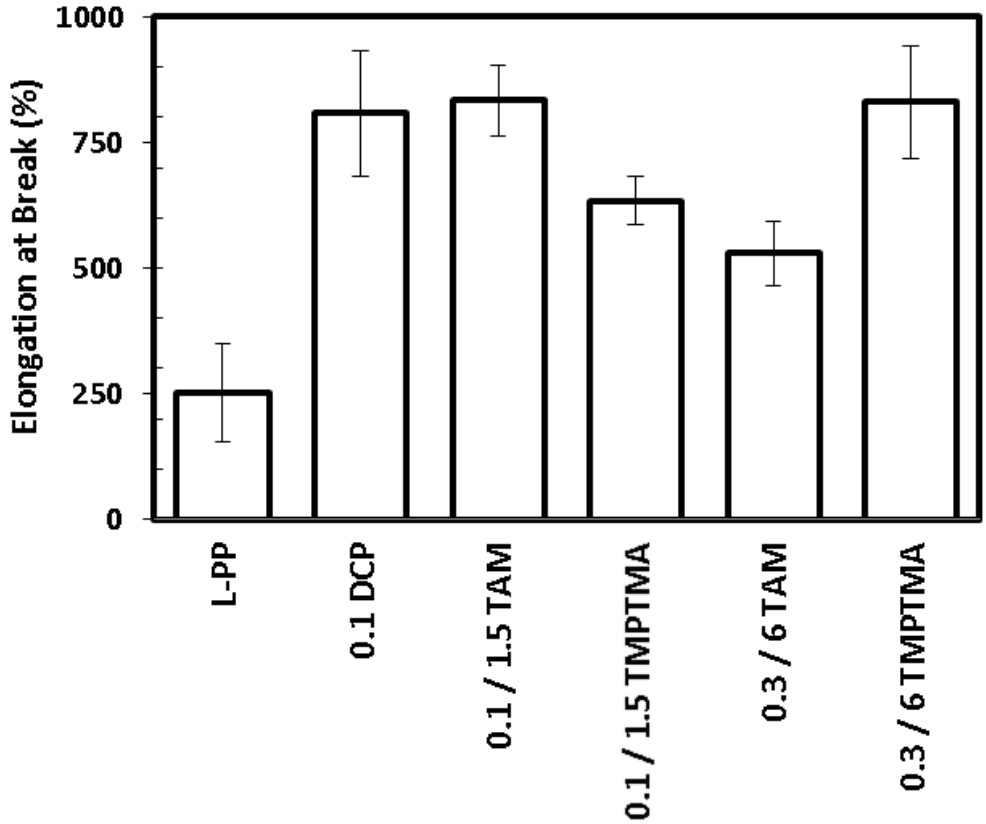

Figure 4.9 Elongation at Break of L-PP, DCP-PP and CM-PP.

The presence of uniform and small crystals, which are homogeneously distributed throughout the areas, and the absence of skin and core layers is also expected to influence positively the impact properties. Evidence of this is provided by the notched Izod impact strength measurements, shown in **Table 4.3**. As expected, the degraded DCP-PP, as well as the lightly modified CM-PPs had lower impact strength than L-PP. The smaller spherulites and improved sample uniformity afforded in the presence of high amounts of coagents improved significantly the notched Izod impact strengths, which surpassed the impact strength of neat L-PP. It is also noted that the fracture behavior of the samples modified with high amount of coagents changed from complete break (CB) in to hinged break (HB).

Table 4.3 Notched Izod impact strength of various PPs (CB: complete break, HB: Hinge break)

Formulation	**Notched Izod impact strength (J/m)**
L-PP	25 ± 5 (CB)
0.1 DCP	21 ± 4 (CB)
0.1 / 1.5 TAM	18 ±1 (CB)
0.1 / 1.5 TMPTMA	19 ± 3 (CB)
0.3 / 6 TAM	28 ± 1 (HB)
0.3 / 6 TMPTMA	31 ± 1 (HB)

These coagent modified PLAs are expected to have significant differences in cell size during foaming process owing to differences in crystallization rates and viscosities. This is dealt in Appendix A.

4.4. Conclusions

Reactive extrusion of linear isotactic polypropylene in the melt state in the presence of peroxide and coagents produced materials that had lower viscosity and molar mass, narrower molar mass distribution and chain branching, depending on the type and amount of coagent. Additionally CM-PPs had higher crystallization temperatures and a finer spherulitic structure, consistent to the properties commonly seen in nucleated PP. The altered crystallization kinetics of these materials

resulted in the disappearance of the distinctive core-skin layer in injection molded specimens, and consequently in a significant enhancement in their mechanical properties.

The production of controlled rheology and nucleated PP is generally a two-step process, which involves a first reactive extrusion step to obtain controlled rheology PP and a second compounding step where nucleating agents are added, to enhance the crystallization kinetics and alter the crystalline structure. In addition to being more costly and energy intensive, this procedure often results in a significant deterioration of the mechanical properties of the material. The solution proposed in this work is a one-pot approach to produce controlled rheology and/or branched nucleated polypropylene formulations with mechanical properties that match closely those of polypropylenes of much higher molecular weight. This research implements therefore a practical and industrially relevant reactive processing technique to upgrade the properties of an important commodity thermoplastic and thus make it more applicable in common processing techniques such as injection molding, which require fine-tuned rheological and thermal properties. As shown in Appendix A, the cell size of coagent modified PPs were observed to be significantly lower than linear counterparts owing to the differences in crystallization kinetics and viscosities.

In the next chapter of this thesis, the process of peroxide mediated reactive extrusion is applied to a biopolymer: poly(lactide), PLA.

4.5 References

[1] S.H. Ryu, C.G. Gogos, M. Xanthos, Melting behaviour of controlled rheology polypropylene, Polymer. 32 (1991) 2449–2455. doi:10.1016/0032-3861(91)90088-Z.

[2] C. Tzoganakis, J. Vlachopoulos, A.E. Hamielec, Production of controlled-rheology polypropylene resins by peroxide promoted degradation during extrusion, Polym. Eng. Sci. 28 (1988) 170–180.

[3] E. Passaglia, S. Coiai, S. Augier, Control of macromolecular architecture during the reactive functionalization in the melt of olefin polymers, Prog. Polym. Sci. 34 (2009) 911–947. doi:10.1016/j.progpolymsci.2009.04.008.

[4] S. Coiai, E. Passaglia, M. Aglietto, F. Ciardelli, Control of degradation reactions during radical functionalization of polypropylene in the melt, Macromolecules. 37 (2004) 8414–8423. doi:10.1021/ma0400315.

[5] H. Beck, Heterogeneous nucleating agents for polypropylene crystallization, J. Appl. Polym. Sci. 11 (1967) 673–685. doi:10.1002/app.1967.070110505.

[6] N. Patil, C. Invigorito, M. Gahleitner, S. Rastogi, Influence of a particulate nucleating agent on the quiescent and flow-induced crystallization of isotactic polypropylene, Polymer. 54 (2013) 5883–5891. doi:10.1016/j.polymer.2013.08.004.

[7] A.D. Gotsis, B.L.F. Zeevenhoven, A.H. Hogt, The effect of long chain branching on the processability of polypropylene in thermoforming, Polym. Eng. Sci. 44 (2004) 973–982. doi:10.1002/pen.20089.

[8] P. Spitael, C.W. Macosko, Strain hardening in polypropylenes and its role in extrusion foaming, Polym. Eng. Sci. 44 (2004) 2090–2100. doi:10.1002/pen.20214.

[9] Ä. Supe, D. Graebling, Synthesis of branched polypropylene by a reactive extrusion process, Macromolecules. 35 (2002) 4602–4610. doi:10.1021/ma0109469.

[10] W. Zhao, Y. Huang, X. Liao, Q. Yang, The molecular structure characteristics of long chain branched polypropylene and its effects on non-isothermal crystallization and mechanical properties, Polymer. 54 (2013) 1455–1462. doi:10.1016/j.polymer.2012.12.073.

[11] B.K. Kim, K.J. Kim, Cross-linking of polypropylene by peroxide and multifunctional monomer during reactive extrusion, Adv. Polym. Technol. 12 (1993) 263–269. doi:10.1002/adv.1993.060120304.

[12] E. Borsig, M. van Duin, a. D. Gotsis, F. Picchioni, Long chain branching on linear polypropylene by solid state reactions, Eur. Polym. J. 44 (2008) 200–212. doi:10.1016/j.eurpolymj.2007.10.008.

[13] J.S. Parent, A. Bodsworth, S.S. Sengupta, M. Kontopoulou, B.I. Chaudhary, D. Poche, et al., Structure–rheology relationships of long-chain branched polypropylene: Comparative analysis of acrylic and allylic coagent chemistry, Polymer . 50 (2009) 85–94. doi:10.1016/j.polymer.2008.11.014.

[14] G.J. Nam, J.H. Yoo, J.W. Lee, Effect of long-chain branches of polypropylene on rheological properties and foam-extrusion performances, J. Appl. Polym. Sci. 96 (2005) 1793–1800. doi:10.1002/app.21619.

[15] Y. Wang, Q. Ni, Z. Liu, J. Zou, X. Zhu, Grafting modification and properties of polypropylene with pentaerythritol tetra-acrylate, J. Polym. Res. 18 (2011) 2185–2193. doi:10.1007/s10965-011-9629-z.

[16] S.A. Mousavi-Saghandikolaei, M. Frounchi, S. Dadbin, S. Augier, E. Passaglia, F. Ciardelli, Modification of isotactic polypropylene by the free-radical grafting of 1,1,1-trimethylolpropane trimethacrylate, J. Appl. Polym. Sci. 104 (2007) 950–958. doi:10.1002/app.25796.

[17] J. Tian, W. Yu, C. Zhou, Crystallization behaviors of linear and long chain branched

polypropylene, J. Appl. Polym. Sci. 104 (2007) 3592–3600. doi:10.1002/app.26024.
[18] W. Wu, J.S. Parent, S.S. Sengupta, B.I. Chaudhary, Preparation of crosslinked microspheres and porous solids from hydrocarbon solutions: A new variation of precipitation polymerization chemistry, J. Polym. Sci. Part A Polym. Chem. 47 (2009) 6561–6570. doi:10.1002/pola.23699.
[19] M. Gahleitner, J. Wolfschwenger, C. Bachner, K. Bernreitner, W. Neil, Crystallinity and mechanical properties of PP-homopolymers as influenced by molecular structure and nucleation, J. Appl. Polym. Sci. 61 (1996) 649–657. doi:10.1002/(SICI)1097-4628(19960725)61:4<649::AID-APP8>3.0.CO;2-L.
[20] M. Sentmanat, E.B. Muliawan, S.G. Hatzikiriakos, Fingerprinting the processing behavior of polyethylenes from transient extensional flow and peel experiments in the melt state, Rheol. Acta. 44 (2004) 1–15. doi:10.1007/s00397-004-0398-z.
[21] K. El Mabrouk, J.S. Parent, B.I. Chaudhary, R. Cong, Chemical modification of PP architecture: Strategies for introducing long-chain branching, Polymer. 50 (2009) 5390–5397. doi:10.1016/j.polymer.2009.09.066.
[22] C.W. Macosko, Rheology: Principles, Measurements, and Applications, Wiley Subscription Services, Inc., A Wiley Company, 1994.
[23] J.S. Parent, S.S. Sengupta, M. Kaufman, B.I. Chaudhary, Coagent-induced transformations of polypropylene microstructure: Evolution of bimodal architectures and cross-linked nano-particles, Polymer. 49 (2008) 3884–3891. doi:10.1016/j.polymer.2008.07.007.
[24] F. Manero, M.R. Kamal, R.A. Lai-Fook, A.E. Varela, W.I. Patterson, Measurement and Prediction of Temperature Distribution in an Injection Molding Cavity, Int. Polym. Process. 18 (2003) 185–193. doi:10.3139/217.1728.
[25] M.R. Kamal, P.G. Lafleur, Heat transfer in injection molding of crystallizable polymers, Polym. Eng. Sci. 24 (1984) 692–697. doi:10.1002/pen.760240911.
[26] V. Tan, M.R. Kamal, Morphological Zones and Orientation in In jection-Molded Polyethylene, 22 (1978) 2341–2355. doi:10.1002/app.1978.070220824.
[27] M.R. Kantz, H.D. Newman, F.H. Stigale, The Skin-Core Morphology and Structureproperty Relationships in Injection-Molded Polypropylene, J. Appl. Polym. Sci. 16 (1972) 1249–1260. doi:10.1002/app.1972.070160516.
[28] W. Wenig, F. Herzog, Injection molding of polypropylene: x-ray investigation of the skin-core morphology, J. Appl. Polym. Sci. 50 (1993) 2163–2171. doi:10.1002/app.1993.070501216.
[29] M.R. Kamal, F.H. Moy, Microstructural characterization of injection-molded articles, J. Appl. Polym. Sci. 28 (1983) 1787–1804. doi:10.1002/app.1983.070280521.
[30] M. Gahleitner, C. Bachner, E. Ratajski, G. Rohaczek, W. Neißl, Effects of the catalyst system on the crystallization of polypropylene, J. Appl. Polym. Sci. 73 (1999) 2507–2515.
[31] Y. Feng, X. Jin, J.N. Hay, Effect of nucleating agent addition on crystallization of isotactic polypropylene, J. Appl. Polym. Sci. 69 (1998) 2089–2095.
[32] J. Cao, K. Wang, W. Cao, Q. Zhang, R. Du, Q. Fu, Combined effect of shear and nucleating agent on the multilayered structure of injection-molded bar of isotactic polypropylene, J. Appl. Polym. Sci. 112 (2009) 1104–1113. doi:10.1002/app.29540.
[33] Y.-H. Chen, G.-J. Zhong, Y. Wang, Z.-M. Li, L. Li, Unusual Tuning of Mechanical Properties of Isotactic Polypropylene Using Counteraction of Shear Flow and β-Nucleating Agent on β-Form Nucleation, Macromolecules. 42 (2009) 4343–4348. doi:10.1021/ma900411f.
[34] H. Azizi, I. Ghasemi, Reactive extrusion of polypropylene: production of controlled-rheology polypropylene (CRPP) by peroxide-promoted degradation, Polym. Test. 23 (2004) 137–143. doi:10.1016/S0142-9418(03)00072-2.
[35] B. Pukanszky, I. Mudra, P. Staniek, Relation of crystalline structure and mechanical

properties of nucleated polypropylene, J. Vinyl Addit. Technol. 3 (1997) 53–57.
[36] F. Mai, K. Wang, M. Yao, H. Deng, F. Chen, Q. Fu, Superior reinforcement in melt-spun polyethylene/multiwalled carbon nanotube fiber through formation of a shish-kebab structure., J. Phys. Chem. B. 114 (2010) 10693–702. doi:10.1021/jp1019944.
[37] T.J. McCallum, M. Kontopoulou, C.B. Park, A. Wong, S.G. Kim, Effect of branched PP content on the physical properties and cell growth during foaming of TPOs, J. Appl. Polym. Sci. 110 (2008) 817–824. doi:10.1002/app.28648.

Chapter 5

Rheological Characterization of Long-Chain Branched Poly(lactide) prepared by reactive extrusion in the presence of allylic and acrylic coagents

5.1 Introduction

Thermoplastic polyesters, such as poly(ethylene terephthalate) (PET), and more recently polylactide or polylactic acid (PLA) are widely used in the packaging industry and other commodity applications, due to their suitable mechanical and barrier properties, and transparency. PLA has additional advantages, being bio-derived and biodegradable/compostable under certain conditions. Polyesters lack strain hardening, because of their linear structure. This limits their applicability in processes that require extensional flows, such as film casting and blowing, foaming and blow molding. Polyesters are also prone to thermal/hydrolytic degradation, which makes their processing more challenging. These deficiencies are commonly addressed by reactive processing, which aims at modifying the polymer architecture by introducing chain extension and/or branching, thus limiting the loss in molecular weight and improving the strain hardening behavior.

Polyesters, such as PET, poly(butylene terephthalate) (PBT), and PLA are commonly modified using multifunctional chain extenders, that react with the end groups and create branched structures. Pyromellitic dianhydride (PMDA), epoxy-based tetraglycidyl diamino diphenyl methane (TGDDM), and multi-functional styrene-acrylic oligomers are commonly used chain extenders for PET and PBT [1–7]. In addition to PMDA, PLA has been modified using polyisocyanates [8–12] which have been essentially abandoned in favour of the less toxic multifunctional epoxy-based chain extenders [13–19]. Free radical-mediated reactive extrusion in the presence of peroxides has been employed extensively to achieve branching of PLA [20–25]. Addition of multifunctional coagents, such as (PETA), triallyl isocyanurate (TAIC), and triallyl trimesate (TAM) further facilitates the formation of branches [26–28].

Branched structures can be characterized using rheological means, especially measurements in the linear viscoelastic (LVE) regime, as well as in the non-linear regime, using shear and elongational flow experiments, which are very sensitive to shear thinning and strain hardening effects respectively. The rheological properties of branched polymer melts are correlated with their molecular properties, such as molar mass and molar mass distributions, radius of gyration, intrinsic

viscosity that can be characterized through triple detection (light scattering, concentration, viscosity) size-exclusion chromatography (SEC) measurements. These evaluations are very sensitive to the presence of branching, which is manifested through broadening of the molar mass distribution, appearance of high molar mass tails, deviations in the Mark-Houwink plots, etc. [1,2,29–32].

Careful studies of the relation between rheological properties and chain structure of PLA have been conducted by various researchers [2,19,26,33–41]. A variety of LVE responses have been reported, depending upon the type of PLA branched structure (star, comb, hyperbranched etc.). Branching by functional end groups, such as styrene-glycidyl acrylate oligomer (Joncryl®) allows for the formation well-controlled comb-like chain structures [34]. On the other hand given the random character of free-radical mediated reactions, allowing for each chain to be branched at multiple locations, mixtures of structures, including linear, star, comb or tree-like molecules may be obtained [26,42,43]. These materials have been modeled successfully by the branch on branch model [42], which employs the idea of hierarchical relaxation of branched structures, to model the LVE properties of branched polymers [44,45]. You et al. described a branching mechanism involving macroradicals originating from a PLA chain scission mechanism in the presence of peroxide and pentaeythritol triacrylate (PETA) coagent [26]. Free-radical mediated branching by irradiation, in the presence of trimethylolpropane triacrylate (TMPTA) coagent produces bimodal architectures, consisting of mixtures long-chain branched macromolecular structures and some degraded material [38,39,46].

In the present work we compare the effect of the type (allylic versus acrylic) and amount of tri-functional coagents on the LVE properties of PLA branched in the presence of dicumyl peroxide Furthermore we use these results, together with detailed characterization of the molar mass distributions using triple-detector gel permeation chromatography (GPC), to infer the branched architecture of these coagent modified PLAs.

5.2. Experimental

5.2.1 Materials

PLA (grade 3251D, MFI 35 g/10 min at 190°C/2.16 kg) was obtained from Natureworks® LLC. Triallyl trimesate (TAM, 98%) was obtained from Monomer Polymer and Dajac Labs Inc., Trevose, USA.). Trimethylolpropane triacrylate (TMPTA), trimethylolpropane trimethacrylate (TMPTMA), pentaeythritol triacrylate (PETA) and dicumyl peroxide (DCP, 98% purity) were used as received from Sigma-Aldrich, Oakville, Canada. The chemical structures of all the coagents used

in this work are shown in Scheme 5.1. Methanol (HPLC grade), tetrahydrofuran (THF, HPLC grade), and chloroform (HPLC grade) were also obtained from Sigma-Aldrich.

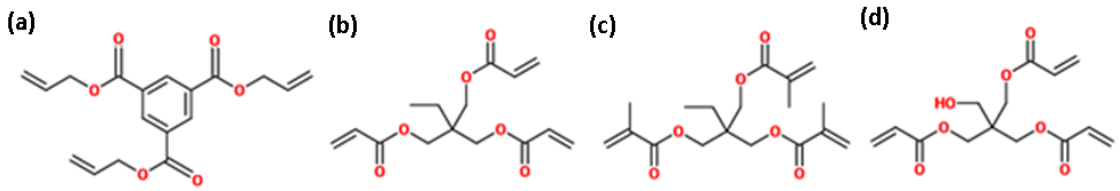

Scheme 5.1: Chemical structure of coagents used in the present work: (a) TAM, (b) TMPTA, (c) TMPTMA, and (d) PETA.

5.2.2 Reactive extrusion

To prepare reactively modified PLA formulations, PLA was ground into powder, mixed with appropriate ratios of DCP and coagent then coated with an acetone solution to yield a batch size of 30 g. Samples were dried in a vacuum oven at 60 °C for 12 hours to remove residual solvent and moisture. The formulations, containing between 0.1 – 3.0 wt.% coagent and 0.3 – 0.6 wt.% DCP were charged to a DSM micro-compounder, equipped with twin-co-rotating screws, at 180 °C and 100 rpm for 6 minutes. After compounding, the strands were chopped into pellets for further characterization. The sample designation used in this work was 'a/b coagent' where 'a' denotes the concentration of DCP in wt.% and 'b' denotes concentration of coagent in wt.%. Neat PLA was processed under the similar conditions outlined above, to provide a suitable basis for comparison.

5.2.3 Gel Permeation Chromatography (GPC)

GPC characterization was performed in a Viscotek 270max separation module equipped with triple detectors as differential refractive index (DRI), viscosity (IV), and light scattering (low angle, LALS and right angle, RALS). The separation module was maintained at 40 °C and contained two porous PolyAnalytik columns in series with an exclusion molecular weight limit of 209,106 Da. Distilled THF was used as the eluent at a flow rate of 1 mL min^{-1}. The PLA samples (5 g) were purified by dissolving in chloroform (20 ml) and precipitating with excess methanol. The purified samples were further dissolved in THF for GPC characterization. The dissolved samples were filtered through a 0.22 µm nylon filter before passing though the column. The refractive index, dn/dc was determined to be 0.0482 $ml.gm^{-1}$. The results from the triple detector train and Viscotek Omnisec software were used to determine polymer molecular weight distribution (MWD) and molecular weight (MW) averages. Gel content was measured by extracting samples in boiling THF

and chloroform as solvents. Samples were sealed in 120 mesh stainless steel sieve and extracted for 6 hours. The samples which were free of gels in THF were used for GPC measurements. Table 5.1 shows the data on all the gel-free samples on which GPC measurements could be performed.

Table 5.1: Molecular weight distributions and Cross model parameters for PLA samples

Sample Designation	M_w (kg.mol^{-1})	Đ	M_z (kg.mol^{-1})	η_o (Pa s)	λ (s)
PLA	83	1.7	130	370^{+}	-
0.1/0.1 TAM	84	2.5	240	570	0.003
0.1/0.3 TAM	102	2.9	300	1,530	0.025
0.2/0.2 TAM	110	4.0	540	1,800	0.04
0.2/0.3 TAM	120	3.6	1100	2,400	0.04
0.3/0.1TAM	94	3.4	400	2,200	0.02
0.3/0.2 TAM	130	3.4	1100	2,410	0.02
0.3/3 TMPTMA	94	1.7	230	520	0.003
0.3/3 TMPTA	100	2	400	2,500	0.06
0.3/3 PETA	90	2.5	250	1, 300	0.01

M_w- weight average molecular weight, Đ – dispersity, M_z- Z-average molecular weight, η_o – zero shear viscosity, and λ – relaxation time, $^{+}$Denotes plateau values as the samples exhibited Newtonian behaviour.

5.2.4 Rheological Characterization

Compression molded discs of 25 mm in diameter were prepared in a Carver hydraulic press at 180 °C and were used for rheological characterization. The linear viscoelastic (LVE) properties of the prepared PLA samples as a function of angular frequency (ω) were measured in the oscillatory mode at 180, 200 and 220 °C using MCR-301 Anton Paar rheometer equipped with 25 mm diameter parallel plates at a gap of 1 mm. Time sweeps performed at 180°C for 15 min. at frequency of 1 Hz confirmed that all samples were thermally stable during the duration of the experiments.Stress sweeps were performed to ensure that all the measurements were within linear viscoelastic regime. The average of three measurements are reported throughout this work. The obtained data was fitted to a modified Cross model.

$$|\eta^*(\omega)| = \frac{\eta_o}{1 + |\lambda\omega|^{1-n}} \qquad (1)$$

where η is the shear viscosity, η_o is the zero shear viscosity, λ is the relaxation time, n is a constant related to the shear thinning behaviour, and ω is the frequency in rad.s^{-1}.

Time-temperature superposition was performed based on the unified framework proposed by Mavridis and Shroff [47] to study the temperature dependence of rheological data and calculate activation energies. Small amplitude oscillatory shear rheology (SAOS) data obtained at different temperatures were shifted to the temperature of 180 °C. A horizontal shift was adequate for all samples and resulted in the estimation of the horizontal activation energy of the flow (E_H).

$$a_T\,(T) = exp\left[\frac{E_H}{R}\left(\frac{1}{T} - \frac{1}{T_0}\right)\right] \qquad (2)$$

where T_0 is reference temperature, T is temperature, $a_T\,(T)$ is horizontal shift factor, and R is universal gas constant.

5.3. Results and discussion

5.3.1 Thermorheological behaviour through LVE characterization

The thermorheological behaviour of polymer melts has emerged as a powerful tool to gain insight into the molecular structure of polymers [48]. While linear and short-chain branched molecules are thermorheologically simple, branched polymers, such as metallocene/single-site catalyzed linear low density polyethylenes (LLDPE) containing long side branches, may exhibit thermorheological complexity [49]. However the highly branched long-chain branched low-density polyethylenes (LDPEs) showed thermorheological simplicity [48], because every molecule in the tree-like LDPEs is long-chain branched, and consequently there is no distribution of relaxation strengths. Cailloux et al. and Kruse et al. also saw thermorheological simplicity in branched PLA and polyester samples respectively, depending upon the type and degree of modification [2,50].

The well-known vanGurp-Palmen plots [51] plot the phase angle versus the complex modulus at different temperatures to detect whether a polymer melt follows thermorheologically simple or complex behaviour. The plots of samples that are thermorheologically simple have similar shape, irrespective of the temperature, resulting in the curves coinciding. Such is the case for the PLA formulations modified by various coagents as shown in **Figure 5.1**.

In addition to its usefulness to establish thermorheological behaviour, the vanGurp plot is very sensitive to the dispersity, and the type of branched architecture. Different shapes have been reported, for linear, star, comb, and hyperbranched polymers [33,52]. Our linear, unmodified PLA showed terminal flow behaviour, indicative of its linear structure. (**Figure 5.1**). On the other hand, even though the modified samples shown in **Figure 5.1** were thermorheologically simple, they

deviated substantially from terminal flow, suggesting the presence of branched architectures. Such deviations have been reported extensively in low density polyethylene (LDPE) [48], LCB PP [30] and LCB PLA [39].

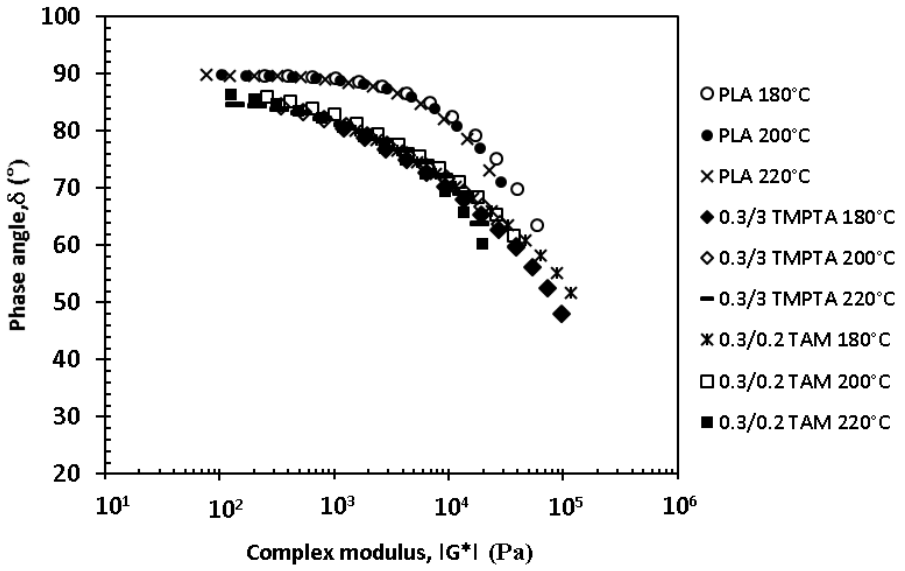

Figure 5.1: Van Gurp-Palmen plot of thermorheologically simple samples

Activation energies for all the thermorheologically simple formulations were calculated by applying the Arrhenius relation, which relates the horizontal shift factor, a_T with temperature (equation 2) and are summarized in **Figure 5.2**. Formulations reacted with DCP and TAM exhibited the largest values of the activation energy, which was as high as 112 kJ/mol in the formulations reacted with the highest amount of DCP and TAM (formulation 0.3/0.2 TAM) (**Figure 5.2a**). In thermorheologically simple samples the increases in the activation energies provide strong evidence of branching, as long branches are known to affect strongly the flow energy. This has been demonstrated in the case of polyolefins, such as short-chain and long-chain branched polyethylene [31,48,53], and polypropylene [29,30,48,54], as well as thermoplastic polyesters, such as PET and PLA [1,2,13,19]. Cailloux et al. reported energy of about 120 kJ.mol^{-1} for star-shaped PLA [50].

Significantly larger amounts of the acrylate-based TMPTA coagent were needed to produce the same effect at similar DCP loadings (**Figure 5.2b**), whereas PETA produced only modest increases in the activation energy, and TMPTMA was totally ineffective. These results suggest that acrylate coagents are much less efficient in introducing branching.

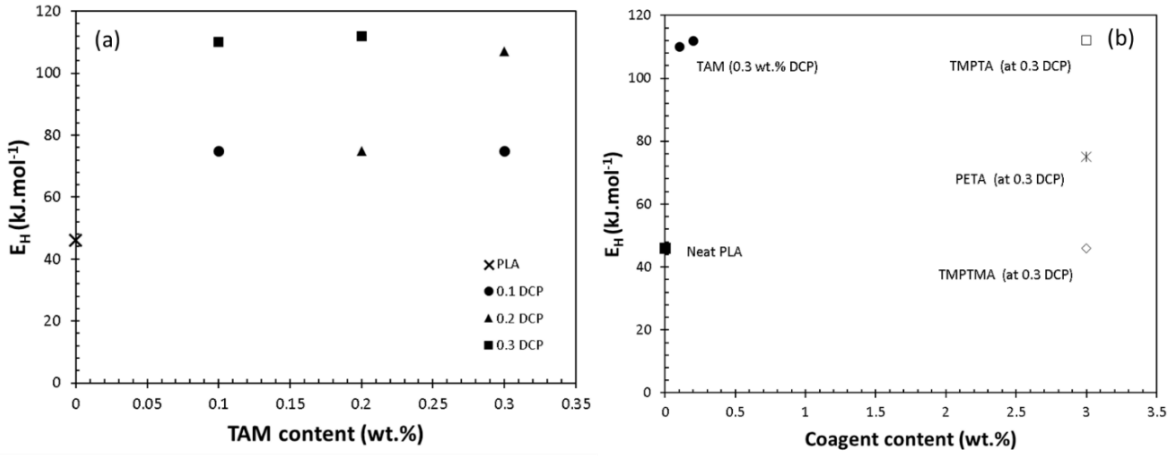

Figure 5.2: Activation energy of flow for a) TAM coagent at various DCP and TAM contents, (b) comparison of coagents at 0.3 wt.% DCP.

It must be noted that increasing the TAM amount beyond 0.3 resulted in thermorheologically complex melts, with the appearance of additional relaxation modes (**Figure 5.3**). This suggests that increasing the amount of the trifunctional coagent resulted in more complex branched structures, manifested by the appearance of additional relaxation modes as the samples approach the gel point. Fang et al [38], also reported thermorheological complexity in gamma-ray irradiated PLA in the presence of TMPTA coagent.

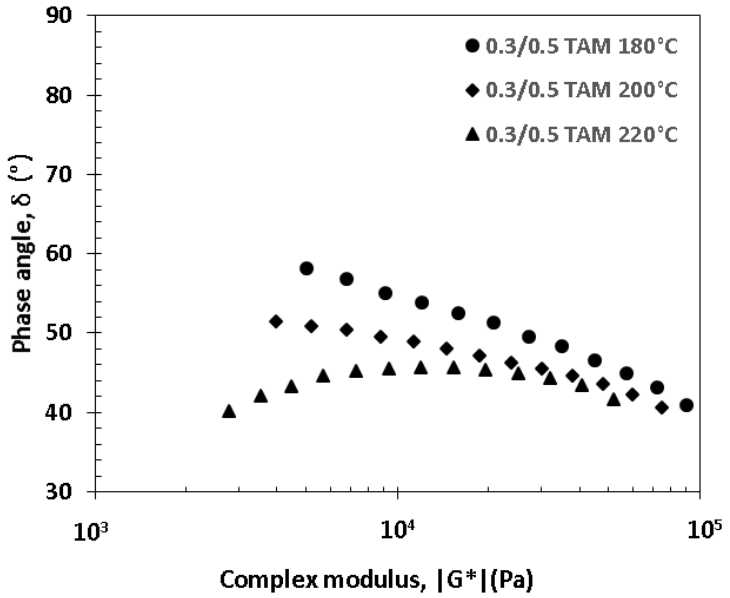

Figure 5.3: Van Gurp-Palmen plot of a thermorheologically complex sample (0.3/0.5 TAM)

5.3.2. SAOS characterization

Depending upon the coagent type and amount, branched architectures have a profound effect on the complex viscosity of the coagent modified system, as shown by the master curves in **Figure 5.4**. The modified samples exhibited increases in zero shear viscosity and enhanced shear thinning depending upon the concentration of peroxide and coagent, compared to the starting PLA, which showed essentially Newtonian behaviour. It must be noted that reaction of PLA with DCP alone did not produce measurable differences compared to neat PLA, and therefore the results are not shown here.

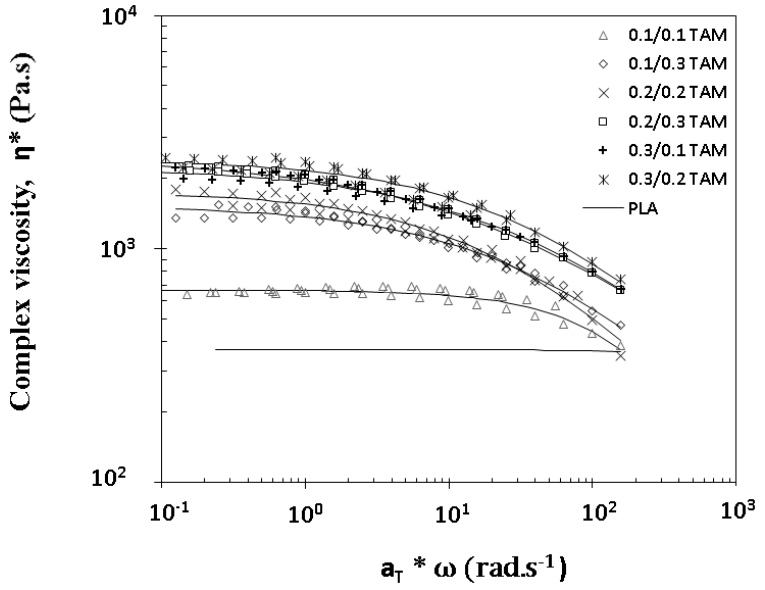

Figure 5.4: Complex viscosity as a function of angular frequency for various TAM formulations, at a reference temperature of 180°C; solid lines represent respective Cross model fits, solid lines represent experimental data for neat PLA as samples exhibited Newtonian behavior

As mentioned in section 5.3.1 above, increasing the amount of TAM beyond 0.3 wt.% resulted in loss of thermorheological simplicity. In this case it was impossible to construct master curves. The SAOS frequency sweeps obtained at 180°C are shown in **Figure 5.5a**, and the corresponding VanGurp plots are shown in **Figure 5.5b**.

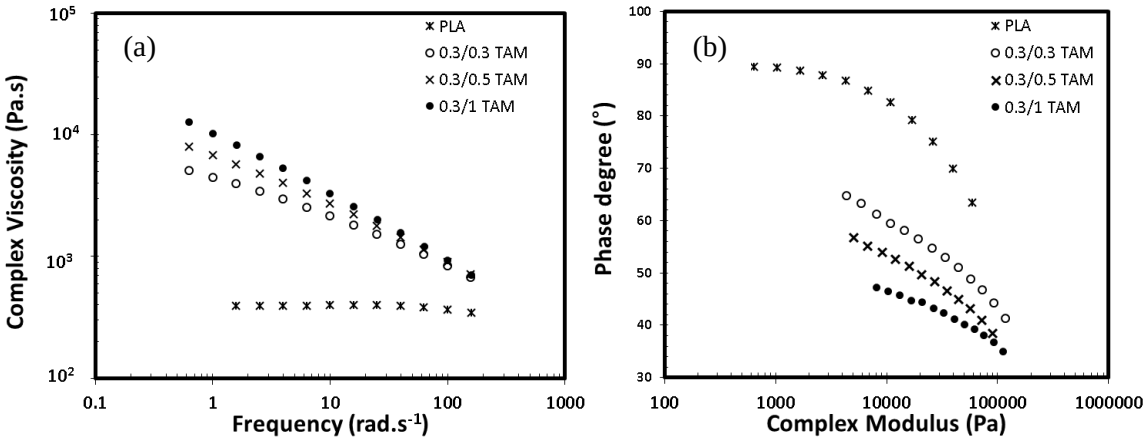

Figure 5.5: (a) Complex viscosity as a function of angular frequency and (b) VanGurp-Palmen plots of thermorheologically complex samples at 180°C.

These samples demonstrated a gradual loss of the Newtonian plateau, whereas the 0.3/1 TAM formulation approached the gel point, based on the phase degree values. It must be noted that these samples appeared gel-free in chloroform, but did have gels in THF, thus inhibiting further GPC characterization.

Plots of complex viscosity with respect to angular frequency for various coagents reveal further interesting insights (**Figure 5.6**). At similar concentration of DCP (0.3 wt.%), and coagent loading, TMPTA influenced the oscillatory response most, followed by PETA, whereas TMPTMA had negligible effect. Comparison with a composition containing 0.3 wt.% DCP and only 0.1 wt.% TAM, demonstrates the overwhelming effectiveness of the allylic-based TAM, compared to the acrylate coagents. These findings are consistent with the activation energy results, presented in **Section 5.3.1**.

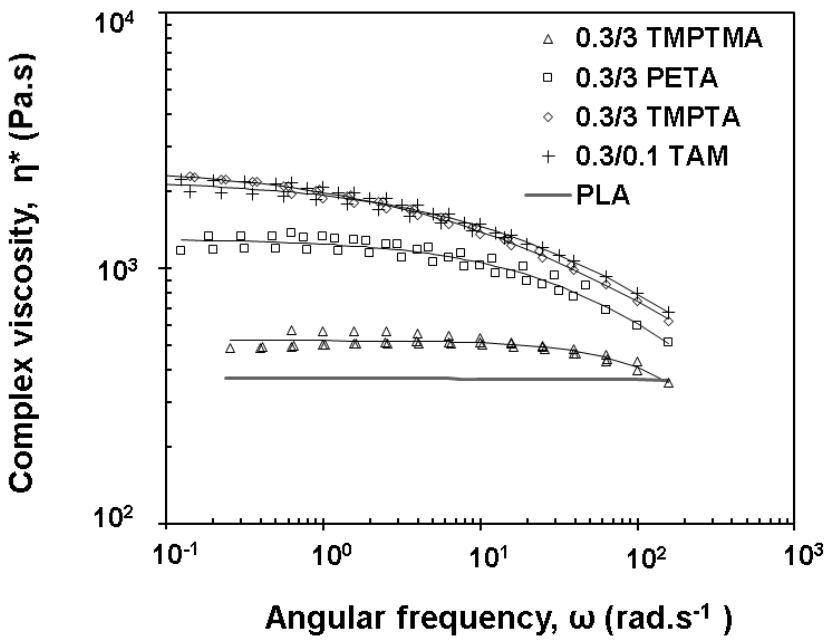

Figure 5.6: Complex viscosity with respect to angular frequency for allylic and acrylic coagents reacted with 0.3 wt % DCP. Solid lines represent corresponding Cross model fits.

To facilitate comparisons, **Figures 5.7 (a)** and **(b)** summarize the zero shear viscosities (**Table 5.1**), and **Figures 5.7(c)** and **(d)** the relaxation times (**Table 5.1**), obtained by fitting the Cross model (Equation 1) to the master curves shown in **Figure 5.4** and **5.6**. For the neat PLA and 0.3/1 TAM, the viscosity cannot be described by the Cross model therefore the viscosity at the lowest measured frequency is shown.

While the zero shear viscosities should be influenced by both the increase in the molar mass and branching, the relaxation times provide an indication of the degree of shear thinning, attributed to changes in the polydispersity and/or the presence or branching. The increase of the relaxation time by orders of magnitude in the modified samples confirms the presence of branching. These figures show clearly the effectiveness of TAM compared to the other coagents, and the profound effects of increasing the amount of DCP and TAM coagent on both parameters.

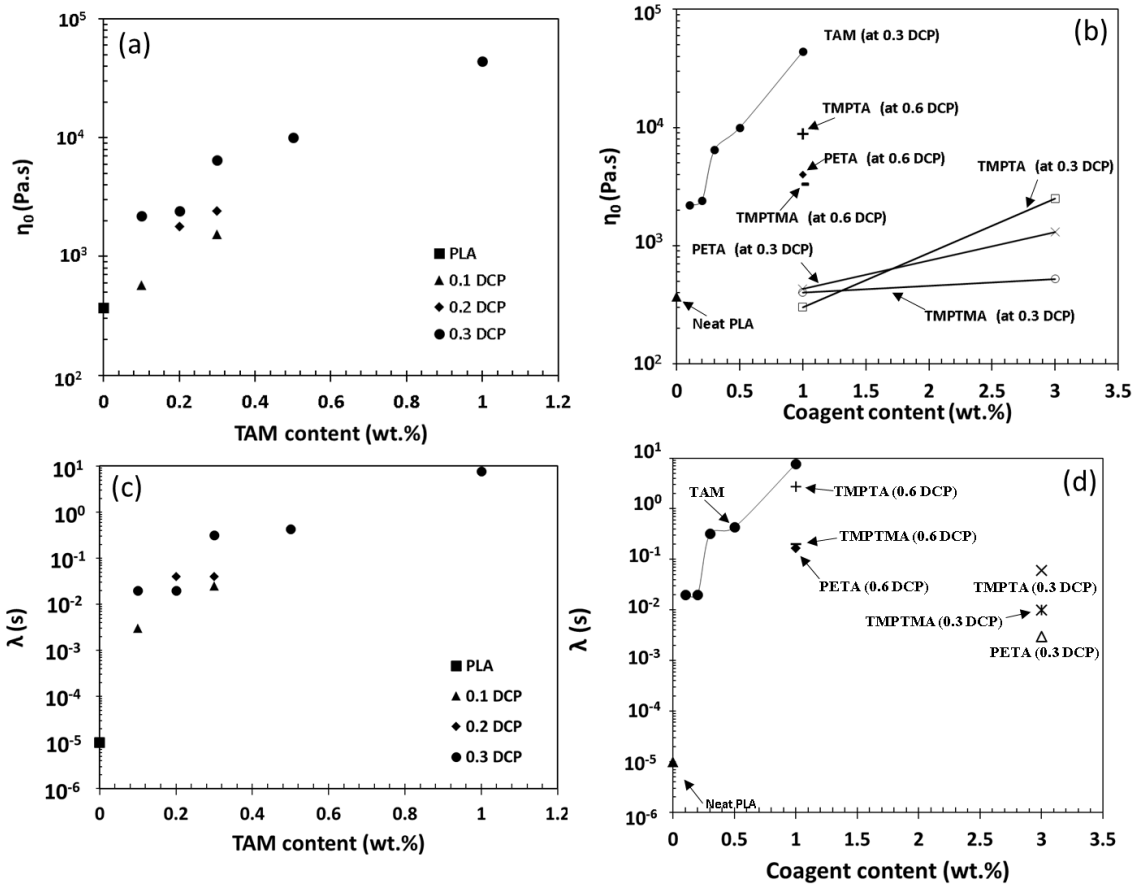

Figure 5.7: (a) Zero shear viscosity as a function of TAM content, (b) zero shear viscosity as a function of coagent type and amount (c) relaxation time as a function of TAM content and (d) relaxation times as a function of coagent type and amount; lines are shown to guide the eye.

5.3.3 Molar Mass Distributions

The LVE properties presented above are influenced by the molecular architecture of the polymers. Even though SEC characterization is not always fully capable of characterizing branched structures in polymer melts, it can still provide instructive insights. The SEC results showed that the neat linear PLA had M_w of 83 kg.mol^{-1} (**Figure 5.8a, Table 5.1**) and followed a linear relation between radius of gyration and M_w calculated through light scattering (M_{LS}), which follows a scaling law shown in equation (3) [38,55] (**Figure 5.8b**).

$$\langle R_g^2 \rangle^{0.5} = K M_{LS}^{\alpha} \qquad (3)$$

The value of α was found to be 0.58 from Figure 5.8b, in good agreement with the theoretical value [38].

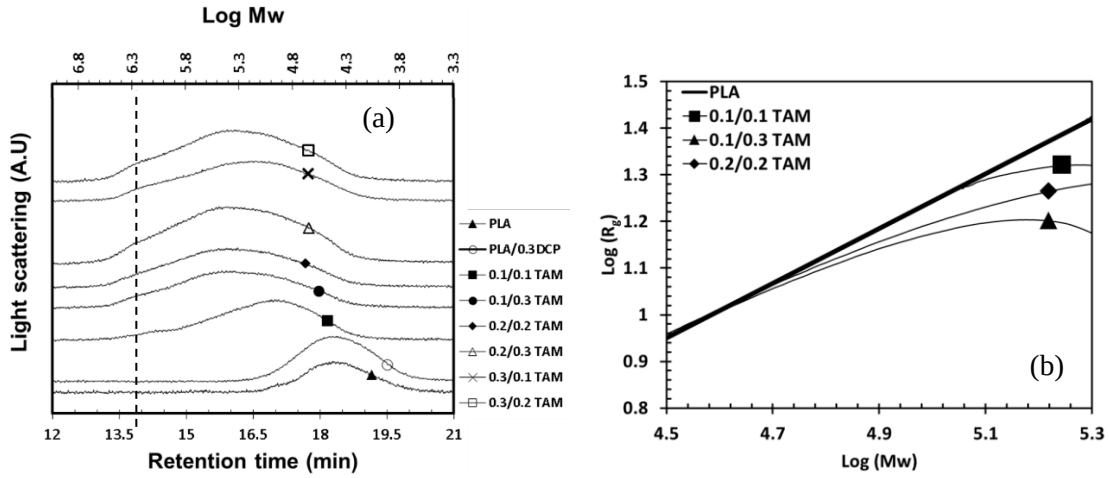

Figure 5.8: (a) Light scattering response of PLAs reacted with various amounts of TAM coagent plotted against retention volume; the secondary abscissa shows molecular weight calculated from universal calibration corresponding to retention volume on primary abscissa and (b) Radius of gyration as a function of molecular weight. PLA/0.3 DCP follows the same trend as PLA, formulations 0.2/0.3 TAM, 0.3/0.1 TAM, and 0.3/0.2 TAM follow the same trend as 0.2/0.2 TAM and hence are not shown here.

In **Figure 5.8a** we present the unprocessed results obtained from light scattering results, as they are more sensitive to the presence of branched structures [56]. Modification of the PLA with peroxide alone did not result in significant changes in chain architecture (see PLA/0.3DCP in **Figure 5.8a**). This is in contrast with reports by Fang et al [38], who used irradiation to generate free-radicals and reported the presence of degraded structures, attributed to chain scission.

Reaction in the presence of both peroxide and TAM resulted in increased molecular weight when compared to neat PLA. The light scattering curve of all samples modified by TAM and peroxide showed shifts toward higher molecular weight regions with a minor peak appearing at retention time of 14 min (shown by a vertical line in **Figure 5.8a**) which is reflected in the higher z-average molecular weight (M_z) values and broadening of distribution peak when compared to neat PLA (**Table 5.1**). These results suggest that high molecular weight fractions were produced in the presence of TAM and peroxide, and that there is no evidence of degradation.

The pronounced deviations of the radius of gyration of the branched polymers from the radius of gyration of the linear counterparts can be expressed by using a coil contraction factor g which relates the mean square radius of linear polymer, $\langle R^2_{g,lin} \rangle$, to that of branched polymer, $\langle R^2_{g,br} \rangle$, of equal molar mass [2,55]:

$$g = \frac{\langle R^2_{g,br} \rangle}{\langle R^2_{g,lin} \rangle} \quad (4)$$

The deviation from the linear reference toward lower values suggests contraction of the coiling chains, as expected in the case of branched polymers. The slopes of the linear portion for the branched PLA samples (α in equation 3) varied between 0.4-0.44. The deviation from the slope of 0.58 corresponding to linear PLA provides solid evidence of branching.

Comparison of the light scattering response of samples modified by the three acrylic (TMPTA, TMPTMA, and PETA) coagents showed that they did not produce shifts of similar degree as the TAM coagent (**Figure 5.9**). Interestingly however, a very pronounced peak appears at very short elution times in unpurified samples (**Figure 5.9a**). This peak, which appears at short elution times and was absent in the purified samples, corresponds to the presence of very high molar mass material (**Figure 5.9b**). It is well known that acrylic coagents, which are very reactive, oligomerize in the presence of peroxide [57]; in doing so they would create cross-linked structures, which further elute at short times without grafting onto the PLA chain. Even though we have alluded to this before in the previous chapters of this thesis, this is the first time that evidence of these structures has been demonstrated using GPC. This may explain the apparent lack of efficiency of these coagents in generating branches, when contrasted with TAM. This mechanism would be absent in the case of irradiated PLA, thus explaining that TMPTA coagent was more efficient in the work by Fang et al [38].

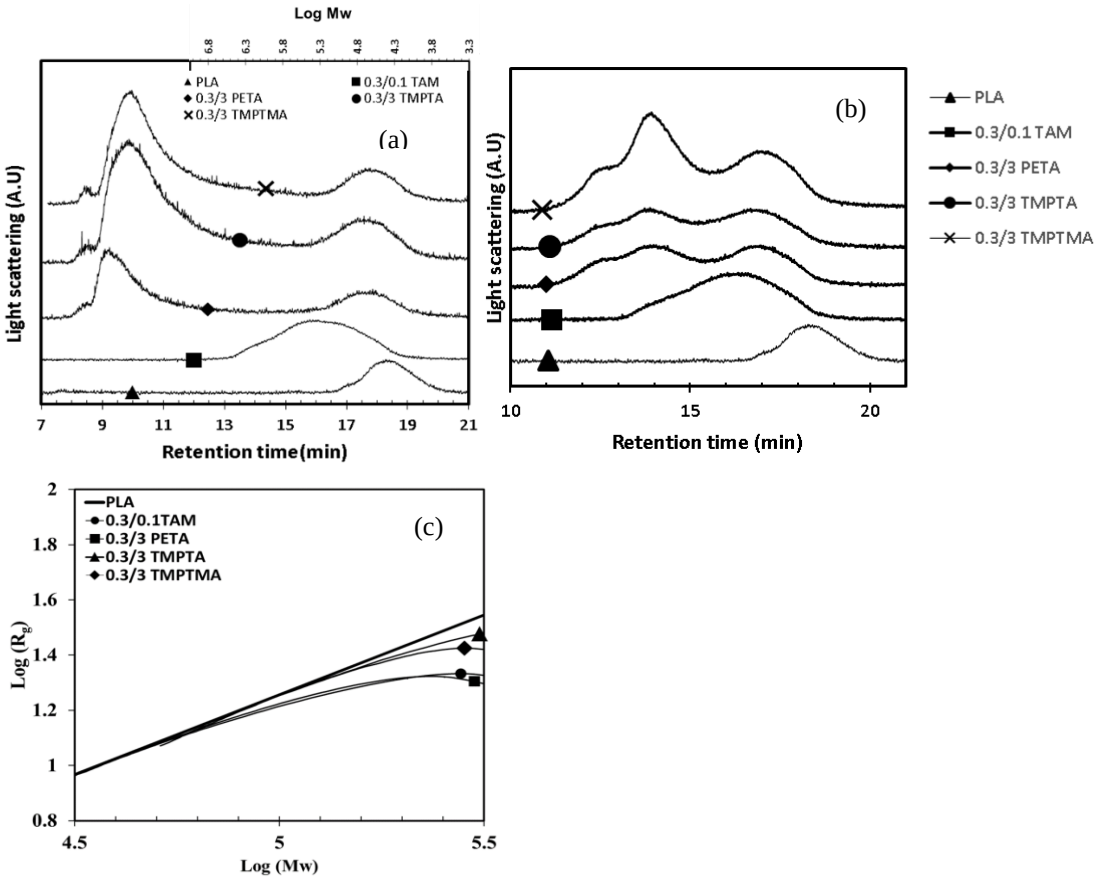

Figure 5.9: (a) Light scattering response of PLAs reacted by various coagents before purification plotted against retention volume; the secondary abscissa shows molecular weight calculated from universal calibration corresponding to retention volume on primary abscissa, and (b) Light scattering response of PLAs reacted by various coagents after purification (c) Radius of gyration as a function of molecular weight.

Figures 5.10 (a)-(d) and **Table 5.1** serve to present a comparison between the molar mass measurements obtained for the various coagents, at different coagent loadings. Even though the M_w increased only modestly upon modification with coagents, there is a very pronounced effect in the M_z, suggesting that the branching effects are represented by this quantity. These figures demonstrate once more that TAM is much more effective compared to the acrylate coagents, which have more modest effects, and that Mz is particularly affected by the coagent amount. It becomes apparent here that, consistently with previous findings the TMPTA coagent was more effective compared to the rest of the acrylate ones, whereas TMPTMA and PETA did not alter the PLA structure substantially. The ineffectiveness of TMPTMA in engaging in branching reactions has been demonstrated previously in PP due to stearic hindrance of methyl group [57,58].

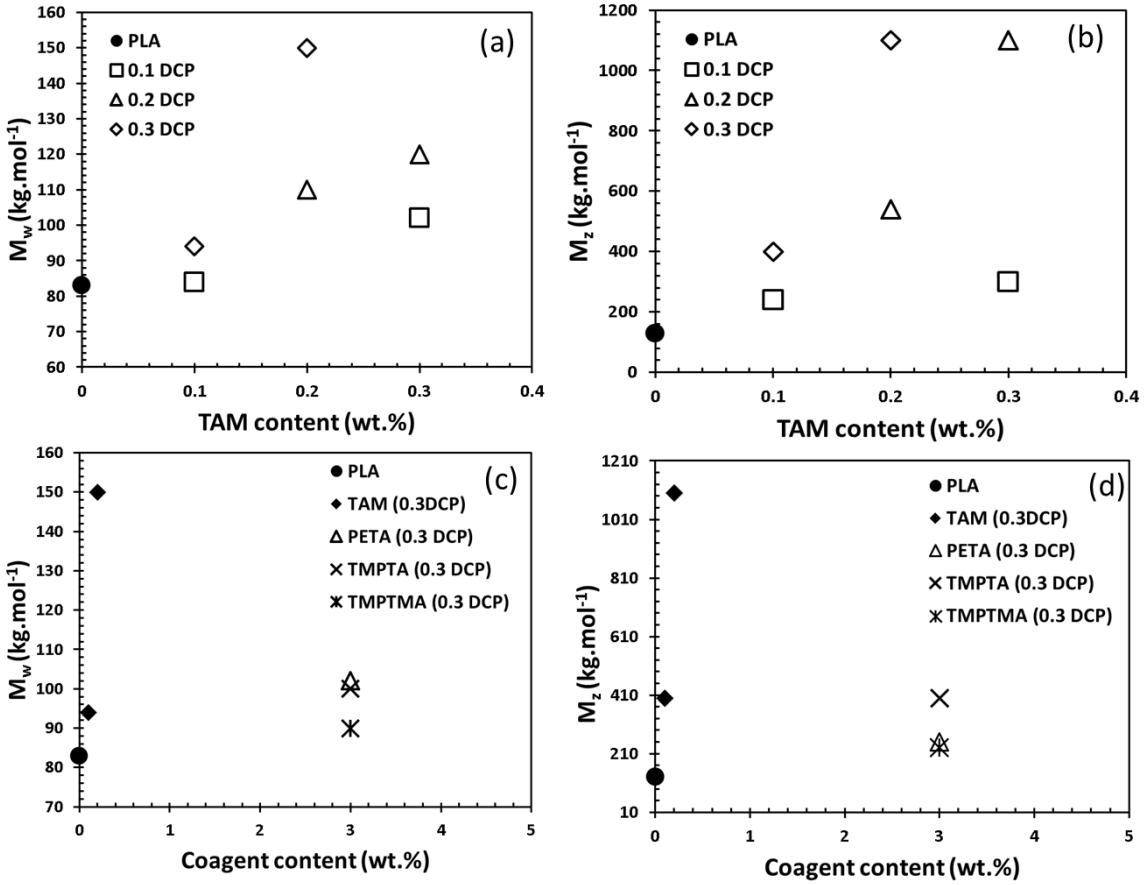

Figure 5.10: **(a) M_w as a function of DCP and TAM content (b) M_z as a function of DCP and TAM content (c) M_w as a function coagent type and amount (d) M_z as a function coagent type and amount.**

5.3.4 Branched PLA Structure

The structure of PLA branched through free-radical means, in the presence of coagents has been studied previously [26,38,39]. The presence of mixtures of linear and long-chain branched macromolecular structures have been speculated in PLA irradiated by electron beam and gamma ray radiation [38,39]. In these reports, there is also evidence of chain scission, which generates a distribution of branch lengths. In fact comb-like structures were also reported in the presence of PETA coagent [26], stemming from the presence of macroradicals generated through chain scission.

However, in the present case, we saw no evidence of chain scission. Therefore, given the most likely mechanism for free-radical reaction suggested by Nerkar et al. [59], a plausible chain structure would consist of mixtures of linear PLA chains that are unreacted, and LCB structures that are generated through combination of the tri-functional coagent with the PLA macroradicals. This type

of branched structure would be very prone to network formation through cross-linking as the amount of the trifunctional coagents increases further. This conceptual branched structure is supported by the LVE characterization, and specifically the activation energy measurements, which follow the behaviour that is expected for uniformly long-chain branched melts. The presence of LCB is also supported by the enhanced shear thinning behaviour seen in coagent modified samples (**Figure 5.6**), and the pronounced deviations seen in the plots of radius of gyration versus molar mass (**Figure 5.8b and 5.9b**).

Even though not strictly applicable for the types of complex structures generated through free-radical reactions, the Zimm-Stockmeyer equation has been used extensively as a means to compare the amount of branching between different samples in PP [60,61] and PLA [39]. According to the model the contraction factor, g (equation 5) can be used to calculate branch points per molecule, m. For a trifunctional randomly branched polymer, g can be related to m by equation 5 as [55]:

$$g = \left[\left(1 + \frac{m}{7}\right)^{0.5} + \frac{4m}{9\pi}\right]^{-0.5} \qquad (5)$$

These evaluations applied to the GPC data obtained for the purified samples are shown in Figure 5.11, and show clearly that increasing the amount of TAM in the formulations resulted in more branching, and that among the acrylate coagents, TMPTA was the most effective

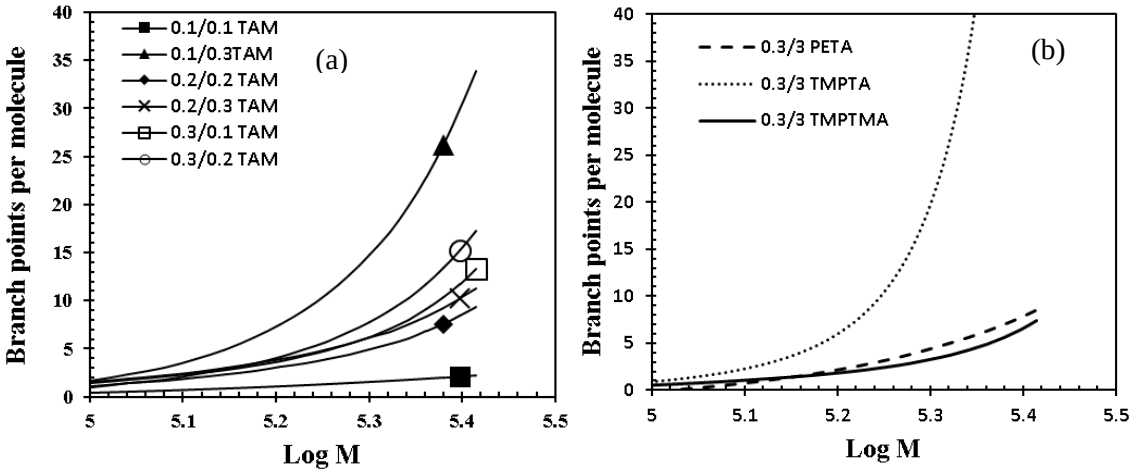

Figure 5.11: Branch points per molecule (m) plotted against weight average molecular weight for (a) Allylic coagent, (b) Acrylate coagents.

Whereas SEC characterization by itself cannot provide evidence of the type of branching, the combination of the zero shear viscosity measurements with the SEC results, in the form of a plot of zero shear viscosity versus M_w provides useful insight (**Figure 5.12**). In this plot the dependence of η_0 on M_w is well-established for linear PLA as [62]:

$$\eta_0 = K.M_w^a \quad (6)$$

where η_0 is zero shear viscosity, M_w is weight average molecular weight of linear PLA, and logK = -14.2 while a=3.4 for PLA.

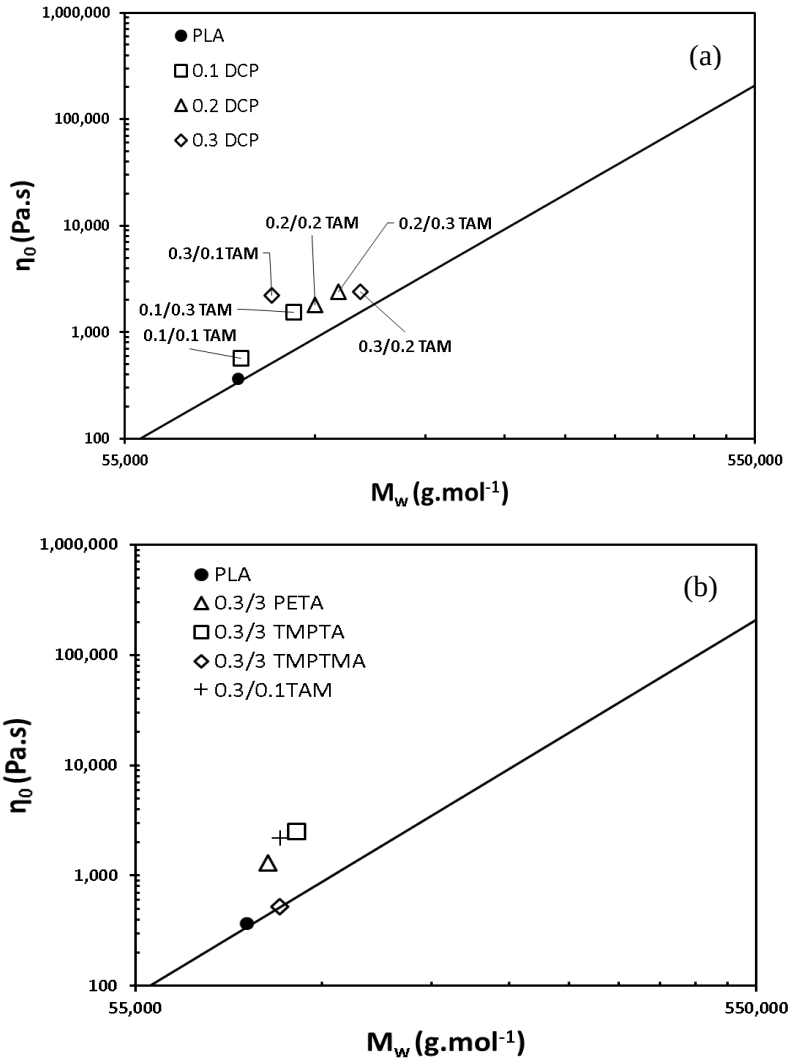

Figure 5.12: Zero shear viscosity, obtained from oscillatory measurements with respect to weight average molecular weight, obtained from light scattering measurements for (a) PLAs modified with TAM, (b) PLAs modified with other coagents.

PLA formulations reacted with DCP and TAM (**Figure 5.12(a)**) showed positive deviation from the power-law dependence. Positive deviations are usually ascribed to a high degree of entanglements in the presence of LCB. [1,33,38,60]

It is interesting to note that samples modified with the acrylate coagents PETA, TMPTA showed deviations as well, whereas TMPTMA did not deviate from the linear fit (**Figure 5.12(b)**). This corroborates that the TMPTMA was able to introducing LCB. This may be attributed to the low grafting efficiencies, owing to the oligomerization side-reaction, which results in the formation of a separate phase [56] eluting as high molar mass material (**Figure 5.9a**), as explained earlier

In spite of the moderate effects seen in these charts, it is worth noting that the zero shear viscosity had a very pronounced dependence on M_z, following a power-law trend, up to an M_z of about 10^6, before leveling off **(Figure 5.13a)**. This suggests that the branching is mostly reflected in the high molecular weight tail and influences profoundly the LVE properties. Similar is the case for relaxation time calculated from the Cross model which shows a strong dependence on M_z (**Figure 5.13b**).

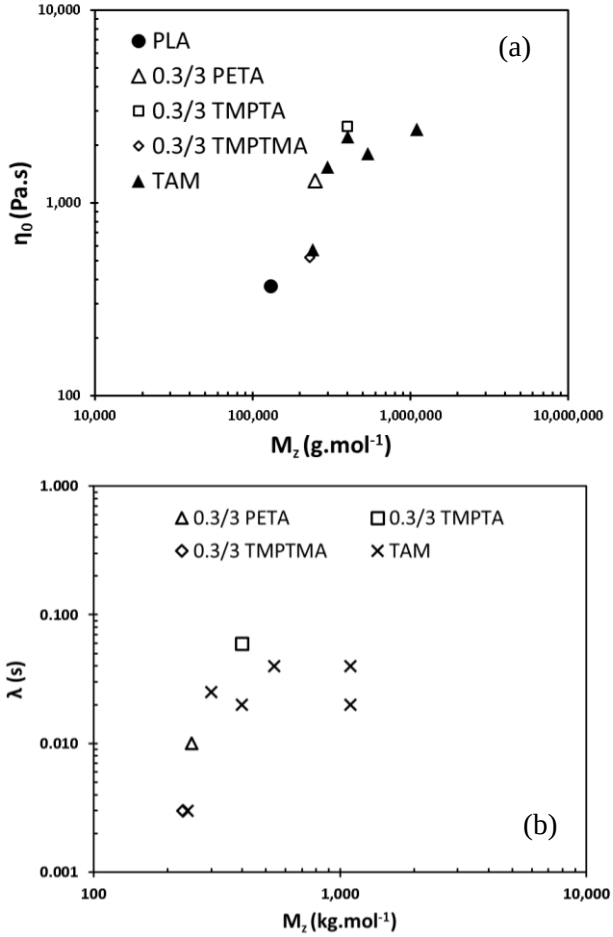

Figure 5.13: (a) Zero shear viscosity as a function of M_z (b) Relaxation time as a function of M_z. The solid line in (a) represents a power-law trendline

5.4. Conclusions

This chapter has compared the effect of the type (allylic versus acrylic) and amount of tri-functional coagents on the LVE properties of PLA branched in the presence of dicumyl peroxide. Based on detailed rheological and size exclusion chromatography measurements, differences between the activity of allylic and acrylic coagent in introducing long chain branching (LCB) was evident. PLA modified with allylic coagent (TAM) in the presence of peroxide exhibited higher zero shear viscosity, more pronounced shear thinning, and higher activation energy of flow when compared to neat PLA. In PLA modified with TAM, the broadening of molecular weight distribution peak and deviation from linearity in the radius of gyration versus molecular weight graph as well as deviation from power-law dependence of zero shear viscosity versus molecular weight suggested formation of LCB architecture in the high molecular weight fractions. The three acrylate coagents studied (TMPTA, TMPTMA, and PETA) generated more moderate effects, when compared to TAM, suggesting relatively poor grafting efficiency.

In the next chapter of this thesis, the most efficient coagent TAM is further studied for its ability to influence the thermal and sold-state properties of branched PLA.

5.5 References

(1) Härth, M.; Kaschta, J.; Schubert, D. W. Shear and elongational flow properties of long-chain branched poly(ethylene terephthalates) and correlations to their molecular structure. *Macromolecules* **2014**, *47* (13), 4471–4478.

(2) Kruse, M.; Wagner, M. H. Rheological and molecular characterization of long-chain branched poly(ethylene terephthalate). *Rheol. Acta* **2017**, *56* (11), 887–904.

(3) Makkam, S.; Harnnarongchai, W. Rheological and mechanical properties of recycled PET modified BY reactive extrusion. *Energy Procedia* **2014**, *56* (C), 547–553.

(4) Villalobos, M.; Awojulu, A.; Greeley, T.; Turco, G.; Deeter, G. Oligomeric chain extenders for economic reprocessing and recycling of condensation plastics. *Energy* **2006**, *31* (15), 3227–3234.

(5) Bikiaris, D. N.; Karayannidis, G. P. Thermomechanical analysis of chain-extended PET and PBT. *J. Appl. Polym. Sci.* **1996**, *60* (1), 55–61.

(6) Inata, H.; Matsumura, S. Chain extenders for polyesters. V. Reactivities of hydroxyl-addition-type chain extender; 2,2′-bis(4h-3,1-benzoxazin-4-one). *J. Appl. Polym. Sci.* **1987**, *34* (7), 2609–2617.

(7) Bikiaris, D. N.; Karayannidis, G. P. Chain extension of polyesters PET and PBT with two new diimidodiepoxides. II. *J. Polym. Sci. Part A Polym. Chem.* **1996**, *34* (7), 1337–1342.

(8) Kylmä, J.; Tuominen, J.; Helminen, A.; Seppälä, J. Chain extending of lactic acid oligomers. Effect of 2,2′-bis(2-oxazoline) on 1,6-hexamethylene diisocyanate linking reaction. *Polymer* **2001**, *42* (8), 3333–3343.

(9) Tuominen, J.; Kylmä, J.; Seppälä, J. Chain extending of lactic acid oligomers. 2. Increase of molecular weight with 1,6-hexamethylene diisocyanate and 2,2′-bis(2-oxazoline). *Polymer.* **2002**, *43* (1), 3–10.

(10) Di, Y.; Iannace, S.; Di Maio, E.; Nicolais, L. Reactively Modified Poly(lactic acid): Properties and Foam Processing. *Macromol. Mater. Eng.* **2005**, *290* (11), 1083–1090.

(11) Ren, J.; Wang, Q.-F.; Gu, S.-Y.; Zhang, N.-W.; Ren, T.-B. Chain-linked lactic acid polymers by benzene diisocyanate. *J. Appl. Polym. Sci.* **2006**, *99* (3), 1045–1049.

(12) Gu, S.; Yang, M.; Yu, T.; Ren, T.; Ren, J. Synthesis and characterization of biodegradable lactic acid-based polymers by chain extension. *Polym. Int.* **2008**, *57* (8), 982–986.

(13) Cailloux, J.; Santana, O. O.; Franco-Urquiza, E.; Bou, J. J.; Carrasco, F.; Gámez-Pérez, J.; Maspoch, M. L. Sheets of branched poly(lactic acid) obtained by one step reactive extrusion calendering process: Melt rheology analysis. *Express Polym. Lett.* **2012**, *7* (3), 304–318.

(14) Li, H.; Huneault, M. A. Effect of chain extension on the properties of PLA/TPS blends. *J. Appl. Polym. Sci.* **2011**, *122* (1), 134–141.

(15) Al-Itry, R.; Lamnawar, K.; Maazouz, A. Improvement of thermal stability, rheological and mechanical properties of PLA, PBAT and their blends by reactive extrusion with functionalized epoxy. *Polym. Degrad. Stab.* **2012**, *97* (10), 1898–1914.

(16) Pilla, S.; Kramschuster, A.; Yang, L.; Lee, J.; Gong, S.; Turng, L.-S. Microcellular injection-molding of polylactide with chain-extender. *Mater. Sci. Eng. C* **2009**, *29* (4), 1258–1265.

(17) Mihai, M.; Huneault, M. A.; Favis, B. D. Rheology and extrusion foaming of chain-branched poly(lactic acid). *Polym. Eng. Sci.* **2010**, *50* (3), 629–642.

(18) Corre, Y.-M.; Duchet, J.; Reignier, J.; Maazouz, A. Melt strengthening of poly (lactic acid) through reactive extrusion with epoxy-functionalized chains. *Rheol. Acta* **2011**, *50* (7–8), 613–629.

(19) Cailloux, J.; Santana, O. O.; Franco-Urquiza, E.; Bou, J. J.; Carrasco, F.; Maspoch, M. L. Sheets of branched poly(lactic acid) obtained by one-step reactive extrusion-calendering process: Physical aging and fracture behavior. *J. Mater. Sci.* **2014**, *49* (11), 4093–4107.

(20) Takamura, M.; Nakamura, T.; Takahashi, T.; Koyama, K. Effect of type of peroxide on cross-linking of poly(l-lactide). *Polym. Degrad. Stab.* **2008**, *93* (10), 1909–1916.
(21) Takamura, M.; Nakamura, T.; Kawaguchi, S.; Takahashi, T.; Koyama, K. Molecular characterization and crystallization behavior of peroxide-induced slightly crosslinked poly(L-lactide) during extrusion. *Polym. J.* **2010**, *42* (7), 600–608.
(22) Takamura, M.; Sugimoto, M.; Kawaguchi, S.; Takahashi, T.; Koyama, K. Influence of extrusion temperature on molecular architecture and crystallization behavior of peroxide-induced slightly crosslinked poly(L-lactide) by reactive extrusion. *J. Appl. Polym. Sci.* **2012**, *123* (3), 1468–1478.
(23) Södergård, A.; Näsman, J. H. Stabilization of poly(l-lactide) in the melt. *Polym. Degrad. Stab.* **1994**, *46* (1), 25–30.
(24) Soedergaard, A.; Niemi, M.; Selin, J.-F.; Naesman, J. H. Changes in Peroxide Melt-Modified Poly(L-lactide). *Ind. Eng. Chem. Res.* **1995**, *34* (4), 1203–1207.
(25) Carlson, D.; Dubois, P.; Nie, L.; Narayan, R. Free radical branching of polylactide by reactive extrusion. *Polym. Eng. Sci.* **1998**, *38* (2), 311–321.
(26) You, J.; Lou, L.; Yu, W.; Zhou, C. The preparation and crystallization of long chain branching polylactide made by melt radicals reaction. *J. Appl. Polym. Sci.* **2013**, *129* (4), 1959–1970.
(27) Yang, S. lin; Wu, Z. H.; Yang, W.; Yang, M. B. Thermal and mechanical properties of chemical crosslinked polylactide (PLA). *Polym. Test.* **2008**, *27* (8), 957–963.
(28) Quynh, T. M.; Mitomo, H.; Nagasawa, N.; Wada, Y.; Yoshii, F.; Tamada, M. Properties of crosslinked polylactides (PLLA & PDLA) by radiation and its biodegradability. *Eur. Polym. J.* **2007**, *43* (5), 1779–1785.
(29) Stange, J.; Uhl, C.; Münstedt, H. Rheological behavior of blends from a linear and a long-chain branched polypropylene. *J. Rheol.* **2005**, *49* (5), 1059.
(30) Auhl, D.; Stange, J.; Münstedt, H.; Krause, B.; Voight, D.; Lederer, A.; Lappan, U.; Lunkwitz, K. Long-chain branched polypropylenes by electron beam radiation and their reological properties. *Macromolecules* **2004**, *37*, 9465–9472.
(31) Costeux, S.; Wood-Adams, P.; Beigzadeh, D. Molecular structure of metallocene-catalyzed polyethylene: Rheologically relevant representation of branching architecture in single catalyst and blended systems. *Macromolecules* **2002**, *35* (7), 2514–2528.
(32) Wood-Adams, P. M.; Dealy, J. M.; DeGroot, A. W.; Redwine, O. D. Effect of molecular structure on the linear viscoelastic behavior of polyethylene. *Macromolecules* **2000**, *33* (20), 7489–7499.
(33) Nouri, S.; Dubois, C.; Lafleur, P. G. Effect of chemical and physical branching on rheological behavior of polylactide. *J. Rheol.* **2015**, *59* (4), 1045–1063.
(34) Gu, L.; Xu, Y.; Fahnhorst, G.; Macosko, C. W. Star vs long chain branching of poly(lactic acid) with multifunctional aziridine. *J. Rheol.* **2017**, *61*, 785–796.
(35) Meng, Q.; Heuzey, M. C.; Carreau, P. J. Control of thermal degradation of polylactide/clay nanocomposites during melt processing by chain extension reaction. *Polym. Degrad. Stab.* **2012**, *97* (10), 2010–2020.
(36) Najafi, N.; Heuzey, M. C.; Carreau, P. J.; Therriault, D.; Park, C. B. Rheological and foaming behavior of linear and branched polylactides. *Rheol. Acta* **2014**, *53* (10–11), 779–790.
(37) Najafi, N.; Heuzey, M. C.; Carreau, P. J.; Wood-Adams, P. M. Control of thermal degradation of polylactide (PLA)-clay nanocomposites using chain extenders. *Polym. Degrad. Stab.* **2012**, *97* (4), 554–565.
(38) Fang, H.; Zhang, Y.; Bai, J.; Wang, Z.; Wang, Z. Bimodal architecture and rheological and foaming properties for gamma-irradiated long-chain branched polylactides. *RSC Adv.* **2013**, *3* (23), 8783.

(39) Wang, Y.; Yang, L.; Niu, Y.; Wang, Z.; Zhang, J.; Yu, F.; Zhang, H. Rheological and topological characterizations of electron beam irradiation prepared long-chain branched polylactic acid. *J. Appl. Polym. Sci.* **2011**, *122* (3), 1857–1865.
(40) Liu, J.; Zhang, S.; Zhang, L.; Bai, Y. Crystallization behavior of long-chain branching polylactide. *Ind. Eng. Chem. Res.* **2012**, *51* (42), 13670–13679.
(41) Liu, J.; Zhang, S.; Zhang, L.; Bai, Y. Preparation and rheological characterization of long chain branching polylactide. *Polymer.* **2014**, *55* (10), 2472–2480.
(42) Liu, J.; Lou, L.; Yu, W.; Liao, R.; Li, R.; Zhou, C. Long chain branching polylactide: Structures and properties. *Polymer.* **2010**, *51* (22), 5186–5197.
(43) Gu, L.; Xu, Y.; Fahnhorst, G.; Macosko, C. W. Long chain branching of PLA. **2017**, *30006*, 30006.
(44) Das, C.; Read, D. J.; Auhl, D.; Kapnistos, M.; den Doelder, J.; Vittorias, I.; McLeish, T. C. B. Numerical prediction of nonlinear rheology of branched polymer melts. *J. Rheol.* **2014**, *58* (3), 737–757.
(45) Das, C.; Inkson, N. J.; Read, D. J.; Kelmanson, M. A.; McLeish, T. C. B. Computational linear rheology of general branch-on-branch polymers. *J. Rheol.* **2006**, *50* (2), 207–234.
(46) Xu, H.; Fang, H.; Bai, J.; Zhang, Y.; Wang, Z. Preparation and characterization of high-melt-strength polylactide with long-chain branched structure through γ-radiation-induced chemical reactions. *Ind. Eng. Chem. Res.* **2014**, *53* (3), 1150–1159.
(47) Mavridis, H.; Shroff, R. N. Temperature dependence of polyolefin melt rheology. *Polym. Eng. Sci.* **1992**, *32* (23), 1778–1791.
(48) Stadler, F. J.; Kaschta, J.; Munstedt, H. Thermorheological behavior of various long-chain branched polyethylenes. *Macromolecules* **2008**, *41* (4), 1328–1333.
(49) Wood-Adams, P.; Costeux, S. Thermorheological behavior of polyethylene: Effects of microstructure and long chain branching. *Macromolecules* **2001**, *34* (18), 6281–6290.
(50) Cailloux, J.; Santana, O.; Bou, J. J.; Carrasco, F.; Maspoch, M. Using viscoelastic properties to quantitatively estimate the amount of modified poly(Lactic Acid) chains through reactive extrusion. *J. Rheol.* **2015**, *59* (5), 1191–1227.
(51) van Gurp, M.; Palmen, J. Time-temperature superposition for polymeric blends. *J Rheol Bull* **1998**, *65*, 5–8.
(52) Kapnistos, M.; Vlassopoulos, D.; Roovers, J.; Leal, L. G. Linear rheology of architecturally complex macromolecules: Comb polymers with linear backbones. *Macromolecules* **2005**, *38* (18), 7852–7862.
(53) Wood-Adams, P. M.; Dealy, J. M. Using rheological data to determine the branching level in metallocene polyethylenes. *Macromolecules* **2000**, *33* (20), 7481–7488.
(54) Stadler, F. J.; Piel, C.; Kaschta, J.; Rulhoff, S.; Kaminsky, W.; Münstedt, H. Dependence of the zero shear-rate viscosity and the viscosity function of linear high-density polyethylenes on the mass-average molar mass and polydispersity. *Rheol. Acta* **2006**, *45* (5), 755–764.
(55) Zimm, B. H.; Stockmayer, W. H. The Dimensions of Chain Molecules Containing Branches and Rings. *J. Chem. Phys.* **1949**, *17* (12), 1301–1314.
(56) Parent, J. S.; Sengupta, S. S.; Kaufman, M.; Chaudhary, B. I. Coagent-induced transformations of polypropylene microstructure: Evolution of bimodal architectures and cross-linked nano-particles. *Polymer.* **2008**, *49* (18), 3884–3891.
(57) Parent, J. S.; Bodsworth, A.; Sengupta, S. S.; Kontopoulou, M.; Chaudhary, B. I.; Poche, D.; Cousteaux, S. Structure–rheology relationships of long-chain branched polypropylene: Comparative analysis of acrylic and allylic coagent chemistry. *Polymer.* **2009**, *50* (1), 85–94.
(58) Zhang, Y.; Tiwary, P.; Parent, J. S.; Kontopoulou, M.; Park, C. B. Crystallization and foaming of coagent-modified polypropylene: Nucleation effects of cross-linked

nanoparticles. *Polymer.* **2013**, *54* (18), 4814–4819.
(59) Nerkar, M.; Ramsay, J. A.; Ramsay, B. A.; Vasileiou, A. A.; Kontopoulou, M. Improvements in the melt and solid-state properties of poly(lactic acid), poly-3-hydroxyoctanoate and their blends through reactive modification. *Polymer.* **2015**, *64*, 51–61.
(60) Auhl, D.; Stadler, F. J.; Munstedt, H. Comparison of Molecular Structure and Rheological Properties of Electron-Beam- and Gamma-Irradiated Polypropylene. *Macromolecules* **2012**, *45*, 2057–2065.
(61) Auhl, D.; Stange, J.; Münstedt, H.; Krause, B.; Voigt, D.; Lederer, A.; Lappan, U.; Lunkwitz, K. Long-chain branched polypropylenes by electron beam irradiation and their rheological properties. *Macromolecules* **2004**, *37* (25), 9465–9472.
(62) Othman, N.; Jazrawi, B.; Mehrkhodavandi, P.; Hatzikiriakos, S. G. Wall slip and melt fracture of poly(lactides). *Rheol. Acta* **2012**, *51* (4), 357–369.

Chapter 6

Tuning the rheological, thermal and solid-state properties of branched PLA by free-radical-mediated reactive extrusion

6.1 Introduction

Poly(lactide), or poly (lactic acid) (PLA) is a biobased and biodegradable aliphatic polyester. In spite of its potential to replace petroleum derived polyesters in commodity applications, its slow crystallization kinetics and low melt strength limit its application in common polymer processing methods, such as injection molding, blow molding, film processing, foaming, etc. [1–8].

The crystallization kinetics of PLA can be improved by adding nucleating agents such as inorganic fillers, nano-particles, organic nucleants, PLA stereocomplex, etc [9]. To address the lack of melt strength, chain extenders, such as polycarbodiimide, tris (nonylphenyl) phosphite, pyromellitic dianhydride (PMDA), triglycidyl isocyanurate (TGIC) and epoxy-functionalized oligomeric acrylic copolymer (trade name Joncryl® from BASF) have been used to introduce branching, and counteract the degradation of PLA [10–15].

Various structures like star, pom-pom, comb, tree, or highly dense networks have been reported in the resulting products [14–20]. PLA can be also be branched or crosslinked through free-radical processing, initiated by organic peroxides [21,22] or irradiation [23–25], in the presence multifunctional coagents, such as pentaertythritol triacrylate (PETA), trimethylolproprane triacrylate (TMPTA), and triallyl isocyanurate (TAIC) [23,24,26–29].

In comparison to the commonly used acrylate-based coagents an allylic coagent, triallyl trimesate (TAM) has emerged as a particularly potent coagent, at relatively low concentrations, as demonstrated in **Chapter 5.**

---

*A version of this chapter has been accepted for publication: **Praphulla Tiwary**, Marianna Kontopoulou, ACS Sustainable Chemistry & Engineering 2017 (DOI: 10.1021/acssuschemeng.7b03617)

A recent communication by our group [30] has shown that in addition to substantial improvements in the elasticity and strain hardening characteristics of PLA, grafting with TAM resulted in faster crystallization rates, both under isothermal and non-isothermal conditions. Similar improvements have been reported in TAM-modified polypropylene (PP) in the previous chapters of this thesis (**Chapters 2-4**). The potential of using low amounts of peroxide and coagents in these modifications is very attractive, given the desire to keep additives at a minimum level to maintain the designation of a fully bio derived polymer

Given that the macroscopic mechanical properties of polymers are intimately related to their molar mass distribution, chain branching, and crystalline structure, it is expected that the modifications reported earlier will affect profoundly the properties of these coagent-modified formulations. In this chapter we examine in detail the evolution of molecular weight, thermorheological, and mechanical properties of PLA, prepared by reactive extrusion using various amounts of peroxide and TAM coagent, and we present short-term data for their hydrolytic degradation profile. An additional contribution of this chapter is that a more industrially-applicable reactive extrusion process is adopted.

6.2 Materials and Methods

6.2.1 Materials

PLA 3251D, MFI 80 g.10 min^{-1} at 210°C/2.16 kg, injection moulding grade, designated as PLA1 and PLA 2500 HP, MFI 8 g.10 min^{-1} at 210°C/2.16 kg, extrusion grade, designated as PLA2 were obtained from NatureWorks®. Triallyl trimesate (TAM, 98% purity, Monomer-Polymer and Dajac labs.), dicumyl peroxide (DCP, 98% purity), tetrahydrofuran (THF, HPLC grade), chloroform (HPLC grade), and acetone were used as received. The solvents and peroxide were obtained from Sigma-Aldrich Canada. All the chemicals and the polymers were used as received.

6.2.2 Reactive Extrusion

Reactive extrusion was conducted using a twin screw co-rotating extruder (Coperion ZSK 18 ML) equipped with a strand die, water cooling bath, and pelletizer, using the low shear screw design shown in **Fig. 6.1**. A masterbatch was prepared by coating ground PLA powder with an acetone solution containing DCP and coagent and allowing the solvent to evaporate. This masterbatch was mixed with dried neat PLA1 in appropriate ratios to yield the desired concentration of DCP and coagent (**Table 6.1**) in the system. The sample designation is PLA/a/b where ‘a’ denotes

concentration of DCP in weight percentage and 'b' denotes concentration of TAM in weight percentage (**Table 6.1**). The temperature profile was 170/190/190/190/190/190/190 ˚C (hopper to die). The extrusion was performed at a feeder speed of 30 min^{-1} with screw speed of 120 min^{-1} (corresponding to an average throughput of 1.5 $kg.hr^{-1}$) and average residence time of 2 min 30 s, (the half-life time of DCP is $t_{1/2}$= 0.3-0.8 min at 190˚C [31]) to allow for the complete reaction of PLA1. The neat PLAs, were processed in similar fashion.

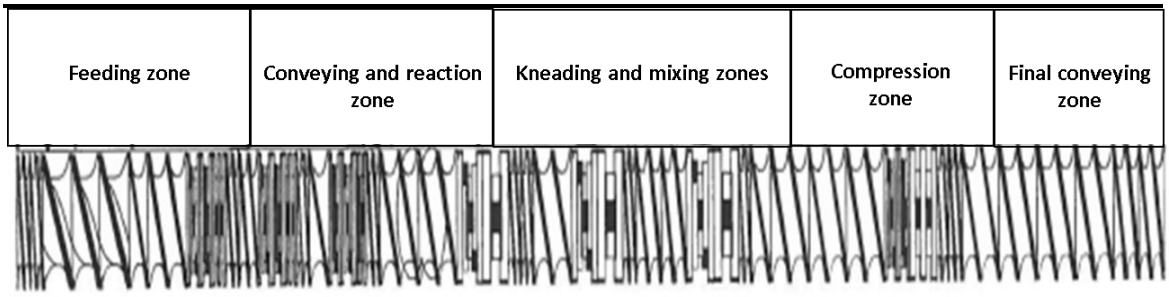

Figure 6.1 Screw design used in the reactive extrusion.

6.2.3 Spectroscopic characterization

To confirm grafting of TAM, a UV-Vis Agilent Cary 100 spectrophotometer equipped with Agilent Cary WinUV software was used. The scans were performed from 800 to 200 nm at the rate of 600 $nm.min^{-1}$. The PLA samples (5 g) were purified by dissolving in chloroform (20 ml) and precipitating with excess methanol. The purified samples were further dissolved in chloroform at a concentration of 20 $mg.ml^{-1}$ and transferred to quartz cuvettes. Baseline scans with only chloroform were performed. Different concentrations of pure TAM in chloroform were used to obtain a calibration curve relating to the peak height at 241 nm, which corresponds to the aromatic ring present in the TAM molecule. The quantitative information of the percentage grafting was obtained for all formulations by using the calibration curve, and is shown in Table 6.1.

Representative spectra for PLA 0.3/0.1, (**Fig. 6.2)** show a distinct peak corresponding to the aromatic ring, confirming that TAM is grafted on PLA. The amount of graft thus estimated for all the formulations reacted with DCP and TAM ranged between 0.1-0.3 wt.% of the amount of TAM originally added, suggesting that the grafting efficiency was very low.

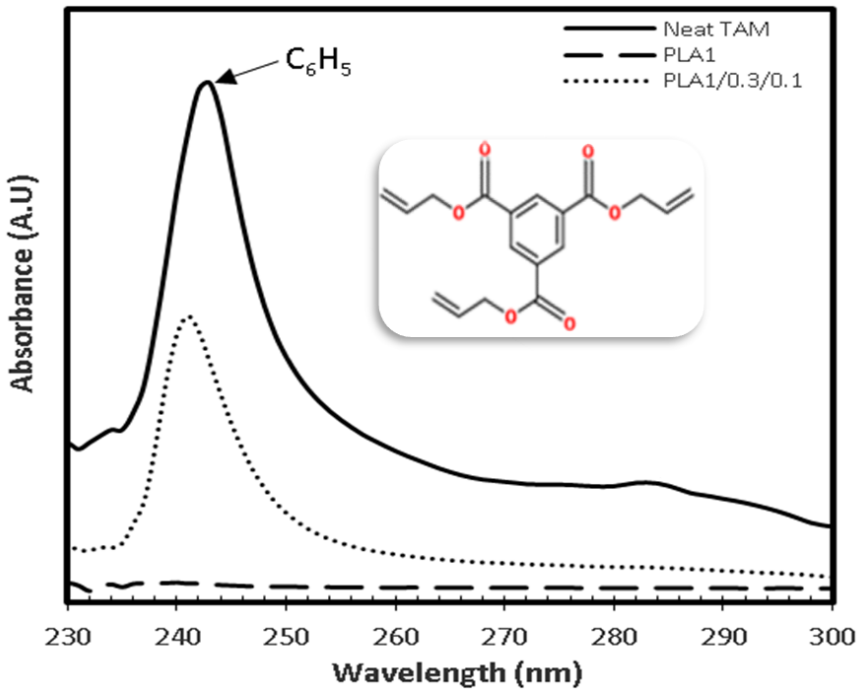

Figure 6.2 UV-Vis spectra of neat TAM, PLA1, and PLA1/0.3/0.1. Inset shows the chemical structure of TAM. Curves have been shifted by arbitrary factor.

6.2.4 Gel Content Analysis and Gel Permeation Chromatography (GPC)

Gel content analysis was conducted by extraction within boiling THF from a 120 mesh stainless steel sieve for 6 h, according to ASTM D 2765. The samples were dried overnight in a vacuum oven at 60° C to remove the residual solvent. The residual polymer was dried to constant weight, with gel contents reported as a weight percentage of unextracted material.

GPC characterization was performed in a Viscotek 270max separation module equipped with triple detectors as differential refractive index (DRI), viscosity (IV), and light scattering (low angle, LALS and right angle, RALS). The separation module was maintained at 40 °C and contained two porous PolyAnalytik columns in series with an exclusion molecular weight limit of 209,106 Da. Distilled tetrahydrofuran (THF) was used as the eluent at a flow rate of 1 $mL.min^{-1}$. The results from the triple detector train and Viscotek Omnisec software were used to determine polymer molar mass distributions using the value of the refractive index (dn/dc) as 0.0478 $ml.mg^{-1}$.

6.2.5 Rheological characterization

A 25mm parallel plate fixture hosted on a MCR-301 Anton Paar rheometer was used in the oscillatory mode with a gap of 1.2 mm to measure linear viscoelastic properties at 180°C under nitrogen atmosphere. Stress sweeps were performed to ensure that all the measurements were within linear viscoelastic regime.

The complex viscosity data were fitted to the Cross model given by equation (3) to estimate the zero shear viscosities.

$$|\eta^*(\omega)| = \frac{\eta_0}{1+|\lambda\omega|^{(1-n)}} \quad (1)$$

where η^* is the complex viscosity, η_0 is the zero shear viscosity, λ is the relaxation time, n is the constant related to shear thinning behavior, and ω is the frequency in rad.s^{-1}.

Equation (4) was used to describe the rheology of formulations that followed a power-law dependence:

$$|\eta^*(\omega)| = K\omega^n \quad (2)$$

where η^* is the complex viscosity, K is consistency index, *n* is the constant related to shear thinning behavior, and ω is the frequency in rad.s^{-1}.

Samples were characterized in a uniaxial testing platform from Xpansion instruments hosted on a MCR-301 Anton Paar rheometer [32]. The measurements were conducted at 180°C at an extension rate of 0.1, 1, and 10 s^{-1}. The linear viscoelastic (LVE) oscillatory measurements obtained at 180 °C were used to calculate the LVE stress growth curve, η^+, and to check the consistency of the extensional measurements. For a more quantitative estimation of the strain hardening phenomena, the strain hardening coefficient, S, was calculated according to

$$S = \frac{\eta_E^+(t,\dot{\varepsilon}_0)}{3.\eta^+(t)} \quad (3)$$

The curve corresponding to $3\eta^+$ represents the LVE envelope in uniaxial extension, according to Trouton's law.

6.2.6 Injection Molding

Injection molding was done using a Nissei ES 200 ELJECT injection molder with a fixed mold temperature of 25°C and mold cooling time of 30 s. The injection pressure was set to 1000 psi with injection speed of 30 mm.min^{-1}. The injection molding temperature was kept constant at 190°C, from hopper to nozzle. Minor adjustments in injection pressure were done to achieve complete filling of the mold.

6.2.7 Mechanical Properties and heat deflection temperature (HDT) testing

Tensile tests were performed in an Instron 3369 universal testing machine equipped with a 50 N load cell. Tensile tests were done on injection molded samples according to ASTM D 638 (type IV sample, cross head speed of 5 mm.min^{-1}). An impact tester from Satec System Inc. equipped with a 7 lbs. hammer was used to perform unnotched Izod impact tests of injection molded specimens according to ASTM D 256. Flexural tests were performed on compression molded specimens according to ISO 178 (cross head speed of 2 mm.min^{-1}). All the mechanical tests were performed after 48 hours of injection molding.

For heat deflection temperature (HDT) measurements, specimens (127 mm x 13 mm x 3 mm) were prepared by compression molding using a Carver press under 5000 N force, at 200 ˚C with a residence time of 3 min. Specimens were lowered in a silicon oil bath and the temperature was increased from 23˚C at a heating rate of 120˚C/h until 0.25 mm deflection occurred under a load of 1.82 MPa, in accordance with ASTM D648. At least three specimens were tested and the average value was reported.

6.2.8 Hot stage Microscopy

A Linkam CSS450 hot stage setup mounted on Olympus BX51 optical microscope was used to observe the growth of crystals under crossed polarizers. Thin films were heated to 200°C at a rate of 30°C/min and held for 10 min to eliminate their thermal history. The melt was then cooled to 155°C at 30°C/min and the temperature was kept constant for 1 hr. The crystallization process was recorded through Sony ExwaveHAD 3 CCD digital recorder.

6.2.9 Differential scanning calorimetry (DSC)

Differential scanning calorimetry was conducted using a DSC Q1000 by TA instruments. Thermal cycles were performed between -30 to 210°C at heating and cooling rates of 5°C.min^{-1}. After the first heating scan, the samples were held isothermally at 210°C for 3 min before cooling at 5°C.min^{-1} to -30°C, to determine the peak crystallization temperatures according to ASTM D 3418. The heats of fusion and melting temperatures were determined from the melting endotherm that were obtained from the first and second heating scans. The percent crystallinity of the polymer, X_c, was estimated using Equation 4.

$$X_c = \frac{\Delta H_m - \Delta H_{cc}}{\Delta H_{100}} \text{ x } 100 \qquad (4)$$

where ΔH_m is the apparent fusion enthalpy, ΔH_{cc} stands for all cold crystallization transitions recorded during the heating scan, and ΔH_{100} is the theoretical fusion enthalpy of a 100% crystalline polymer, which is 93 J.g^{-1} for PLA [33].

6.2.10 Hydrolytic Degradation

Short-term hydrolytic degradation tests were conducted on compression molded discs (25 mm diameter, 1.5 mm thickness), immersed in distilled water, which was maintained at a constant temperature of 60°C. The total duration of the experiment was 5 days (120 hours), with sampling intervals of 12 hours. Discs were dried in a vacuum oven at 60°C for 12 hours to remove residual moisture. The degradation medium was also archived and replaced with fresh distilled water upon each extraction.

Samples were prepared for GPC by dissolving a 25 mg PLA disc cross-section in 10 ml of THF, yielding a solution of 2.5 mg.ml^{-1} concentration which presented good detector response. The details of GPC characterization are mentioned above.

6.3. Results

6.3.1 Effect of reactive modification on molecular weight and linear viscoelastic properties

The starting material, PLA1 was a linear PLA with weight average molar mass (M_w) of 83 kg. mol^{-1} and dispersity of 1.7 (**Table 6.1**) and (**Fig. 6.3a**). This material was modified using various amounts of peroxide and coagent, to produce branched or cross-linked derivatives having higher molar mass. PLA2 is a linear polymer having higher molar mass than PLA1 **(Table 6.1)**, which serves as a suitable comparison to the modified PLA1. The molar mass distributions, light scattering detector responses and Mark-Houwink (M-H) plots of these formulations are summarized in **Fig. 6.3 (a)** to **(c)** respectively.

The differences in molar mass are reflected in the rheological behavior of these materials; PLA2 exhibited higher complex viscosities than PLA1 throughout the measured frequency range **(Fig. 6.4a)**. Both linear PLAs had a pronounced Newtonian plateau, with minimal shear thinning, and a slope of 2 in the terminal region of the storage modulus vs. frequency plot, which is typical of a linear polymer behavior (**Figs. 6.4a and b**).

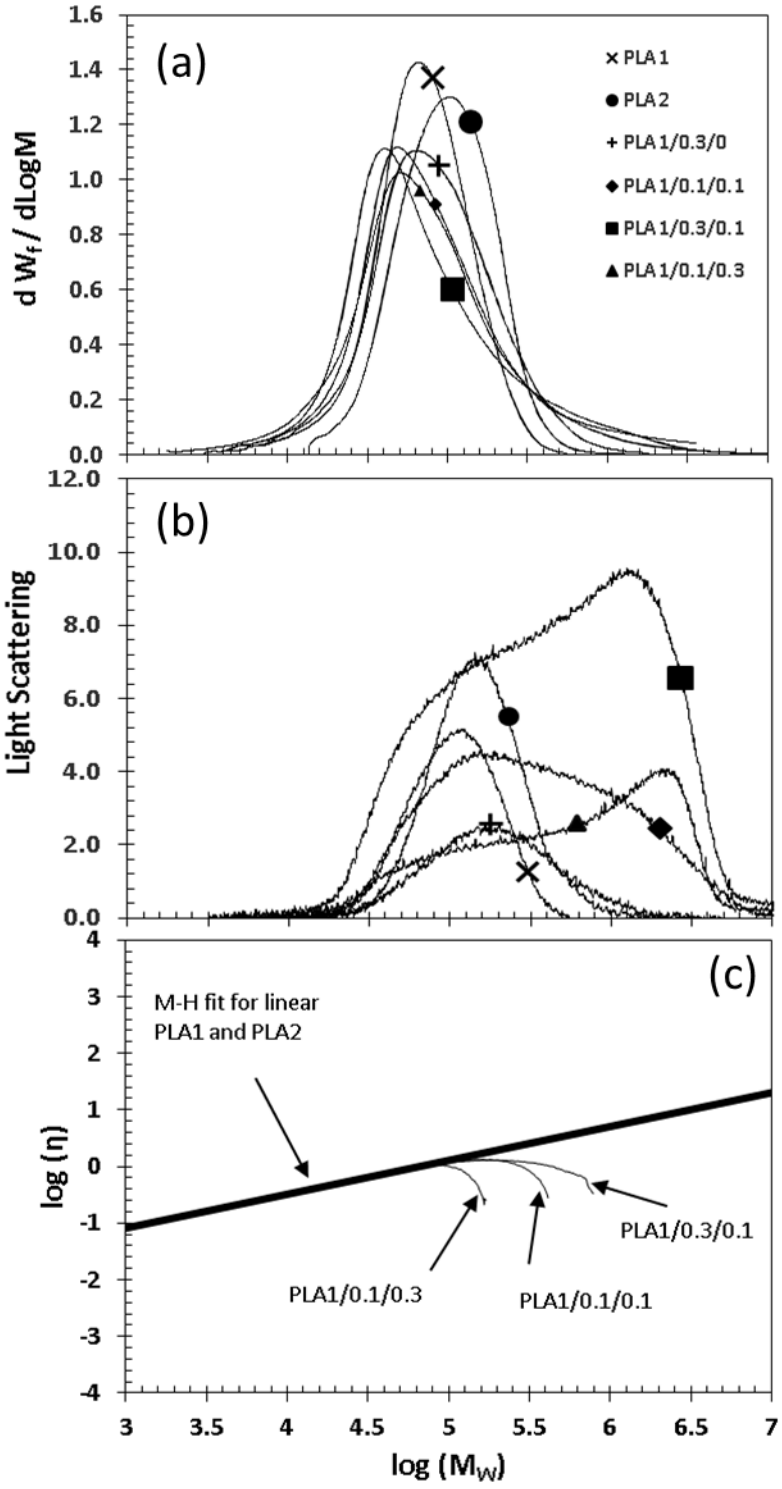

Figure 6.3 a) Molecular weight distribution, b) Light scattering analysis, and c) M-H fit of various PLAs. PLA1 and PLA2 follow power-law relation with Mark-Houwink constants of a=0.61 and log k = -3.96 dl.gm^{-1}.

Table 6.1 Molecular weight and rheological properties

Sample Designation	M_w (kg.mol^{-1})	Đ	M_z (kg.mol^{-1})	η_0 (Pa.s)	λ (s)	n
PLA1	83	1.7	129	400$^+$	-	-
PLA2	126	1.6	189	2,410	2x10^{-3}	0.4
PLA1/0.3/0	119	2.2	267	700	1x10^{-3}	0.5
PLA1/0/0.3	82	1.7	124	360$^+$	-	-
PLA1/0.1/0.1	117	2.8	480	1,070	3x10^{-3}	0.4
PLA1/0.3/0.1	150	4.3	727	3,100	0.15	0.6
PLA1/0.1/0.3	170	3.9	1000	12,000	3	0.6
PLA1/0.3/0.3*				Power law fit: K =20,000 Pa.s^n , n= 0.476		

M_w – Weight average molecular weight, M_z- Z-average molecular weight, Đ – Dispersity, η_o – Zero shear viscosity, λ - relaxation time, n – constant related to shear thinning behavior, $^+$Denotes plateau values as the samples were Newtonian in nature, *GPC measurements could not be performed because of the presence of gels in the formulation.

The zero-shear viscosities of PLA1 and PLA2 followed a linear trend with respect to M_w (**Fig. 6.5**) further confirming the linear structure of the chains [34]. Processing in the presence of peroxide only (sample PLA1/0.3/0) increased the molar mass and resulted in slightly broadened molar mass distribution when compared to neat PLA1 (**Fig. 6.3b**). Reaction of PLA with peroxide generates macroradicals [21,35], which may terminate by recombination resulting in branching. Since free-radical reactions occur randomly along the polymer backbone, a branch-on-branch structure has been suggested for these formulations [20]. However in the present case, the amount of peroxide is low, resulting in negligible amount of branching, when analyzing the M-H plot. These samples exhibited marginal increase in viscosity, attributed to the higher molar mass, and minor deviation from terminal flow (**Fig. 6.4a and b**), which is most likely attributed to the slight increase in dispersity, due to macroradical recombination.

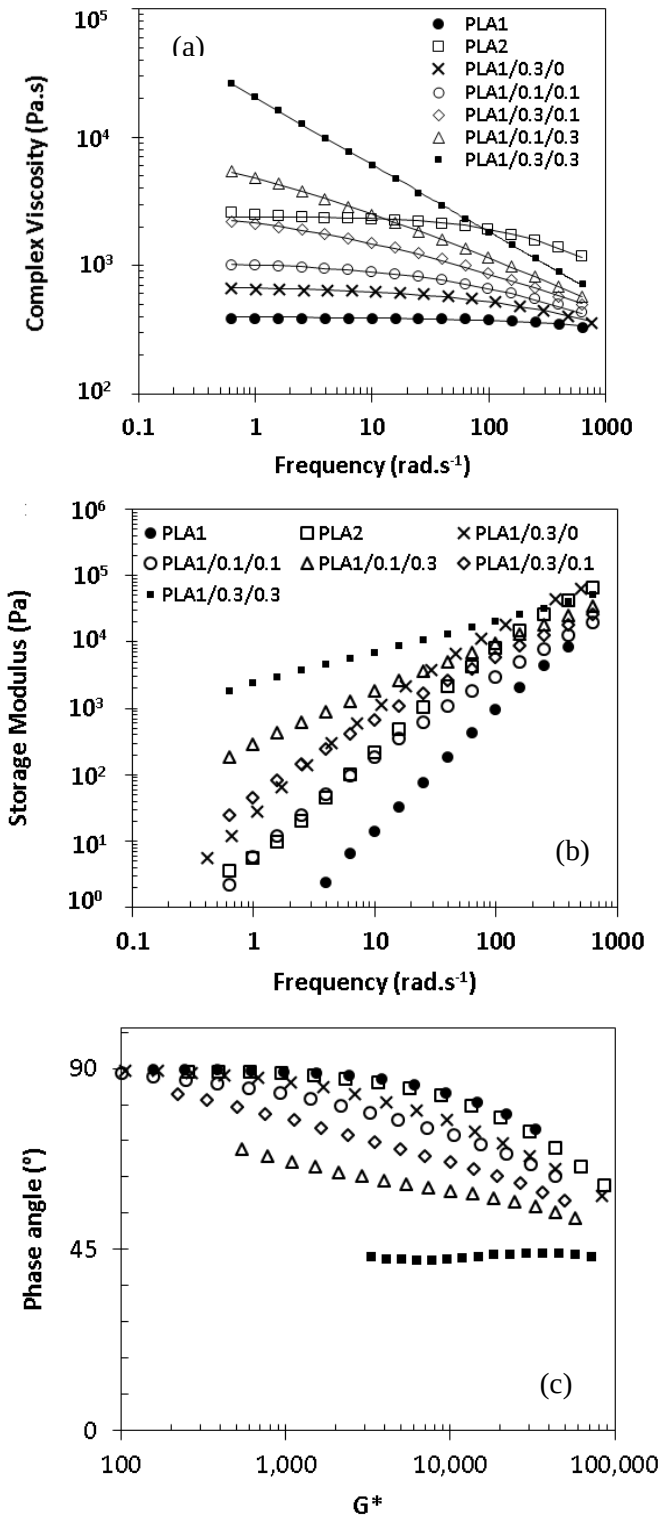

Figure 6.4 a) Complex viscosity and b) storage modulus as a function of frequency c) Van Gurp-Palmen plot. Solid lines in (a) represent the respective Cross model and power-law fit for samples at 180°C.

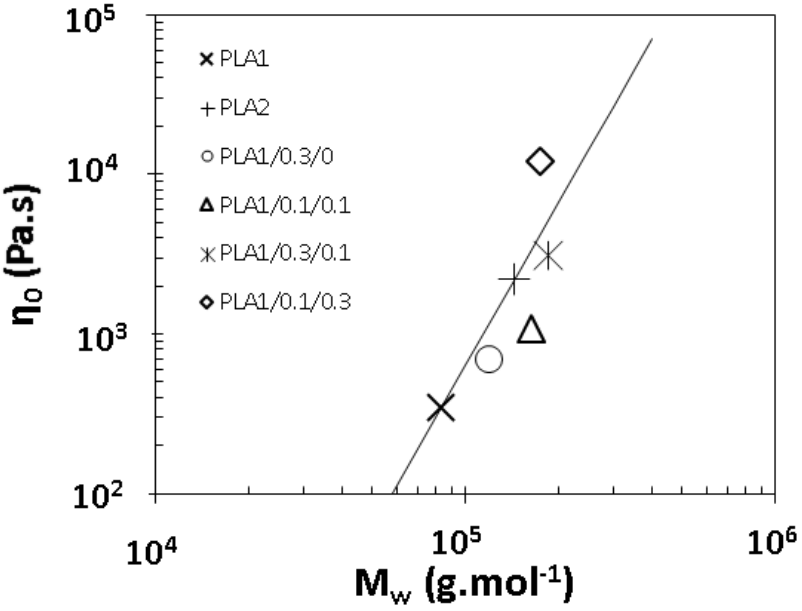

Figure 6.5 Zero shear viscosity obtained through Cross model plotted against weight average molecular weight obtained through light scattering. PLA1 and PLA2 followed the linear fit between Mw and η0 with value of log k= -14.2 and a= 3.4

On the contrary reaction with peroxide and coagent altered the molar mass distributions and the rheological response substantially. In addition to the increase in M_n and M_w, the formation of high molar mass fractions is evident by the increase in the M_z value (**Fig. 6.3a and b, Table 6.1**). Close inspection of the light scattering detector responses (**Fig. 6.3b**), shows broadening in the curves corresponding to the coagent-modified formulations (PLA1/0.1/0.1, PLA1/0.3/0.1) and eventually bimodality when the TAM content increases to 0.3 wt% (PLA1/0.1/0.3), revealing the presence of structures having high molar mass. The corresponding MH plots (**Fig. 6.3c**) deviate from the linear fit beyond $M_w=10^5$ g.mol^{-1} suggesting that the intrinsic viscosity decreased in the high molar mass region, consistent with the formation of branched structures [23,36–39].

The coagent-modified formulations exhibited significant increases in the zero shear viscosity, enhanced shear thinning, and deviation from terminal flow, when compared to the starting PLA1 (**Figure 6.4a, b**). The deviation from the terminal angle of 90° in the Van Gurp-Palmen plot (**Fig. 6.4c**) is indicative of branching. It is interesting to note that both the increases in molar mass and in the viscosity were much more pronounced in formulations prepared in the twin-screw extruder (TSE) in this chapter, compared with the same formulations presented in Chapter 5. This suggests that the improved mixing conditions in the TSE resulted in improved reaction efficiency.
Nevertheless, the deviations from the linear fit of $\log\eta_o$ vs. $\log M_w$ were rather moderate and became more significant only at the highest coagent loading. Auhl et al. [40] have discussed the opposing

effects of the increasing concentration of branched chains, which serves to increase zero shear viscosity, and the decreasing arm length, in the presence of many branches, which results in fewer entanglements and a decrease in viscosity. Harth et al. [41] and Fang et al. [23] showed deviations only when large amounts of branching were present in PET and PLA respectively. This analysis suggests that a relatively small amount of long-chain branches are present in the current system, together with the linear PLA chains that remain unmodified. This is consistent with the very small amounts of TAM that is grafted on the PLA chains (**Table 6.1**)

The system is susceptible to cross-linking upon increasing the amount of the tri-functional coagent [24,25]. Indeed, increasing the amount of DCP and TAM resulted in substantial increases in the viscosity of PLA1 0.3/0.3 and the formation of gels (3 wt.%), signifying the onset of cross-linking, thus making it impossible to measure the molar mass distribution by GPC. The complex viscosity versus frequency data in Fig. 6.4(a) could only be fitted using the power-law equation (4). The 0.3/0.3 TAM formulation showed terminal phase angle below 50°, in the VanGurp plot (**Fig. 6.4c**) right at the onset of gelation, which is also reflected by the power-law type dependence of the complex viscosity versus frequency curve. Increasing TAM content even further, in PLA1 0.3/1 resulted in high gel content (25 wt.%), indicative of high cross-link density, and could not be characterized by GPC or rheology.

6.3.2 Strain hardening

As expected, branching had profound effects on the tensile stress growth coefficient of the modified PLA. (**Fig. 6.6, Table 6.2**). The degree of strain hardening is strain dependent; branches have a stronger effect at low strain rates, whereas the non-strain hardening linear PLA chains dominate at high strain rates [20]. The PLA1 0.3/0.1 formulation, exhibited a small degree of strain hardening at high strain rates only. For the later sample, chain entanglements due to branching were not sufficient to achieve strain hardening, and that the response of the linear PLA chains dominated. Increasing the amount of TAM resulted in more branches (sample PLA1/0.1/0.3, PLA1/0.3/0.3), and a higher strain hardening coefficient.

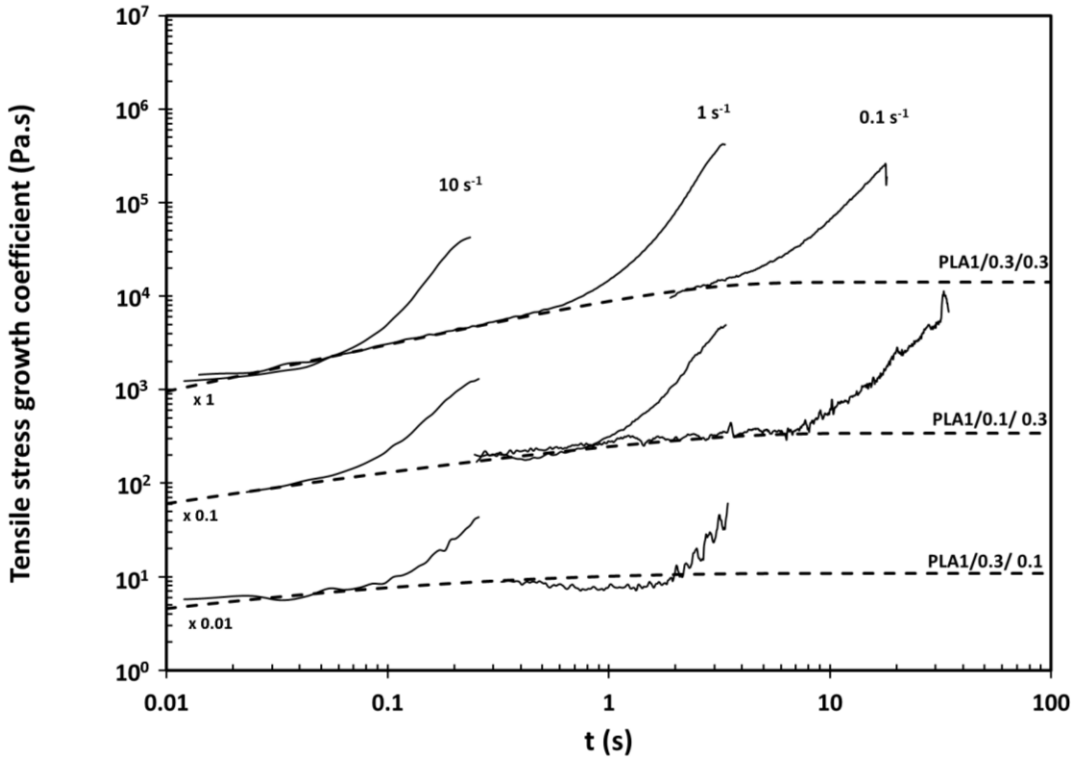

Figure 6.6 Tensile stress growth coefficients of various coagent modified PLAs at various strain rates at 180°C. Measurements on neat PLA, PLA1/0.3DCP, and PLA1/0.1/0.1 could not be performed due to sample sagging. PLA1/0.3/1 could not be loaded, because it was crosslinked. Some samples have been shifted by an arbitrary factor for clarity

Table 6.2 Strain hardening coefficients of coagent modified PLAs at 180°C.

Sample /Strain rate	0.1 s^{-1}	1 s^{-1}	10 s^{-1}
PLA1/0.3/0.1	--	5	5
PLA1/0.1/0.3	20	14	6
PLA1/0.3/0.3	17	20	8

6.3.3 Thermal Properties

It is well known that linear PLA crystallizes very slowly. PLA1 did not show a distinct crystallization peak during the cooling cycle, whereas PLA2 exhibited a subtle transition. In the absence of crystallization upon cooling, these materials typically exhibit pronounced cold

crystallization transitions in the DSC endotherms that are followed by melting. (**Fig. 6.7a and c, Table 6.3**). These characteristics were essentially unaltered upon reaction with DCP or TAM only.

Subtle differences were observed in the thermal properties of the coagent-modified PLAs during the 1st heating scan (**Table 6.3** and **Fig. 6.7a**). Both cold crystallization temperatures were slightly shifted toward lower values as the amount of TAM increased, and became less pronounced in the crosslinked PLA1/0.3/1 formulation. The T_g of the latter also increased by 4°C, indicative of restricted motion of the chains. Neat PLAs and other coagent modified samples (except PLA1/0.3/1) showed negligible crystallinity values, whereas the crystallinity of the PLA1/0.3/1 formulation increased substantially to 31%, consistent with the reduction in the magnitude of the cold crystallization peak.

Table 6.3Thermal properties of PLA formulations.

	1st heating					**Cooling**	**2nd heating**				
Sample	**T_{cc1} (°C)**	**T_{cc2} (°C)**	**T_m (°C)**	**T_g (°C)**	**χ_c (%)**	**T_c (°C)**	**T_{cc1} (°C)**	**T_{cc2} (°C)**	**T_m (°C)**	**T_g (°C)**	**χ_c (%)**
PLA1	95	156	171	60	5		96	154	170	60	5
PLA2	94	162	179	60	8	-	96	154	177	60	15
PLA1/0.3/0	98	154	170	60	1		102	154	168	60	3
PLA1/0/0.3	95	155	171	60	1		96	154	170	60	1
PLA1/0.1/0.1	97	155	171	60	5	124			167	59	47
PLA1/0.1/0.3	90	154	170	60	2	135			169	62	52
PLA1/0.3/0.1	90	153	170	60	4	130	-	-	167	61	52
PLA1/0.3/0.3	90	151	167	60	4	135			167	61	50
PLA1/0.3/1	91	148	165	64	31	132			167	62	45

T_c- crystallization peak temperature measured in cooling, T_{cc1} – cold crystallization peak temperature measured in heating, T_{cc2} – cold crystallization peak temperature measured in heating just before melting, T_m-melting peak temperature measured in heating, χ_c – percentage crystallinity.

Even though the neat PLAs did not have a crystallization peak during the cooling sequence, the crystallization exotherms of the coagent-modified PLAs displayed sharp crystallization peaks (**Table 6.3** and **Fig. 6.7b**). The crystallization temperature, T_c increased with increasing amounts

of TAM. These responses are indicative of improved nucleation in the system, which is capable of nucleating crystals during cooling. Consistently with the observations during the cooling scan, the thermal transitions of the TAM-modified PLA were altered significantly during the 2nd heating scan; the cold crystallization transitions disappeared from the second heating endotherm. (**Fig. 6.7c**). The crystallinity of these polymers increased impressively, by as much as 900%. The changes in the crystallization mechanism produced different types of crystals, affecting slightly their melting temperature, and shifting it below the melting temperature of PLA1. It is noteworthy that the lightly modified PLA1/0.1/0.1 had a broader peak, suggesting the presence of two types of crystals.

Shifts in the cold crystallization temperature, enhanced crystallization kinetics and higher crystallinity have been observed previously upon coagent modification of PLA [28,42]. However the presence of a sharp exothermic crystallization peak, followed by complete disappearance of the cold crystallization in the second heating sequence has never been reported before.

It is well-known that LCB facilitate the formation of stable nucleation sites during crystallization, and therefore induce a nucleating effect in semi-crystalline thermoplastics, such as polyolefins and PLA [14,42–44]. Previous work has shown that PLA branched with Joncryl had improved nucleation capacity[43], but retained the typical characteristics of cold crystallization. Liu et al. [42] speculated that the LCB backbones are likely to act as nucleating sites. The higher segmental mobility of the linear chains facilitates folding of the chains, and thus accelerates the crystallization kinetics. You et al.[44] further attributed the improved nucleation to hydrogen bonding that is established between the PETA coagent and the PLA chains and forms clusters of chains. However in the present PLA/TAM system hydrogen bonding is not possible.

The profound changes in crystallization properties observed in the TAM-modified system observed herein are akin to those characteristic of nucleated systems, similar to what has been observed in our previous work **(chapters 2-4)**, in the presence of a secondary phase consisting of oligomerized coagent.

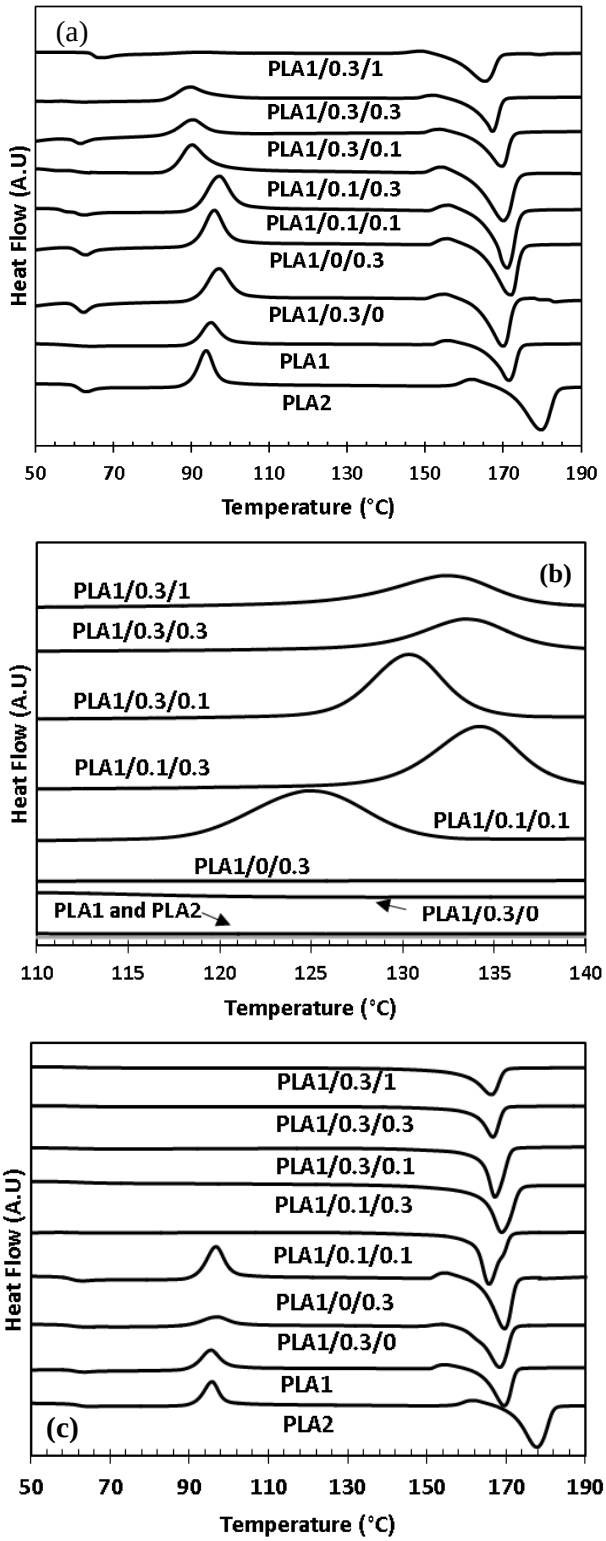

Figure 6.7 (a) 1st heating curve (endothermic), (b) Cooling curve (exothermic) and c) 2nd heating curve (endothermic) of various PLA.

Further insight into the crystallization of the coagent-modified formulations was obtained through isothermal experiments, using hot stage microscopy at 155°C, to enable us to visualize the process of crystallization (**Fig. 6.8**). It is noted that the neat PLAs did not crystallize under these conditions. The lightly modified sample, PLA/0.1/0.1 showed slow crystallite development and a wider distribution of crystal size. This might be the underlying reason behind the broad melting peak observed in the DSC endotherm (**Fig. 6.7c**). On the other hand, the samples modified with higher loadings of TAM crystallized faster, and the crystallization process was essentially complete in 10 min. The resulting microstructure was grainy, with smaller crystallites and higher density of crystals in highly modified sample, consistent with the enhanced nucleation effect.

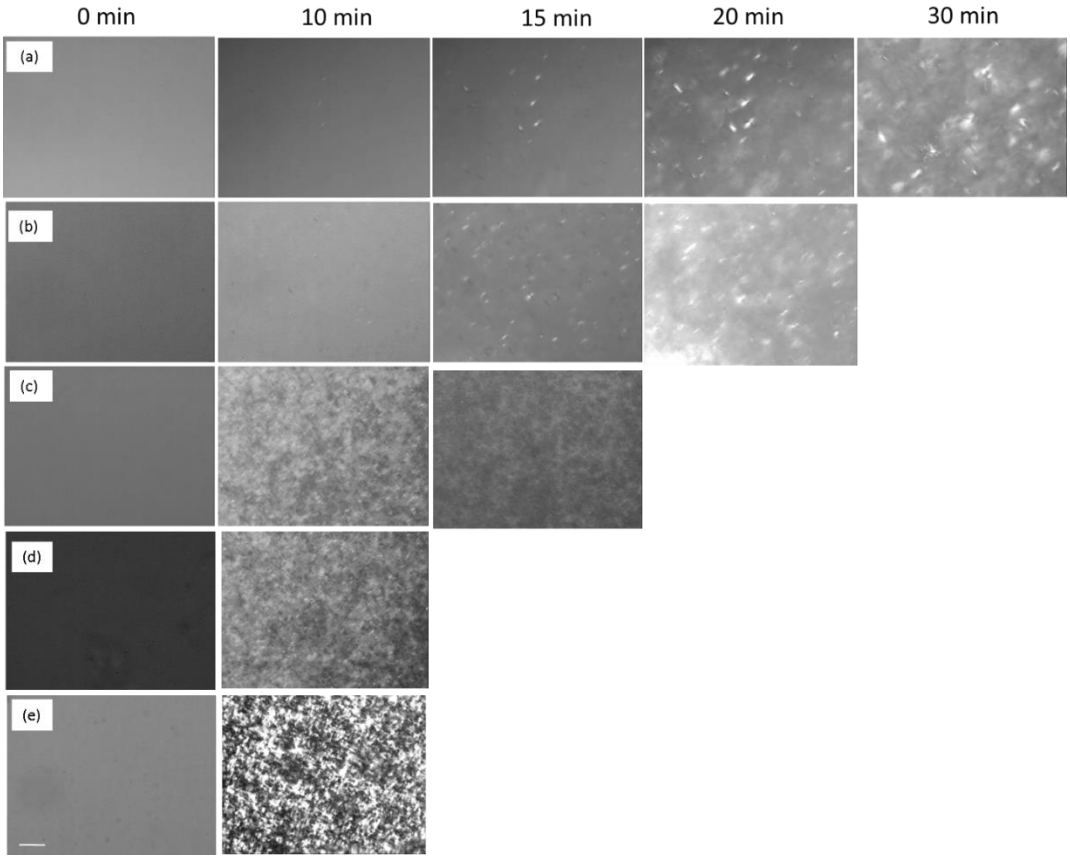

Figure 6.8 Hot stage microscopy images of a) PLA1/0.1/0.1, b) PLA1/0.3/0.1, c) PLA1/0.1/0.3, d) PLA1/0.3/0.3,e) PLA1/0.3/1 at 155°C; the scale bar represents 60㎛. Neat PLA, PLA1/0.3/0, and PLA1/0/0.3 did not crystallize under these conditions.

The results analyzed above confirm that the coagent-modified system behaves similarly to nucleated PLA systems. It should be noted that the effects on crystallinity are only pronounced when the polymer crystallizes slowly, at temperatures above the T_g. Under normal processing

conditions, which include fast crystallization rates the nucleation effect was not evident. This is the case in the injection molded specimens, discussed in Section 6.3.4.

6.3.4 Mechanical properties

The mechanical properties of polymers depend on their molecular weight, chain architecture and crystalline microstructure [45]. In this section we investigate whether the changes in chain architecture imparted by coagent modification, affects the resulting mechanical properties.

Comparing the properties of the two linear PLAs shows that the higher molar mass in PLA2 had higher impact strength, whereas the rest of the properties were similar (**Table 6.4**). The formulation with 0.3/0.3 TAM and 0.3/1 TAM could not be injection molded into parts due to their high viscosity, and are therefore not included in this analysis.

Table 6.4 Mechanical properties of PLAs.

Sample	TS at Break (MPa)	Young's Modulus (MPa)	Flexural Modulus (MPa)	Elongation at Break (%)	Unnotched Izod impact strength ($kJ.m^{-2}$)*	HDT (°C) at 1.82 MPa
PLA1	60±6	1230±54	2670±40	6±1	17±0.5	55
PLA2	65±2	1260±45	2610±115	8±1	32±3	56
PLA1/0.3/0	62±2	1170±46	2400±100	7±0.5	18±0.9	55
PLA1/0/0.3	61±5	1190±44	2600±50	6±0.5	18±0.7	55
PLA1/0.1/0.1	61±6	1220±52	2600±100	7±0.5	34±0.5	55
PLA1/0.1/0.3	63±3	1260±29	2890±90	7±1	23±0.3	56
PLA1/0.3/0.1	62±6	1280±16	2550±100	7±0.5	34±1	55

**All the Izod impact specimen exhibited complete break.*

It must be noted that a cold mold was used in our injection molding process. The PLA samples were therefore cooled fast, at a temperature below their T_g. Under these conditions, the samples did not crystallize, and exhibited similar thermal properties to those of the neat PLA (**Table 6.3** 1st

heating and**, Fig.6.7a**). Therefore the changes observed in the Izod impact strength are only attributed to differences in the PLA chain structure, and specifically to the higher molar mass of the coagent modified samples compared to the parent PLA1. On the other hand the Young's and flexural moduli, elongation at break, tensile stress at break and HDT, were retained upon coagent modification.

The mechanical properties of these TAM modified systems may be altered significantly if the mold is maintained at a temperature above the T_g, to allow for crystals to form during the cooling process. This should be the subject of further investigation.

6.3.5 Hydrolytic degradation

The hydrolytic degradation behaviour of PLA largely depends on the molecular weight, crystallinity, geometry, and the surrounding environment (temperature, moisture, pH, presence of micro-organisms, etc.) [46]. In this work we conducted some preliminary investigations to investigate the effect of the chemical modifications described above on the short-term hydrolytic degradation profiles of the modified PLAs.

As shown in **Fig. 6.9** and **Table 6.5**, the molecular weights of the final samples were lower than those of the initial samples for all formulations, indicating that hydrolytic degradation occurred during this time frame.

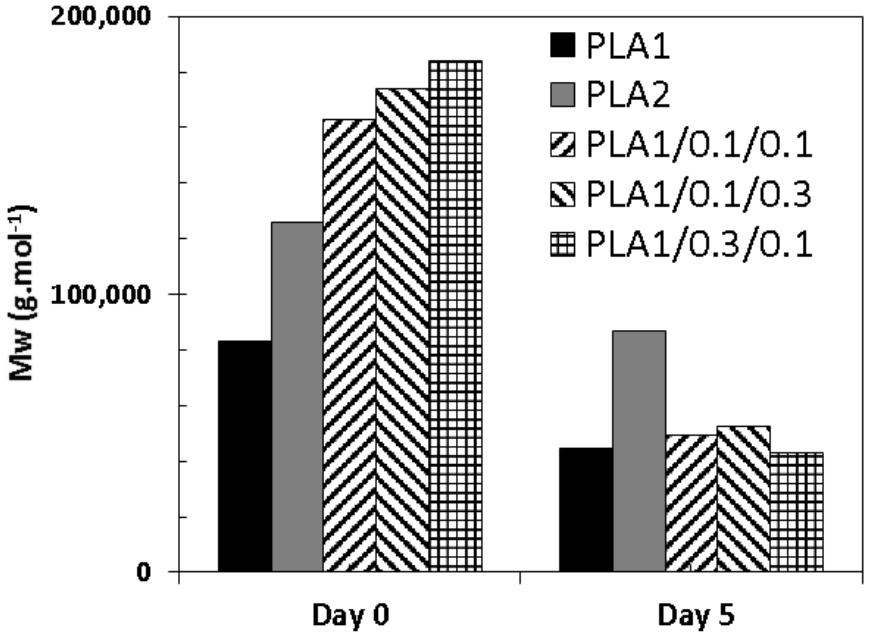

Figure 6.9 Weight average molecular weight of various PLAs on initial (day 0) and final (day 5) day.

The dispersity index of the coagent-modified formulations also decreased significantly, suggesting that the molecular weight distribution was narrowed due to the decrease in high molecular weight fractions. Hydrolysis and cleavage of ester bonds of PLA is considered to occur randomly, with longer chains being more susceptible to cleavage than the shorter chains [47]. On the contrary the observed increase in the dispersity index in the unmodified formulations represents a broadening of the molecular weight distribution peak. This could be ascribed to partial cleavage of some of the amorphous regions and recombination reactions that lead to the addition of low molecular weight crystalline fractions in the polymer [47].

A long-term degradation study was not undertaken in the present work. The preliminary results from the short-term degradation experiment presented here show that the hydrolysis of modified PLA is unaffected by TAM addition at least during the initial stages. Therefore, the modified PLAs should be subjected to further long-term degradation studies.

Table 6.5 Dispersity and molecular weight difference observed during hydrolytic degradation of PLAs

Formulation	M_w ($kg.mol^{-1}$)	Đ	M_W Percent Difference
PLA1 day 0	80	1.7	50
PLA1 day 5	45	2.5	
PLA2 day 0	130	1.6	50
PLA2 day 5	90	1.9	
PLA1/0.1/0.1 day 0	160	3.3	105
PLA1/0.1/0.1 day 5	50	2.4	
PLA1/0.1/0.3 day 0	170	4.1	130
PLA1/0.1/0.3 day 5	50	2.8	
PLA1/0.3/0.1 day 0	180	4.2	80
PLA1/0.3/0.1 day 5	40	2.5	

6.4. Discussion

The mechanism of TAM grafting on PLA in the presence of peroxide has not been studied in detail, but it is evidently a free-radical mediated reaction [48]. It should be noted that reaction of PLA with coagent alone (PLA1/0/0.3) did not result in measurable changes in molar mass, or rheology

(**Table 6.1**). The absence of grafting was confirmed by UV-Vis analysis. Therefore in the absence of peroxide, there is no grafting or transesterification reaction between TAM and PLA. This confirms that grafting of TAM onto the PLA backbone relies on a free-radical mediated mechanism.

In free-radical mediated modifications termination by chain scission and/or crosslinking is possible. In the PLA under investigation herein there is no evidence of a degradation pathway occurring through chain scission (see sample PLA1/0.3/0), and the dominant mechanism in the presence of peroxide only appears to be macroradical recombination. As explained in Chapter 5, the most likely conceptual model is that of two types of chain populations in coagent-modified PLA, comprises of linear chains, which remain unaffected by the modifications, and chains containing long-chain branching. The latter form in the presence of the multifunctional coagent, and cause bimodality in the molar mass distributions that result in deviations from the M-H relationship, and chain entanglements in the melt state, which are responsible for the high viscosities and melt elasticities, and strain hardening (**Fig. 6.4 and 6.6**); these formulations can be further pushed beyond gelation, when the TAM content increases even further.

According to the UV-Vis results the amount of branching present in coagent-modified PLA is low (0.1-0.3 wt.% of added TAM); the analysis of the intrinsic viscosity data revealed that branches are only present in the high molar mass fractions (**Fig. 6.3c**). Looking at both the intrinsic viscosity and zero shear viscosity dependence on molar mass (**Figures 6.3(c) and 6.5**), we conclude that there is a significant reduction in intrinsic viscosity of the higher molar mass fractions, whereas the deviations of the zero shear viscosity from linearity are not very pronounced. This confirms that small amounts of long-chain branched material form, causing a significant reduction in low intrinsic viscosity, manifested as deviation in the M-H plot, while the zero shear viscosity does deviate substantially from the linear $\log\eta_o$ vs. $\log M_w$ dependence [49].

It must be noted that in addition to the reaction pathways discussed in the section above, TAM is prone to oligomerization reactions in the presence of free radicals [50,51], and has also been known to form highly crosslinked structures [19,50]. It is conceivable that in the presence of high amounts of peroxide and TAM, the free radicals formed will tend to react directly with the aliphatic unsaturated sites present in TAM, rather than abstracting hydrogen from the PLA chain. This would favour the oligomerization side-reaction, and could contribute to the formation of complex hyperbranched TAM structures, interpenetrated with the PLA matrix. This side reaction appears to be dominant, since the amount of TAM grafted on PLA was very low. The rest of the ungrafted coagent, may be subject to the oligomerization reactions mentioned above. We suggest that these structures are

responsible for the altered thermal properties described in section 6.3.4, by acting as nucleating agents.

The intricate microstructure of these coagent-modified PLAs can affect profoundly all facets of the properties of these systems, including thermal, mechanical, as well as their degradation profiles, providing interesting possibilities to tailor the structure to suit various polymer processing applications.

6.5. Conclusions

Reactive extrusion PLA in the presence of peroxide and coagent yielded branched formulations with broad molecular weight distributions, depending on the concentration of peroxide and coagent. In spite of its low grafting efficiency, TAM was very effective in producing LCB PLA formulations, having increased viscosity, elasticity, as well as strain hardening characteristics. At high DCP and TAM loadings cross-linked structures were obtained.

The reactively-modified formulations had increased molar mass, which resulted in improved Izod impact strength, whereas the rest of the properties, including their capacity to degrade hydrolytically were maintained. The coagent modified derivatives exhibited a crystallization peak upon cooling in the DSC, higher crystallinity, and a finer and denser spherulitic structure.

These results demonstrated that reactive extrusion of PLA in the presence of peroxide and coagent provides a simple method to produce materials with improved melt strength and crystallization kinetics, without affecting the mechanical properties and the short-term degradation profiles. The present study demonstrates that the rheological and thermal properties of coagent-modified PLA can be modified to suit various polymer processing sectors, by using very small amounts of cross-linking agents. These altered solid and melt state properties of coagent modified PLAs are expected to play a significant role in foaming which is dealt in the next chapter of the thesis.

6.6 References

(1) Nofar, M.; Zhu, W.; Park, C. B.; Randall, J. Crystallization kinetics of linear and long-chain-branched polylactide. *Ind. Eng. Chem. Res.* **2011**, *50* (24), 13789–13798.

(2) Auras, R.; Harte, B.; Selke, S. An overview of polylactides as packaging materials. *Macromol. Biosci.* **2004**, *4* (9), 835–864.

(3) Garlotta, D. A Literature Review of Poly (Lactic Acid). *J. Polym. Environ.* **2002**, *9* (2), 63–84.

(4) Dorgan, J. R.; Williams, J. S.; Lewis, D. N. Melt rheology of poly(lactic acid): Entanglement and chain architecture effects. *J. Rheol.* **1999**, *43* (5), 1141.

(5) Rasal, R. M.; Janorkar, A. V.; Hirt, D. E. Poly(lactic acid) modifications. *Prog. Polym. Sci.* **2010**, *35* (3), 338–356.

(6) Dorgan, J. R.; Lehermeier, H.; Mang, M. Thermal and Rheological Properties of Commercial-Grade Poly (Lactic Acid)s. *J. Polym. Environ.* **2000**, *8* (1), 1–9.

(7) Dorgan, J. R.; Janzen, J.; Clayton, M. P.; Hait, S. B.; Knauss, D. M. Melt rheology of variable L-content poly(lactic acid). *J. Rheol.* **2005**, *49* (3), 607.

(8) Palade, L. I.; Lehermeier, H. J.; Dorgan, J. R. Melt rheology of high L-content poly(lactic acid). *Macromolecules* **2001**, *34* (5), 1384–1390.

(9) Saeidlou, S.; Huneault, M. A.; Li, H.; Park, C. B. Poly(lactic acid) crystallization. *Prog. Polym. Sci.* **2012**, *37* (12), 1657–1677.

(10) Di, Y.; Iannace, S.; Di Maio, E.; Nicolais, L. Reactively Modified Poly(lactic acid): Properties and Foam Processing. *Macromol. Mater. Eng.* **2005**, *290* (11), 1083–1090.

(11) Pilla, S.; Kramschuster, A.; Yang, L.; Lee, J.; Gong, S.; Turng, L.-S. Microcellular injection-molding of polylactide with chain-extender. *Mater. Sci. Eng. C* **2009**, *29* (4), 1258–1265.

(12) Corre, Y.-M.; Maazouz, A.; Duchet, J.; Reignier, J. Batch foaming of chain extended PLA with supercritical CO_2: Influence of the rheological properties and the process parameters on the cellular structure. *J. Supercrit. Fluids* **2011**, *58* (1), 177–188.

(13) Mihai, M.; Huneault, M. A.; Favis, B. D. Rheology and extrusion foaming of chain-branched poly(lactic acid). *Polym. Eng. Sci.* **2010**, *50* (3), 629–642.

(14) Liu, J.; Zhang, S.; Zhang, L.; Bai, Y. Preparation and rheological characterization of long chain branching polylactide. *Polymer* **2014**, *55* (10), 2472–2480.

(15) Liu, J.; Lou, L.; Yu, W.; Liao, R.; Li, R.; Zhou, C. Long chain branching polylactide: Structures and properties. *Polymer* **2010**, *51* (22), 5186–5197.

(16) Cailloux, J.; Santana, O. O.; Franco-Urquiza, E.; Bou, J. J.; Carrasco, F.; Gámez-Pérez, J.; Maspoch, M. L. Sheets of branched poly(lactic acid) obtained by one step reactive extrusion calendering process: Melt rheology analysis. *Express Polym. Lett.* **2012**, *7* (3), 304–318.

(17) Nouri, S.; Dubois, C.; Lafleur, P. G. Effect of chemical and physical branching on rheological behavior of polylactide. *J. Rheol.* **2015**, *59* (4), 1045–1063.

(18) Nouri, S.; Dubois, C.; Lafleur, P. G. Synthesis and characterization of polylactides with different branched architectures. *J. Polym. Sci. Part B Polym. Phys.* **2015**, *53* (7), 522–531.

(19) Kaczmarek, H.; Nowicki, M.; Vuković-Kwiatkowska, I.; Nowakowska, S. Crosslinked blends of poly(lactic acid) and polyacrylates: AFM, DSC and XRD studies. *J. Polym. Res.* **2013**, *20* (3).

(20) Gu, L.; Xu, Y.; Fahnhorst, G.; Macosko, C. W. Star vs long chain branching of poly(lactic acid) with multifunctional aziridine. *J. Rheol.* **2017**, *61*, 785–796.

(21) Takamura, M.; Nakamura, T.; Kawaguchi, S.; Takahashi, T.; Koyama, K. Molecular

characterization and crystallization behavior of peroxide-induced slightly crosslinked poly(L-lactide) during extrusion. *Polym. J.* **2010**, *42* (7), 600–608.
(22) Takamura, M.; Nakamura, T.; Takahashi, T.; Koyama, K. Effect of type of peroxide on cross-linking of poly(l-lactide). *Polym. Degrad. Stab.* **2008**, *93* (10), 1909–1916.
(23) Fang, H.; Zhang, Y.; Bai, J.; Wang, Z.; Wang, Z. Bimodal architecture and rheological and foaming properties for gamma-irradiated long-chain branched polylactides. *RSC Adv.* **2013**, *3* (23), 8783.
(24) Xu, H.; Fang, H.; Bai, J.; Zhang, Y.; Wang, Z. Preparation and characterization of high-melt-strength polylactide with long-chain branched structure through γ-radiation-induced chemical reactions. *Ind. Eng. Chem. Res.* **2014**, *53* (3), 1150–1159.
(25) Wang, Y.; Yang, L.; Niu, Y.; Wang, Z.; Zhang, J.; Yu, F.; Zhang, H. Rheological and topological characterizations of electron beam irradiation prepared long-chain branched polylactic acid. *J. Appl. Polym. Sci.* **2011**, *122* (3), 1857–1865.
(26) Quynh, T. M.; Mitomo, H.; Nagasawa, N.; Wada, Y.; Yoshii, F.; Tamada, M. Properties of crosslinked polylactides (PLLA & PDLA) by radiation and its biodegradability. *Eur. Polym. J.* **2007**, *43* (5), 1779–1785.
(27) Yang, S. lin; Wu, Z. H.; Yang, W.; Yang, M. B. Thermal and mechanical properties of chemical crosslinked polylactide (PLA). *Polym. Test.* **2008**, *27* (8), 957–963.
(28) You, J.; Lou, L.; Yu, W.; Zhou, C. The preparation and crystallization of long chain branching polylactide made by melt radicals reaction. *J. Appl. Polym. Sci.* **2013**, *129* (4), 1959–1970.
(29) Chen, C. Q.; Ke, D. M.; Zheng, T. T.; He, G. J.; Cao, X. W.; Liao, X. An Ultraviolet-Induced Reactive Extrusion to Control Chain Scission and Long-Chain Branching Reactions of Polylactide. *Ind. Eng. Chem. Res.* **2016**, *55* (3), 597–605.
(30) Nerkar, M. Preparation and characterization of biopolymer compounds containing poly-3-hydroxyalkanoates and polylactic acid, PhD Thesis, Queen's University at Kingston, Ontario, Canada, 2014.
(31) Arkema Inc. Di-Cup https://www.arkema.ca/export/shared/.content/media/downloads/products-documentations/organic-peroxides/dicup-tds.pdf (accessed Dec 19, 2017).
(32) Sentmanat, M.; Muliawan, E. B.; Hatzikiriakos, S. G. Fingerprinting the processing behavior of polyethylenes from transient extensional flow and peel experiments in the melt state. *Rheol. Acta* **2004**, *44* (1), 1–15.
(33) Fischer, E. W.; Sterzel, H. J.; Wegner, G. Investigation of the structure of solution grown crystals of lactide copolymers by means of chemical reactions. *Kolloid-Zeitschrift Zeitschrift fur Polym. Polym.* **1973**, *251* (11), 980–990.
(34) Othman, N.; Jazrawi, B.; Mehrkhodavandi, P.; Hatzikiriakos, S. G. Wall slip and melt fracture of poly(lactides). *Rheol. Acta* **2012**, *51* (4), 357–369.
(35) Nemoto, T.; Takagi, J.; Ohshima, M. Nanocellular foams—cell structure difference between immiscible and miscible PEEK/PEI polymer blends. *Polym. Eng. Sci.* **2010**, *50* (12), 2408–2416.
(36) Chen, H.; Kong, J. Polymer Chemistry Hyperbranched polymers from A 2 + B 3 strategy: recent advances in description and control of fi ne topology Hyperbranched polymers from A 2 + B 3 strategy: recent advances in description and control of fine topology. *Polym. Chem.* **2016**, *7* (3643), 3635–3774.
(37) Striegel, A. M.; Timpa, J. D. Gel permeation chromatography of polysaccharides using universal calibration. *Int. J. Polym. Anal. Charact.* **1996**, *2* (3), 213–220.
(38) Kruse, M.; Wagner, M. H. Rheological and molecular characterization of long-chain branched poly(ethylene terephthalate). *Rheol. Acta* **2017**, *56* (11), 887–904.
(39) Bikiaris, D. N.; Karayannidis, G. P. Chain extension of polyesters PET and PBT with two

new diimidodiepoxides. II. *J. Polym. Sci. Part A Polym. Chem.* **1996**, *34* (7), 1337–1342.
(40) Auhl, D.; Stadler, F. J.; Munstedt, H. Comparison of Molecular Structure and Rheological Properties of Electron-Beam- and Gamma-Irradiated Polypropylene. *Macromolecules* **2012**, *45*, 2057–2065.
(41) Härth, M.; Kaschta, J.; Schubert, D. W. Shear and elongational flow properties of long-chain branched poly(ethylene terephthalates) and correlations to their molecular structure. *Macromolecules* **2014**, *47* (13), 4471–4478.
(42) Liu, J.; Zhang, S.; Zhang, L.; Bai, Y. Crystallization behavior of long-chain branching polylactide. *Ind. Eng. Chem. Res.* **2012**, *51* (42), 13670–13679.
(43) Najafi, N.; Heuzey, M. C.; Carreau, P. J.; Therriault, D.; Park, C. B. Rheological and foaming behavior of linear and branched polylactides. *Rheol. Acta* **2014**, *53* (10–11), 779–790.
(44) You, J.; Yu, W.; Zhou, C. Accelerated Crystallization of Poly (lactic acid): Synergistic effect of Poly (ethylene glycol), Dibenzylidene Sorbitol , and Long-Chain Branching. *Ind. Eng. Chem. Res.* **2014**, *53*, 1097–1107.
(45) Tan, V.; Kamal, M. R. Morphological Zones and Orientation in In jection-Molded Polyethylene. *J. Appl. Polym. Sci.* **1978**, *22*, 2341–2355.
(46) Hoüglund, A.; Odelius, K.; Albertsson, A. C. Crucial differences in the hydrolytic degradation between industrial polylactide and laboratory-scale poly(L -lactide). *ACS Appl. Mater. Interfaces* **2012**, *4* (5), 2788–2793.
(47) Ndazi, B. S.; Karlsson, S. Characterization of hydrolytic degradation of polylactic acid/rice hulls composites in water at different temperatures. *Express Polym. Lett.* **2011**, *5* (2), 119–131.
(48) Nerkar, M.; Ramsay, J. A.; Ramsay, B. A.; Vasileiou, A. A.; Kontopoulou, M. Improvements in the melt and solid-state properties of poly(lactic acid), poly-3-hydroxyoctanoate and their blends through reactive modification. *Polymer* **2015**, *64*, 51–61.
(49) Giumanca, R. The Effects of Long Chain Branching on the Rheological Properties of Polymers.MASc Thesis, Univeristy of British Columbia, Canada **2002**.
(50) Wu, W.; Parent, J. S.; Sengupta, S. S.; Chaudhary, B. I. Preparation of crosslinked microspheres and porous solids from hydrocarbon solutions: A new variation of precipitation polymerization chemistry. *J. Polym. Sci. Part A Polym. Chem.* **2009**, *47* (23), 6561–6570.
(51) El Mabrouk, K.; Parent, J. S.; Chaudhary, B. I.; Cong, R. Chemical modification of PP architecture: Strategies for introducing long-chain branching. *Polymer.* **2009**, *50* (23), 5390–5397.

Chapter 7

Transition from microcellular to nanocellular PLA foams by controlling viscosity, branching and crystallization*

7.1. Introduction

Polylactide, or poly(lactic acid) (PLA) is a renewable-resource based aliphatic polyester, which can be biodegradable and compostable under favourable conditions [1]. Being a thermoplastic with properties that are comparable to some commodity polymers, it is viewed as a viable alternative to petroleum-sourced plastics. As part of the drive for renewable-source based products, thermoplastic foams made out of PLA have attracted considerable attention in sectors such as packaging, cushioning, thermal and sound insulation [1].

PLA is a linear polyester, which crystallizes slowly. Its chain architecture dictates its melt-state rheological properties, which are characterized by low melt elasticity and melt strength. The slow crystallization rates and low melt strength pose major obstacles in conventional polymer processing operations. Specifically in foaming, it is challenging to generate uniform cell morphology, because the low melt strength and slow crystallization kinetics lead to cell rupture and coalescence during the cell growth process, resulting in gas loss and foams with low expansion ratios [1–3].

Incorporation of branching through reactive extrusion is a cost-effective and versatile means to enhance melt viscosity, molecular weight, and elasticity in PLA [4–8]. In terms of foam processing the improved melt strength, which hinders cell coalescence and prevents gas from escaping from the cells, results in decreased foam cell size, higher cell density, and increased expansion ratio [6,9–12].

Supercritical foam processing involves rapid decrease in the pressure or temperature of the molten polymer to generate thermodynamic instabilities, leading to the formation of a cellular structure. Crystalline nucleation and growth are highly influential in this process, when it takes place at the vicinity of the crystallization temperature [5,13]. The formation of a network of nucleated crystals during foaming and stabilization increases the expansion ratio by minimizing gas loss and cell coalescence [1,6,14,15]. These benefits can be accomplished through careful choice of processing conditions, and addition of nucleating agents, such as talc and nanosilica [1,16].

---

*A version of this chapter has been published in**: Praphulla Tiwary**, Chul B. Park, Marianna Kontopoulou, European Polymer Journal **2017**, 91, 283-296

In addition to promoting crystallization of the matrix, nucleating agents also help in the generation of nucleation sites from where the cells grow [17,18].

However, excessive crystallization may prevent, or even inhibit completely foam expansion, due to diminished gas diffusion and increased matrix stiffness; therefore, this process must be fine-tuned [1].

Nano-cellular polymers may offer improved properties compared to commodity foams for high value-added applications in the field of membranes, sensors and insulation materials and have therefore been the subject of intense research. By fine-tuning the crystallization properties, Fujimoto et al. [19] prepared PLA/silicate nanocomposite foams ranging from micro-cellular (average size of 2.6 μm) to nano-cellular (average size 360 nm) dimensions, having homogeneous cell morphology. Furthermore, multi-modal cell structures in PLA foams are advantageous in various applications involving sound and thermal insulation [20–22]. Such bimodal structures can be obtained through using mixture of gases or using etching techniques, which are however difficult to scale up to bulk production platforms [20,22]. From the above, it is obvious that the ability to control and fine-tune the cellular morphology and structure of PLA foams is pertinent in the effort to develop biodegradable foams suitable not only for commodity, but also for high-value added applications.

Recent work in our group [7,8] and in the previous chapters (**Chapter 5 and 6**) employed a simple reactive modification approach, utilizing solvent-free, peroxide-initiated grafting of the multi-functional co-agent triallyl-trimesate (TAM) to introduce branching and achieve substantial improvements in the strain hardening characteristics of PLA. This approach also resulted in faster crystallization kinetics, under both isothermal and non-isothermal conditions. This gives us an opportunity to carefully fine tune the rheological and thermal properties of the PLA matrix to attain foams of uniform cell structure and controlled cell sizes. In this manuscript, PLA formulations having well-controlled structure, rheological and thermal properties are selected to investigate systematically the effect of these properties on the resulting foams. The ultimate objective is to provide guidelines on the ranges of material property values that are most conducive to the production of micro- and sub-micron sized foams.

7.2. Materials and Methods

7.2.1 Materials

Two PLA grades, PLA 3251 D (Melt flow index 80 g/10 min at 210°C / 2.16 kg) and PLA 2500 HP (Melt flow index 8 g/10 min at 210°C / 2.16 kg) were obtained from Natureworks®. These are

denoted as PLA 1 and PLA 2 respectively. Joncryl ® ADR 4368, which is a multifunctional epoxide styrene-acrylic oligomeric chain extender with Glycidyl methacrylate (GMA) functionality of 9 and epoxy equivalent weight 285 g.mol^{-1}, and molecular weight of 6,800 g.mol^{-1}, was supplied by BASF®. TAM (98% purity, Monomer-Polymer and Dajac labs.), dicumyl peroxide (DCP, 98% purity, Sigma Aldrich), tetrahydrofuran (THF, HPLC grade, Sigma Aldrich), and dichloromethane (DCM, HPLC grade, Sigma Aldrich) were used as received. Boron Nitride (BN) powder (CarboTherm®, Grade CTP 05) was obtained from Saint-Gobain Ceramics and was used as a nucleating agent.

7.2.2 Reactive modification

PLA was dried in a vacuum oven at 100°C for 3 h, following standard recommended procedures. PLA1/TAM was prepared by coating PLA 3251 D powder (14.8 g) with an acetone solution containing TAM (0.15g, 0.11 wt.%) and DCP (0.045g, 0.3 wt.%) and allowing the solvent to evaporate. The resulting mixture was charged to a co-rotating DSM micro-compounder which was operated at 100 rpm at the temperature of 180°C. The reaction was carried out for 6 min. Neat PLA was processed under similar conditions. A compound containing 1.2 wt. % of GMA (PLA1/GMA), which was required to yield similar zero shear viscosity at 180°C as PLA1/TAM, was prepared under similar conditions, and was used for comparison. Boron Nitride (0.5 ppm) was added to powdered PLA and was extruded in similar fashion to give PLA1/BN for low molecular weight PLA and PLA2/BN for high molecular weight PLA.

7.2.3 Rheological Characterization

Compression molded discs of 25 mm in diameter at 180 °C were prepared in a Carver hydraulic press and were used for rheological characterization. The linear viscoelastic properties of the prepared PLA samples as a function of angular frequency (ω) were measured in the oscillatory mode at 140, 160, and 180 °C using MCR-301 Anton Paar rheometer equipped with 25 mm-diameter parallel plates at a gap of 1 mm. Stress sweeps were performed to ensure that all the measurements were within linear viscoelastic regime. The samples were loaded at 180 °C and cooled down to the measuring temperature for the frequency sweep measurements, to better simulate the thermal history experienced during foaming experiments. The measurements were performed after thermal equilibrium was achieved. The average of three measurements is reported throughout this work. Time sweeps, to detect shear-induced crystallization were performed at 0.1 rad.s^{-1} and 140˚C by loading samples at 180˚C and cooled to perform the tests. Samples were

characterized in a uniaxial testing platform from Xpansion instruments hosted on a MCR-301 Anton Paar rheometer [23]. The measurements were conducted at 180°C at an extension rate of 0.1, 1, and 10 s^{-1}. The linear viscoelastic (LVE) oscillatory measurements obtained at 180 °C were used to calculate the LVE stress growth curve, η^+, and to check the consistency of the extensional measurements. The curve corresponding to $3\eta^+$ represents the LVE envelope in uniaxial extension, according to Trouton's law.

7.2.4 Batch Foaming

Compression molded sheets 0.75 mm - thick were prepared at 180 °C for 2 min in a Carver hydraulic press. These sheets were cut into small specimens (0.5 X 0.5 cm^2) and loaded into a high pressure cylindrical chamber (radius: 1 cm, length: 8 cm). A schematic of the batch foaming setup is shown in **Figure 7.1a**. The chamber was heated to saturation temperature of 180 ˚C through a heat gun. The samples were saturated at 180°C with N_2 at 2,000 psi for 30 min. These conditions were chosen following a series of preliminary experiments.

The pressure cell was cooled with a spray of water. Once the desired foaming temperature was reached (within 5 sec, as monitored by a thermocouple), the pressure was released to allow the samples to foam. The samples were then quenched to room temperature to freeze in the foam morphology. A detailed schematic of the processing conditions is shown in **Figure 7.1(b).**

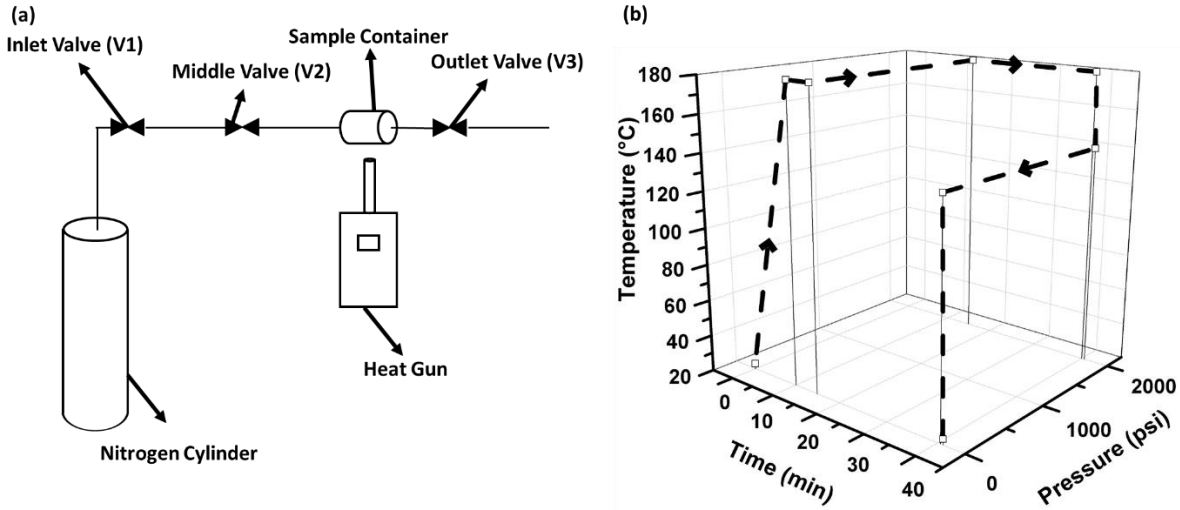

Figure 7.1 a) Schematic of setup used for batch foaming, (b) Schematic of the processing conditions used for batch foaming at a representative foaming temperature of 140°C; the dashed black line represent the process; arrows are used to guide the eye.

7.2.5 Foam characterization

The samples were cryogenically fractured under liquid nitrogen and sputtered with gold. A JEOL JSM-840 scanning electron microscope was used to observe the morphology of the foams. The cell size was determined by using ImageJ software (version 1.48). At least three images from each formulation were used to calculate averages. The volume expansion ratio (*VER*) was calculated as the ratio of bulk density of pure PLA material ρ_p to the bulk density of the foam sample ρ_f :

$$VER = \frac{\rho_p}{\rho_f} \quad (1)$$

The void fraction (V_f), which is the ratio of the volume of the gas phase contained in a foam sample to the total volume of the foam, was calculated by

$$V_f = 1 - \frac{1}{VER} \quad (2)$$

The cell density of the foams with respect to the unfoamed polymer volume (N) was calculated by the following equation:

$$N = \left(\frac{N_0}{A}\right)^{3/2} VER \quad (3)$$

where N_0 is the number of cells in a specified area A. At least three images from each formulation were used to calculate the cell density.

7.2.6 Molecular weight characterization

Gel permeation chromatography (GPC) was performed in a Viscotek 270max separation module equipped with triple detectors as differential refractive index (DRI), viscosity (IV), and light scattering (low angle, LALS and right angle, RALS). The separation module was maintained at 40 °C and contained two porous PolyAnalytik columns in series with an exclusion molecular weight limit of 209,106 Da. Distilled tetrahydrofuran (THF) was used as the eluent at a flow rate of 1 $mL.min^{-1}$. All the samples were passed through a 0.22 µm filter to remove gels before injecting in to the column. The results from the triple detector train and Viscotek Omnisec software were used to determine polymer MWDs and MW averages using the values of the refractive index ($dn.dc^{-1}$). The refractive index values were measured by a Wyatt Optilab DSP refractometer at 40 °C and 690 nm calibrated with sodium chloride. Five samples of 3–18 $mg.mL^{-1}$ were prepared in THF for each polymer and injected sequentially to construct a curve with slope $dn.dc^{-1}$ [24]. The refractive index values for PLA, PLA-TAM, and PLA-GMA were determined to be 0.0482 $ml.gm^{-1}$, close to values reported in the literature [25].

7.2.7 Gel content measurement and characterization of dissolved particles

Gel content analysis was conducted by extraction into boiling THF from a 120 mesh stainless steel sieve for 6 hours, according to ASTM D 2765. The residual polymer was dried to constant weight, with gel contents reported as a weight percentage of unextracted material.

To detect the presence of gels or particles within the sample, which could not be isolated using the ASTM method described above, PLA samples were dissolved in dichloromethane, DCM (0.01 wt.%) and deposited on carbon grids. The grids were then dried in vacuum oven for 3 hours at 60°C to remove all the solvent. The deposited samples were imaged, using a Hitachi H-7000 TEM, operated at 75 kV. The size of the dissolved particles was estimated by Dynamic Light Scattering (DLS), using a MalvernZetasizer Nano ZS equipped with 633nm laser. PLA samples were dissolved in THF (0.01 wt.%) for 5 hours and the resulting solution was transferred to quartz cuvettes to perform DLS measurements.

7.2.8 Differential Scanning Calorimetry (DSC)

DSC was performed on a Q100 DSC from TA Instruments, under dry nitrogen. All samples were first heated to 200 °C at a heating rate of 5°C·min^{-1} to erase previous thermal history, then cooled to 0 °C and reheated to 200 °C at 5°C·min^{-1}. The % crystallinity of the polymers, χ_c, was estimated using equation (4)

$$\chi_c = \frac{\Delta H_m - \Delta H_{cc}}{\Delta H_{100}} X\ 100 \qquad (4)$$

where, ΔH_m is the enthalpy of fusion, ΔH_{cc} is the exothermic enthalpy (cold crystallization) recorded during DSC heating cycle and ΔH_{100} is the theoretical enthalpy of a 100% crystalline polymer, which is equal to 93.6 J.g^{-1} [26].

To compare the nucleation capacity of the various formulations, the nucleation activity, φ, was calculated. This quantity reveals whether a foreign substrate introduced into a polymer aids in nucleation from the melt state. As nucleation activity approaches 0, the foreign substrate is increasingly active in nucleation. As suggested by Dobreva et al. [27], nucleation activity is calculated by comparing nucleation between homogeneous materials (B) and those with nucleating agents (B^*) through the following ratio:

$$\varphi = \frac{B^*}{B} \tag{5}$$

where B can be experimentally determined from the slope of a $\ln \beta$ versus $1/\Delta T_p^2$ graph as shown in equation 6

$$\ln \beta = Const - \frac{B}{\Delta T_p^2} \tag{6}$$

with ΔT_P^2 as the squared degree of supercooling ($\Delta T_P = T_m - T_p$) and β is cooling rate of the cycle and T_p is the crystallization temperature of the polymer measured during second heating. Equation 6 holds for homogeneous nucleation near the melting temperature. Heterogeneous nucleation achieved by using a nucleating agent results in the following equation:

$$\ln \beta = Const - \frac{B^*}{\Delta T_p^2} \tag{7}$$

Linear plots are obtained for $\ln \beta$ versus $1/\Delta T_p^2$ for all samples. Using the slopes of the lines, values for *B* and *B** were obtained for all the samples.

7.3. Results

7.3.1 Effect of PLA viscosity and temperature on foaming

When foaming takes place in the molten state, the viscosity of the polymer melt largely controls the cell size, with lower viscosities promoting cell growth and resulting in larger cells [28]. PLA1 and PLA 2, with low and high molar mass respectively (**Table 7.1**) serve as our two reference linear polymer samples, having high and low viscosity, respectively. Their viscosity curves at the foaming temperatures of 140, 160, and 180°C are shown in **Figure 7.2.**

Figure 7.3 (a-f) compares the cell sizes PLA1 and PLA2 foams. The insets in Figure 3 show the cell size distribution, and the average cell sizes. The average cell sizes at the foaming temperature of 180˚C were 51 μm (**Figure 7.3a**), and 32 μm for PLA1 and PLA2, respectively. This confirms that the lower viscosity of PLA1 facilitated the cell expansion process and led to large cell diameter when compared to PLA2. Foams based on PLA 2 had a broad cell size distribution, indicative of coalescence, and unfoamed regions. These characteristics are also reflected by the lower *VER*, void fraction and cell density in PLA2 (**Figures 7.4a and b, 7.5**). The lower void fraction in PLA2 may be attributed to the lower gas solubility, because of its higher viscosity [1]. In all experiments the saturation time was maintained at 30 min at a temperature of

180°C. This saturation time might not have been sufficient in the case of PLA2, which has a higher melt viscosity.

Table 7.1 Molecular weight and thermal properties of PLA formulations

Sample	M_w (kg.mol^{-1})	Đ	T_c (°C)	T_{cc} (°C)	T_m (°C)	χ_c (%)
PLA1	71	1.7	-	109	170	24
PLA2	140	1.9	-	106	175	29
PLA1/TAM (0.3wt. %DCP/ 0.1wt.% TAM)	138	2	135	-	170	52
PLA1/GMA (1.2 wt.% GMA)	157	3	-	94	170	35
PLA1/BN (500ppm BN)	71	1.7	115	-	166, 172	43
PLA2/BN (500ppm BN)	140	1.9	128	-	175	53

wt.% – weight percentage, M_w – Weight average molecular weight, Đ – Dispersity, T_m – Melting peak temperature, T_c – Crystallization peak temperature, T_{cc} – Cold crystallization peak temperature measured on 2nd heating, χ_c – percentage crystallinity.

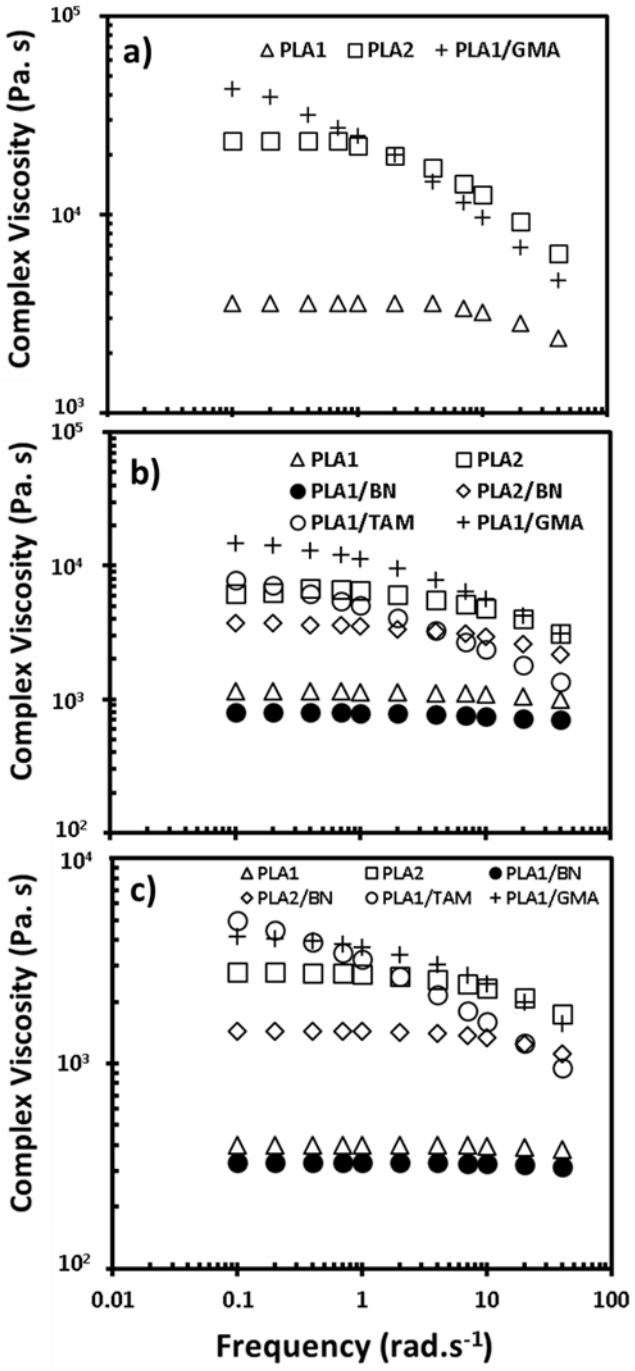

Figure 7.2 Complex viscosity vs frequency plots of various PLAs at three foaming temperatures a) 140°C, b) 160°C and c) 180 °C. The nucleated and PLA1/TAM samples are not shown in Figure a), due to intense crystallization phenomena which prevented reliable measurements (see also section 7.3.2)

Decreasing the temperature resulted in higher viscosity (**Figures 7.2 and 7.6**), which had a substantial effect on the cell size, thus confirming that controlling the temperature provides a powerful means to tailor the cellular structure [29,30]. In both materials, the cells became smaller and more uniform with decrease in the foaming temperature. The higher viscosity suppressed cell growth; at the same time the melt strength would increase, thus preventing coalescence during the later stages.

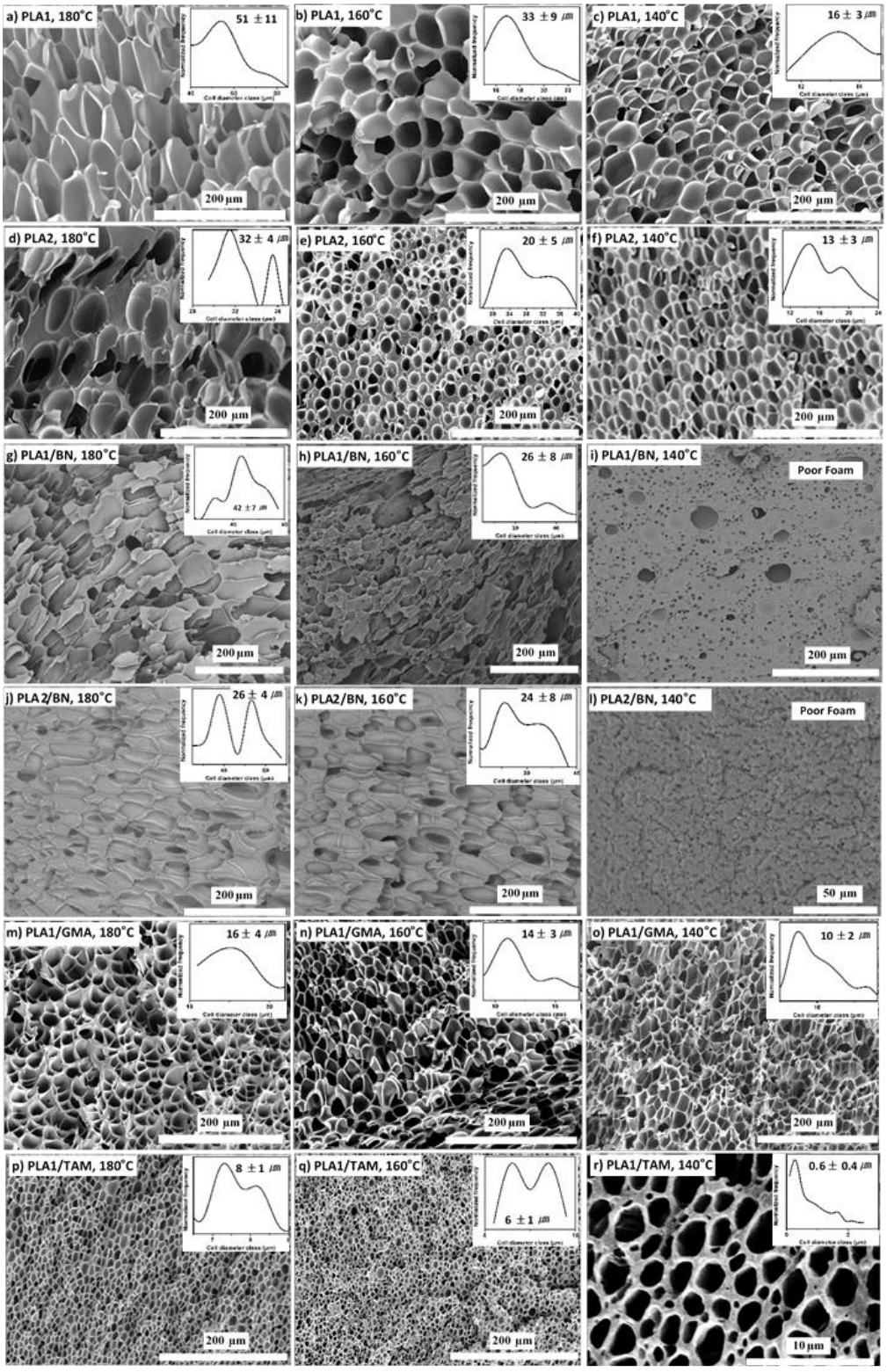

Figure 7.3 Effect of foaming temperature on cell size of PLAs. The insets show cell diameter distribution graph.

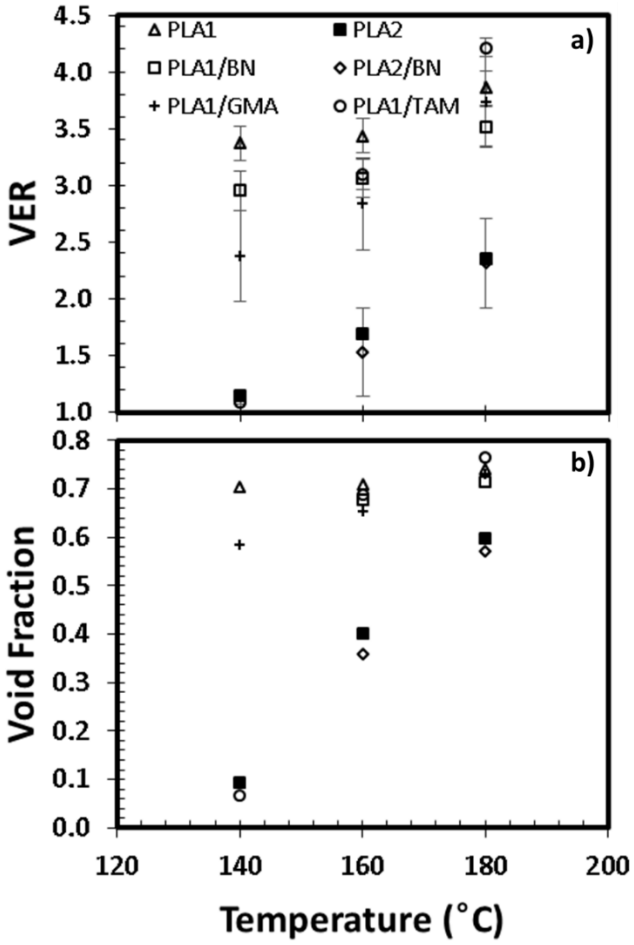

Figure 7.4 (a) VER as a function of foaming temperature and (b) void fraction as a function of foaming temperature, PLA1/BN and PLA2/BN did not foam at 140°C.

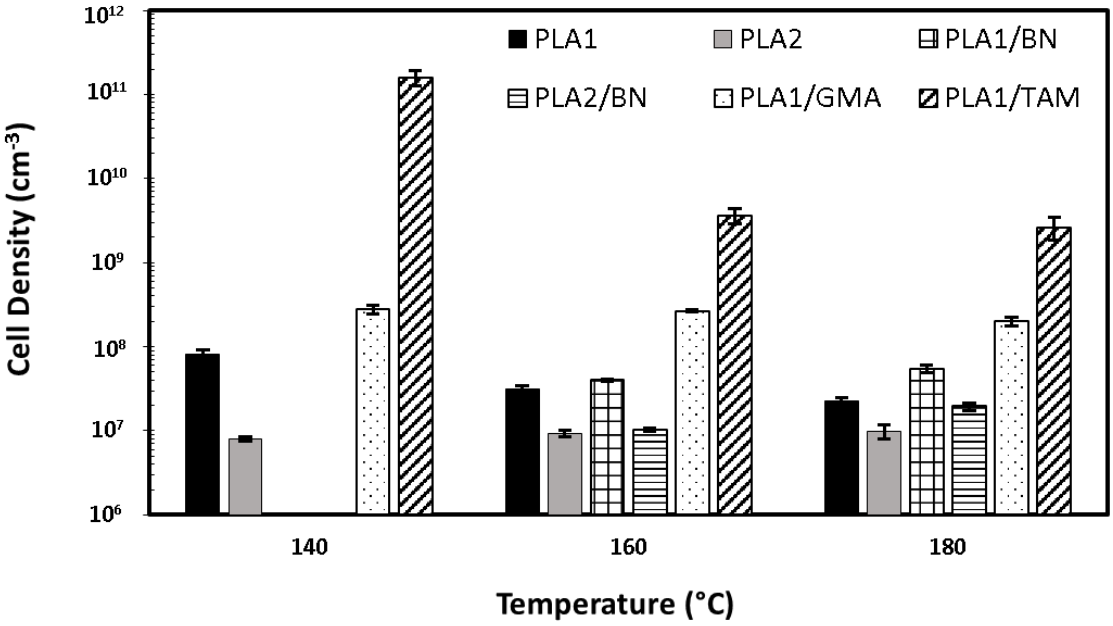

Figure 7.5 Cell density of various PLAs as a function of foaming temperatures, PLA1/BN and PLA2/BN did not foam at 140°C.

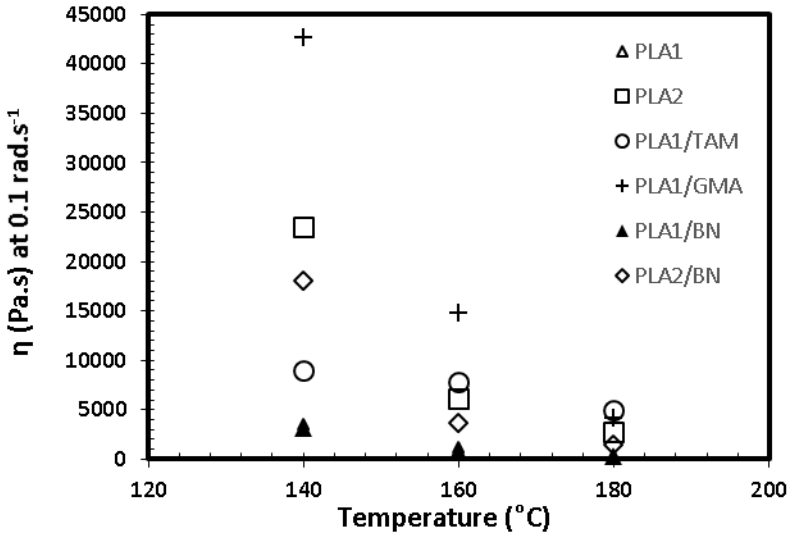

Figure 7.6 Complex viscosity at 0.1 rad.s^{-1}as a function of foaming temperature

PLA1 foams retained much larger *VER*, cell density and void fraction than PLA2 at all temperatures, whereas these quantities in PLA2 showed strong temperature dependence, with the *VER* and void fraction dropping substantially at 140°C (**Figure 7.4**). Figure 7.4 shows the volume expansion ratio (*VER*) and void fraction as a function of foaming temperature. Both followed a decreasing trend with decrease in the foaming temperature. The controlling mechanism governing the volumetric expansion of the foam is either through crystallization and melt stiffening, or through gas loss occurring via diffusion [6,31,32]. High foaming temperatures lead to longer solidification times, allowing the gas to escape from the cells by diffusing to the melt. When this mechanism dominates, the expansion ratio decreases at higher foaming temperatures. On the other hand, *VER* also depends on the stiffness of the matrix; expansion is facilitated as the stiffness drops, upon increasing the foaming temperature. This is apparently the case in the present study, where *VER* increases as foaming temperature increases (**Figure 7.4a**). The *VER* of PLA-2 shows much greater sensitivity as a function of temperature, apparently because its viscosity, and therefore matrix stiffness is also more sensitive to temperature (**Figure 7.6**).

The downward trend in cell size and *VER* as viscosity increases is summarized in **Figures 7.7a and b**, which show the average cell diameter of foams obtained from all the formulations as a function of their viscosity. A corresponding figure of *VER* versus viscosity is presented in **Figures 7.7c and d**. The shear rate profile during cell growth is complex, and varies with location and time [33,34]. Here the viscosities at shear rates of 0.1 and 40 rad.s^{-1} were chosen to cover the entire range of deformation rates happening during cell growth [35].

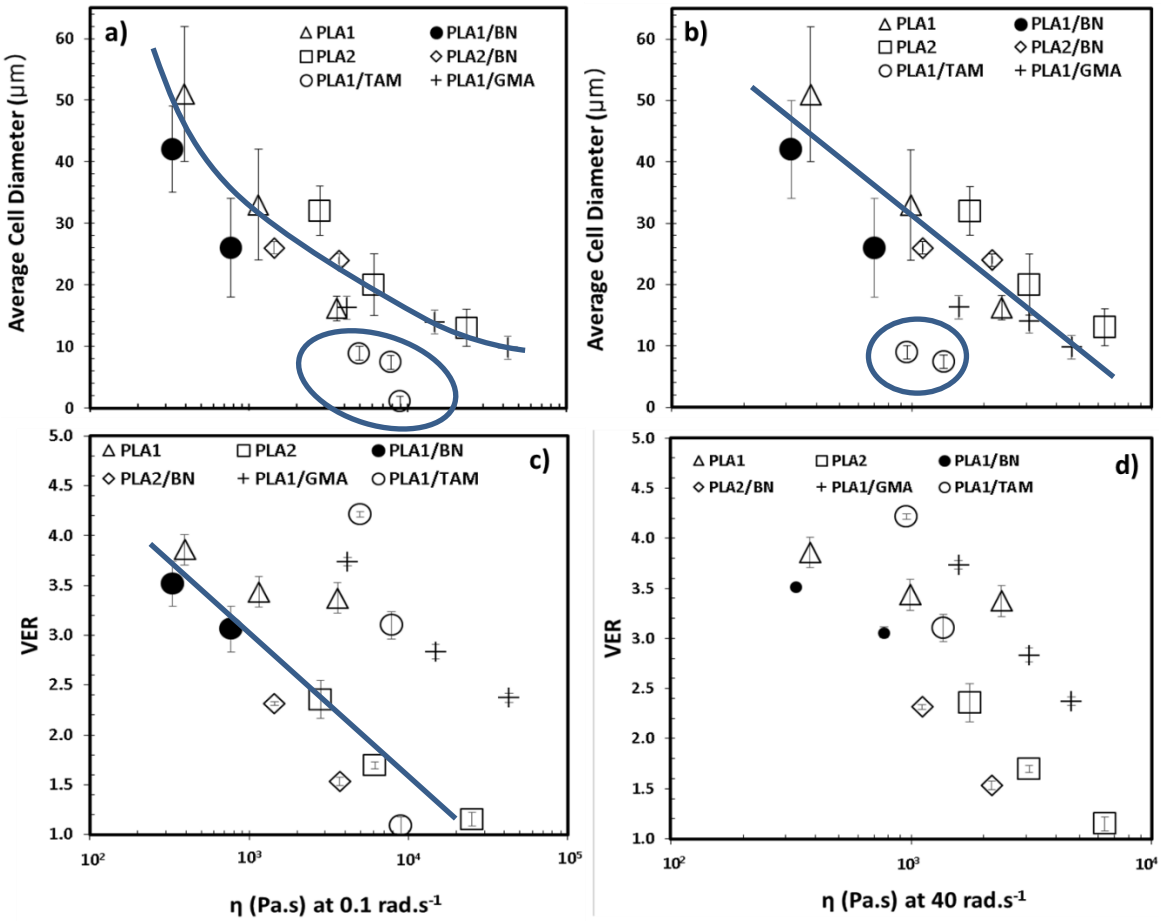

Figure 7.7 Average cell diameter of various PLAs as a function of complex viscosity at 0.1 and 40 rad.s^{-1}. Nucleated PLAs (PLA1/BN and PLA2/BN) did not foam at 140°C while the complex viscosity values for PLA1/TAM, PLA1/BN, and PLA2/BN was not measured due to fast crystallization (refer to Fig. 7.9)

7.3.2 Effect of nucleating agents

Enhancing foaming by adding nucleating agents is a common approach in foaming technology [34,36]. Nucleating agents affect the crystallization properties of the polymeric matrix, with potentially important consequences in the foaming characteristics, especially when foaming takes place at the proximity of the crystallization temperature.

In this section, PLA was modified with a boron nitride (BN) nucleating agent, and the foaming performance is compared with the systems shown previously. BN was chosen as it is a very effective nucleating agent for thermoplastics at low contents, and therefore, it would not affect other important properties of the compounds, such as rheology. Introduction of very low mounts of BN (500 ppm) altered drastically the thermal properties of the PLA, as shown in Table 7.1. The

main difference was that an exothermic crystallization peak appeared at 128 °C for PLA2 and 115 °C for PLA1, whereas the cold crystallization peak diminished. The crystallinity of the materials also increased. The Dobreva analysis (Equation 6 and 7) revealed enhanced nucleation activity in these materials (**Figure 7.8**). It must be noted that the lower the value of nucleation activity, the higher is the ability of the samples to crystallize.

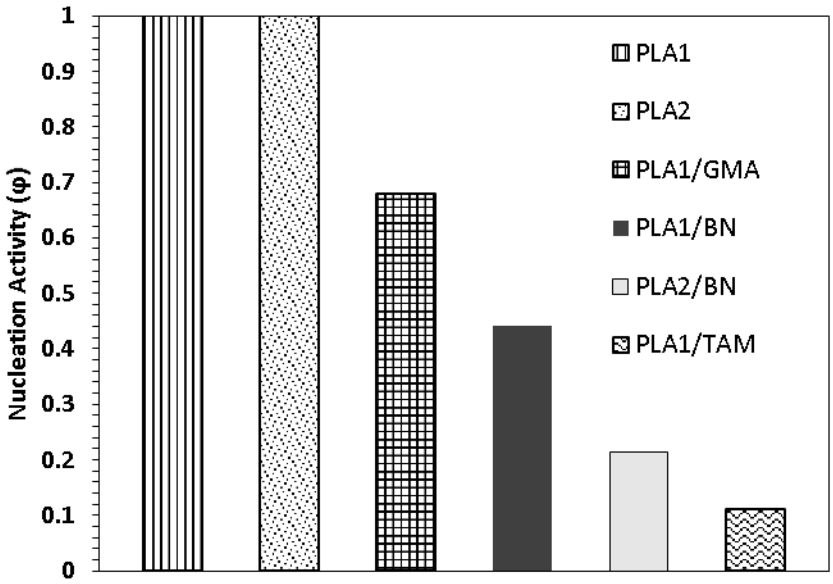

Figure 7.8 Nucleation activity of various PLAs

In terms of viscosities, the nucleated PLAs had slightly lower viscosity than the respective neat PLAs (**Figure 7.2**), due to the lubricating effect of the BN on the PLA chains [16]. This small decrease in viscosity should not play an important role in the overall analysis.

The enhanced nucleation activity in these samples gives rise to shear induced crystallization phenomena at temperatures below the melting and above the crystallization point [6,37]. These phenomena were pronounced at the foaming temperature of 140°C, as revealed by the time sweep experiments of these samples at 140°C (**Figure 7.9**), which demonstrated a dramatic increase in the complex viscosity throughout the experimental time frame. This is the reason why reliable data for these nucleated samples could not be obtained in frequency sweeps at this temperature (and therefore they are not shown in **Figure 7.2**). The fact that the increase starts right away suggest that crystallization was a factor, even during the short foam processing times.

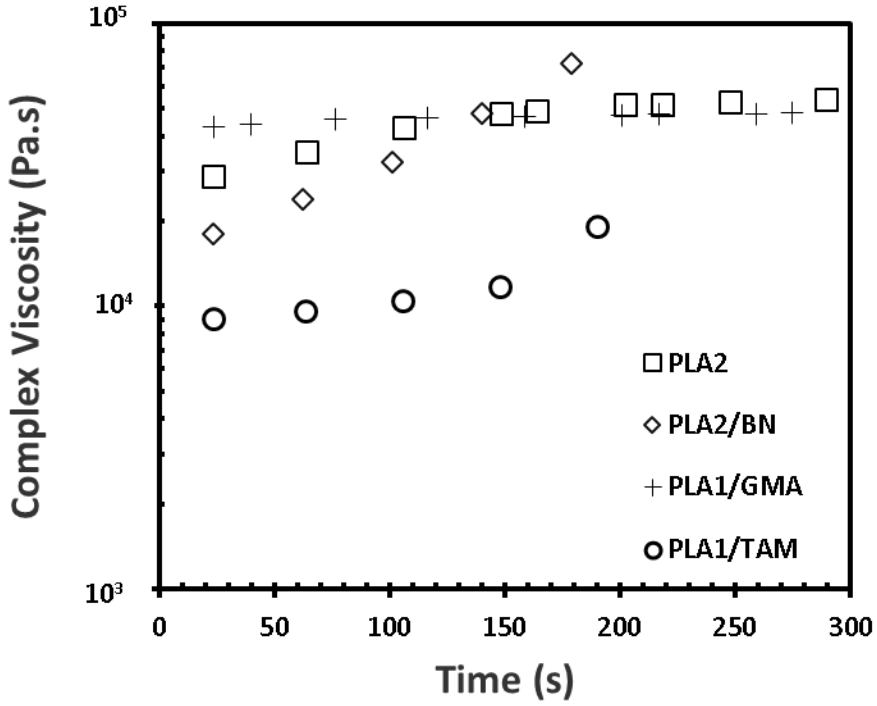

Figure 7.9 Time sweep of various PLAs at 140°C at a frequency of 0.1 rad.s^{-1}

In the presence of nucleating agents, the quality of the cells changed, as shown in **Figures 7.3(g)-(l)**. More cells were heterogeneously nucleated, but this also brought increased chance of coalescence. This resulted in a coarse and irregular cellular structure, with a broad cell size distribution. The *VER* and void fractions showed the same trend as the respective non-nucleated material, suggesting that the foaming behaviour is governed mostly by viscosity factors (**Figure 7.4a and b**).

The results however were completely different when foaming at 140°C. The images in figure 3(i) and (l) show that many cells nucleated, however growth was severely inhibited, because of the crystallization that took place at this temperature (**Figure 7.9**). The formation of crystals suppressed cell growth and hindered the diffusion of the gas, to only a few pockets, resulting in very non-uniform pores (**Figure 7.3 (i) and (l)**).

7.3.3 Effect of branching

In addition to the addition of nucleating agents, it is well known that branched polymers have enhanced foaming behaviour. Epoxy-based chain extenders, containing glycidyl methacrylate

(GMA) functionality have been used in the past to improve the melt strength of PLAs and thus limit cell coalescence and produce better quality foams [9–12,33].

In the present work PLA1 was modified with GMA to produce a product with comparable M_w and viscosity as PLA2, and thus provide a direct comparison with the linear PLA2 (**Table 7.1, Figure 7.2**). Modification with GMA resulted in broader molar mass distribution and branching, as evident by the deviation from the linear trend in the double-log plot of polymer intrinsic viscosity [η] versus molecular weight (M_W), (Mark-Houwink plot) (**Figure 7.10b**), and the pronounced shear thinning in the complex viscosity versus frequency curves (**Figure 7.2**).

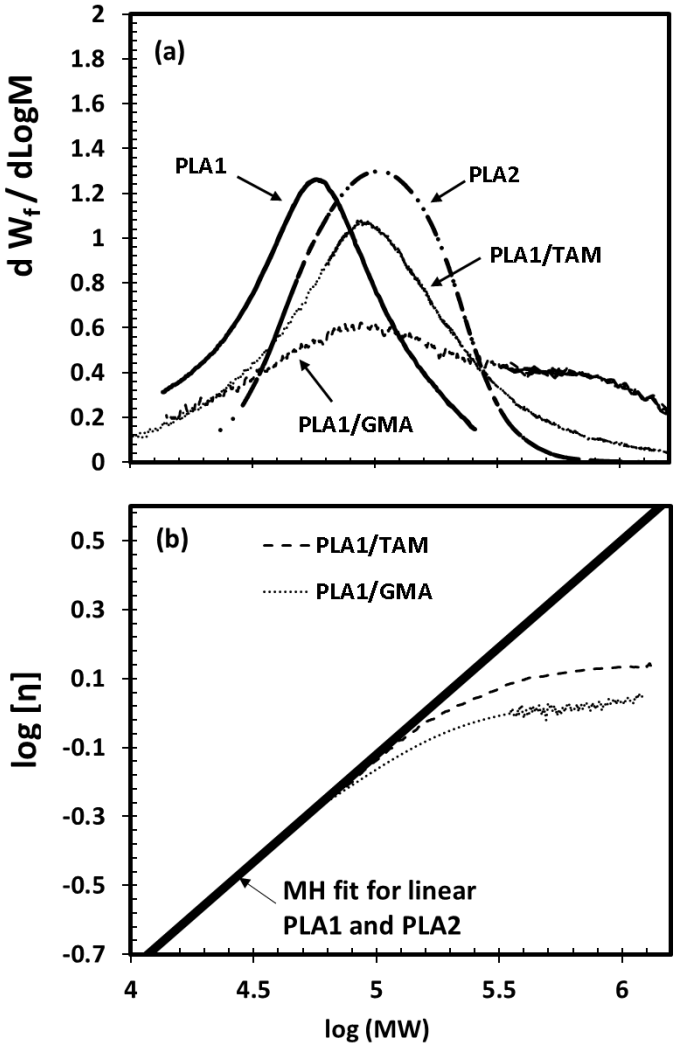

Figure 7.10 (a) Molecular weight distribution graph and (b) MH fit of various PLAs. PLA1 and PLA2 follow power-law relation (solid line) with Mark-Houwink (MH) constants of a = 0.609 and log k = -3.96 dl.gm^{-1}.

The enhanced strain hardening of this branched material under uniaxial extension (**Table 7.2**) suggests improved melt strength, which in turns resulted in a finer cell structure compared to the linear material, which is within the limits of microcellular foams (**Figure 7.3m, n, and o**) [4,39]. These foams also had enhanced *VER*, higher void fraction and higher cell densities (**Figures 7.4 and 7.5**). Decreasing the foaming temperature to 140°C resulted in a further refinement of the cellular structure. It should be noted that for this material there was no evidence of shear-induced crystallization, therefore these results scale with the effects of viscosity (**Figure 7.7**).

Table 7.2 Strain hardening coefficient of branched PLAs at different strain rates at 180°C (data obtained from reference (original data from Nerkar et al.[8])

Sample/Strain rate	**0.1 s^{-1}**	**1 s^{-1}**	**10 s^{-1}**
PLA1/TAM	3.4	2.4	2.1
PLA1/GMA	2.3	2	3

Free-radical initiated reaction of PLA with peroxides and multi-functional coagents is an alternative effective means to produced PLA having a branched structure [40,41]. Reaction of PLA1 with DCP and TAM resulted in a product having comparable M_w with PLA1/GMA and PLA2 (**Figure 7.2 and Table 7.1**). This material showed deviations from the M-H plot, pronounced high molecular weight tail in the molar mass distribution, and enhanced shear thinning, which has been commonly reported in polyolefins branched following this method, and is attributed to the presence of a highly branched population (**Figure 7.10 a and b**) [42,43].

Foaming of PLA1/TAM at 180 and 160°C generated very fine micro-cellular foams (Figure 7.3p and q), with comparable *VER* and void fraction as PLA1/GMA (**Figure 7.4**). The average cell sizes were smaller than those of the respective foams made of PLA1/TAM, and the cell density was higher. At 140°C a transition to sub-micron size foams, with very high cell density, in the order of 10^{11} cells/cm^3 is seen (Figure 7.5). For this material the *VER* dropped drastically, which is a characteristic of nanocellular foams [43]. Comparison of the data shown in **Figure 7.7** shows that the points corresponding to the cell diameter of PLA1/TAM were consistently lower compared to what is expected based on viscosity alone.

These differences cannot be attributed to branching, as this material had similar strain hardening characteristics as PLA1/GMA (**Table 7.2**). We suggest that altered crystallization kinetics, brought upon by the chemical modification were responsible for these effects, as described in the next section.

7.3.4 Combined branching and nucleation effect on foaming

It is well-known that long chain branches facilitate the formation of stable nucleation sites during crystallization, and therefore they have a nucleating effect in semi-crystalline thermoplastics, such as polyolefins and PLA [6]. Whereas the non-isothermal properties of PLA1/GMA were not altered substantially compared to PLA1 (**Table 7.1**), the crystallinity of the material was higher than the parent PLA, and its crystallization half-time was lower [8]. PLA1/GMA also had lower nucleation activity, compared to the linear PLA (**Figure 7.8**). However in this material there is no strong evidence of crystallization [8], or shear-induced crystallization at 140°C (**Figure 7.9**) during the time frame of the experiment.

PLA1/TAM, on the other hand, had the lowest nucleating activity compared to all other formulations, including the nucleated ones (**Figure 7.8**). This material demonstrates an intense exothermic peak, disappearance of the cold crystallization peak and higher crystallinity, together with significantly enhanced crystallization kinetics [8]. The highly branched chain population, characteristic of materials modified through this approach, may enhance crystallization as mentioned above. In addition, even though the material was gel free when tested using the standard test methods for gels, careful solvent extraction experiments revealed the presence of sub-micron particles dispersed within the modified PLA matrix (**Figure 7.11**). Dynamic light scattering (DLS) analysis confirmed that these particles had size of 200 ± 35 nm.

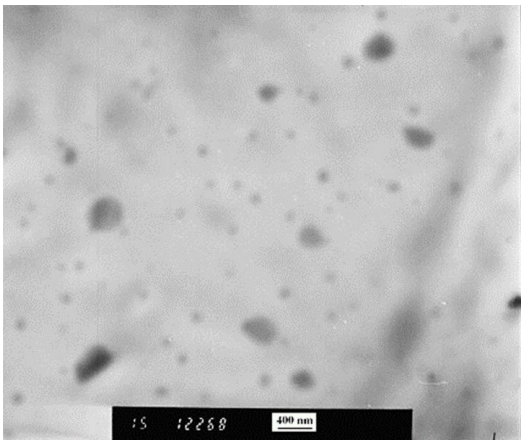

Figure 7.11 Coagent rich particles (~200 nm) observed in TEM micrograph of PLA1/TAM

Whereas this is first time that the formation of such nanoparticles is demonstrated in a reactively modified PLA system, we have reported previously that the modification of polypropylene by allylic coagents, not only results in the formation of significant amounts of long chain branching,

but also generates a population of coagent-rich submicron-sized particles, resulting from the homopolymerization side-reaction of the coagent (dealt in previous chapters). Owing to their size and shape, these particles have the potential to act as nucleating agents for PLA crystallization, thus explaining the enhanced crystallization kinetics reported previously [8].

This material is very prone to shear induced crystallization, as demonstrated by the intense increase in viscosity during the time sweep conducted at 140°C (**Figure 7.9**). Together with branching, this enhanced nucleation effect is responsible for the profound effects on the foam properties of L-TAM, through two mechanisms: Firstly an enhanced heterogeneous cell nucleation effect at the interface between the dispersed particles and polymer would lead to the increased cell densities observed at all temperatures [34]. Secondly, the transition from micro to sub-micron cellular foams observed at 140°C (**Figure 7.3r**) is associated to the shear-induced crystallization and, consequently, the appearance of crystallites at this temperature. These crystallites act to stabilize the foams, and prevent coalescence during the stabilization stage [29,36]. Stabilization during the cell growth/coalescence stage is also facilitated by the higher viscosity, which results from the onset of crystallization.

Based on the above findings, we suggest that the increase in viscosity, together with the presence of branching and the enhanced crystallization ability at low temperatures are responsible for the very fine cellular structure obtained in PLA1/TAM, compared to PLA1/GMA, which only has branching.

7.4. Discussion

The phenomena involved in the foaming of thermoplastics are very complex, and involve the interplay between material properties (rheological and thermal), which depend intimately upon the polymer structure, foaming conditions (temperature, pressure, and saturation time), and transport properties (diffusivity, and thermal conductivity). In this work, we focus on the material properties, while keeping the foaming conditions constant. A careful review of the ranges of values of the materials tested provides the means to predict the quality of the foams that can be achieved.

First of all, the effect of viscosity is dominant, as discussed in **Figure 7.7**, which shows a pronounced downward trend in cell size and *VER*, due to hindrance in cell growth and expansion as viscosity increases. **Figure 7.7** inherently includes the effect of temperature as well, as viscosity depends strongly on temperature. The decrease in the cell size as viscosity increases implies a limiting effect, wherein very high viscosities might completely suppress cell growth and *VER* [1]. Indeed, modification of PLA2 with DCP and TAM (results now shown here) resulted in compounds

with viscosities of the order of 10^5, which could not be foamed, suggesting that this would be the upper limit of viscosity. This region is highlighted in **Figure 7.12.**

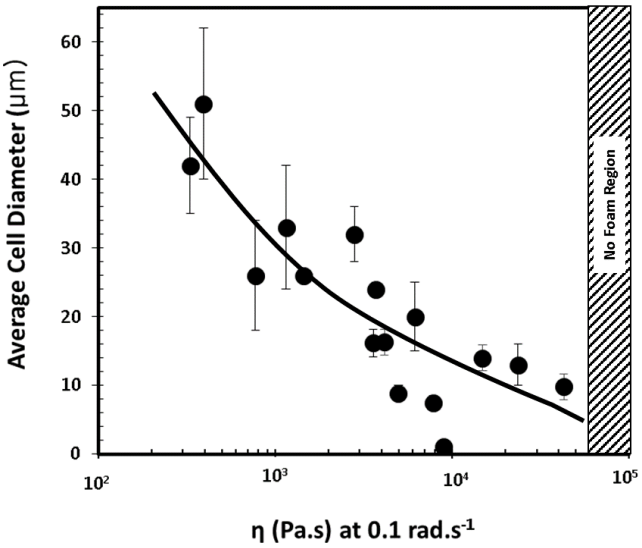

Figure 7.12 Cell diameter vs complex viscosity at 0.1 rad.s^{-1} graph summarizing all experimental data. The solid line is used to guide the eye.

Addition of a NA alone in this work did not generate better foams, as the improved cell-nucleating capacity was counteracted with increased coalescence, without net improvement in foam quality. The enhanced crystallization inhibited significantly foam growth at the lowest temperature tested. This suggests that there may be a region between 140-160°C, which could be further optimized to generate foams with improved cell structure out of these nucleated samples.

The cell size versus viscosity trends were followed in samples branched by GMA, confirming that cell growth depends mainly on viscosity. However, the *VER* and void fractions were substantially higher in these branched samples, when compared to the linear samples of similar viscosity, revealing the dominant effect of strain hardening, which enables expansion of the material without cell rupturing. Our experimental data suggest that branched PLAs with strain hardening coefficients between 2 and 3 at strain rates of 10 s^{-1} can generate foams with average cell diameters between 10-20 μm, and *VER*s between 2.5 and 4, respectively, depending on the foaming temperature, with cell densities between 10^8-10^9 cells/cm^3.

Branching through a free-radical technique generally results in bimodal structures, comprising of linear material and a small fraction of LCB polymer. PLA1/TAM had similar strain hardening characteristics as the PLA1/GMA, and produced similar *VER*s. However, its cell densities were significantly higher, of the order of 10^{11} cells/cm^3 and it produced outliers in the cell diameter vs.

viscosity trends. The only other property that differentiates PLA1/TAM is its enhanced nucleation capacity (denoted by a nucleation activity below 0.5) (**Figure 7.8**), which is comparable to that of materials containing conventional nucleating agents. In addition to promoting cell nucleation, the enhanced strain hardening, attributed to the formation of crystallites at foaming temperatures close to the exothermic crystallization temperature of PLA/TAM (Table 7.1), hinders the loss of gas, thus facilitating cell stabilization.

Given that the nucleated materials alone did not produce such results, it is evident that the presence of both nucleation and strain hardening aides in generating foams with sub-micron cell sizes and very high cell densities, bordering those observed in nanocellular foams.

In summary, the pertinent material properties that can be used to select industrial materials suitable for foaming are viscosity, strain hardening and nucleation activity. Out of these, the viscosity can be a predictor of cell size, whereas strain hardening can ensure higher *VER*s. On the other hand, nucleation activities below 0.5 can generate higher cell densities and smaller cell sizes in branched polymers, if the foaming conditions are within the range where active polymer matrix crystallization takes place.

It should be noted that the fact that dissolved gas at high pressures plasticizes the polymer and thus alters dramatically the rheological and thermal/crystallization properties complicates the phenomena even further. This is not considered in the present analysis, but the trends observed should be consistent to what would happen at high pressures.

7.5. Conclusions

This study investigated systematically the effects of viscosity, crystallization properties, and strain hardening on the cellular structure of PLA foams, prepared through a batch foaming process in the presence of N_2. These material parameters were manipulated through the choice of formulations having different molar mass, degree of branching, as well as through the addition of nucleating agents and choice of foaming temperature.

Viscosity (which in turn is influenced by temperature) was the main factor determining the cell size of the foams. Depending on the viscosity, foams having average cell sizes between 20 and 50 μm were obtained for low and high viscosities respectively. High viscosities hindered cell growth and *VER*; viscosities of the order of 10^5 Pa.s completely suppressed cell growth.

Branched PLAs with strain hardening coefficients between 2 and 3 at strain rates of 10 s^{-1} generated foams with average cell diameters between 10-20 μm, *VER*s between 2.5 and 4 respectively, and

cell densities between 10^8-10^9 cells/cm^3, depending on the foaming temperature. These results confirmed the beneficial effect of branching.

Coagent-modified PLA displayed not only strain hardening, because of its branched structure, but, owing to the presence of sub-micron coagent-rich particles, it also had enhanced nucleation activity. The cell densities of foams made out of this formulation were significantly higher compared to the rest of the formulations, of the order of 10^{11} cells/cm^3. Very fine, sub-micron sized foams were obtained when this material was foamed at temperatures close to its crystallization temperature.

7.6. References

[1] M. Nofar, C.B. Park, Poly (lactic acid) foaming, Prog. Polym. Sci. 39 (2014) 1721–1741.

[2] M. Nofar, W. Zhu, C.B. Park, J. Randall, Crystallization kinetics of linear and long-chain-branched polylactide, Ind. Eng. Chem. Res. 50 (2011) 13789–13798.

[3] S.T. Lee, L. Kareko, J. Jun, Study of thermoplastic PLA foam extrusion, J. Cell. Plast. 44 (2008) 293–305.

[4] S. Pilla, A. Kramschuster, L. Yang, J. Lee, S. Gong, L.S. Turng, Microcellular injection-molding of polylactide with chain-extender, Mater. Sci. Eng. C. 29 (2009) 1258–1265.

[5] Y.M. Corre, J. Duchet, J. Reignier, A. Maazouz, Melt strengthening of poly (lactic acid) through reactive extrusion with epoxy-functionalized chains, Rheol. Acta. 50 (2011) 613–629.

[6] N. Najafi, M.C. Heuzey, P.J. Carreau, D. Therriault, C.B. Park, Rheological and foaming behavior of linear and branched polylactides, Rheol. Acta. 53 (2014) 779–790.

[7] M. Nerkar, J. A. Ramsay, B.A. Ramsay, A.A. Vasileiou, M. Kontopoulou, Improvements in the melt and solid-state properties of poly(lactic acid), poly-3-hydroxyoctanoate and their blends through reactive modification, Polymer. 64 (2015) 51–61.

[8] M. Nerkar, J.A. Ramsay, B. A. Ramsay, M. Kontopoulou, Dramatic improvements in strain hardening and crystallization kinetics of PLA by simple reactive modification in the melt state, Macromol. Mater. Eng. 299 (2014) 1419–1424.

[9] Y. Di, S. Iannace, E. Di Maio, L. Nicolais, Reactively modified poly(lactic acid): properties and foam processing, Macromol. Mater. Eng. 290 (2005) 1083–1090.

[10] Y.M. Corre, A. Maazouz, J. Duchet, J. Reignier, Batch foaming of chain extended PLA with supercritical CO_2: Influence of the rheological properties and the process parameters on the cellular structure, J. Supercrit. Fluids. 58 (2011) 177–188.

[11] M. Mihai, M. A. Huneault, B.D. Favis, Rheology and extrusion foaming of chain-branched poly(lactic acid), Polym. Eng. Sci. 50 (2010) 629–642.

[12] J. Wang, W. Zhu, H. Zhang, C.B. Park, Continuous processing of low-density, microcellular poly(lactic acid) foams with controlled cell morphology and crystallinity, Chem. Eng. Sci. 75 (2012) 390–399.

[13] A. Wong, Y. Guo, C.B. Park, Fundamental mechanisms of cell nucleation in polypropylene foaming with supercritical carbon dioxide—Effects of extensional stresses and crystals, J. Supercrit. Fluids. 79 (2013) 142–151.

[14] M. Nofar, A. Ameli, C.B. Park, Development of polylactide bead foams with double crystal melting peaks, Polymer. 69 (2015) 83–94.

[15] M. Nofar, A. Ameli, C.B. Park, A novel technology to manufacture biodegradable polylactide bead foam products, Mater. Des. 83 (2015) 413–421.

[16] A. Huang, P. Yu, X. Jing, H.-Y. Mi, L.-H. Geng, B.-Y. Chen, et al., The effect of talc on the mechanical, crystallization and foaming properties of poly(lactic acid), J. Macromol. Sci. Part B. 2348 (2016) 00–00.

[17] X.S. Tianyi Ke, Melting behavior and crystallization kinetics of starch and poly(lactic acid) Composites, J. Appl. Polym. Sci. 89 (2003) 1203–1210.

[18] J.J. Kolstad, Crystallization kinetics of poly(L-lactide-co-meso-lactide), J. Appl. Polym. Sci. 62 (1996) 1079–1091.

[19] Y. Fujimoto, S. Sinha Ray, M. Okamoto, A. Ogami, K. Yamada, K. Ueda, Well-controlled biodegradable nanocomposite foams: From microcellular to nanocellular, Macromol. Rapid Commun. 24 (2003) 457–461.

[20] S. Ghaffari Mosanenzadeh, H.E. Naguib, C.B. Park, N. Atalla, Design and development of novel bio-based functionally graded foams for enhanced acoustic capabilities, J. Mater. Sci. 50 (2015) 1248–1256.

[21] S.G. Mosanenzadeh, O. Doutres, H.E. Naguib, C.B. Park, N. Atalla, A semi-empirical

model relating micro structure to acoustic properties of bimodal porous material, J. Appl. Phys. 117 (2015).
[22] S. G. Mosanenzadeh, O. Doutres, H.E. Naguib, C.B. Park, N. Atalla, A numerical scheme for investigating the effect of bimodal structure on acoustic behavior of polylactide foams, Appl. Acoust. 88 (2015) 75–83.
[23] M. Sentmanat, E.B. Muliawan, S.G. Hatzikiriakos, Fingerprinting the processing behavior of polyethylenes from transient extensional flow and peel experiments in the melt state, Rheol. Acta. 44 (2004) 1–15.
[24] A.L. Dupont, G. Harrison, Conformation and dn/dc determination of cellulose in N,N-dimethylacetamide containing lithium chloride, Carbohydr. Polym. 58 (2004) 233–243.
[25] N. Othman, B. Jazrawi, P. Mehrkhodavandi, S.G. Hatzikiriakos, Wall slip and melt fracture of poly(lactides), Rheol. Acta. 51 (2012) 357–369.
[26] E.W. Fischer, H.J. Sterzel, G. Wegner, Investigation of the structure of solution grown crystals of lactide copolymers by means of chemical reactions, Kolloid-Zeitschrift Zeitschrift Fur Polym. 251 (1973) 980–990.
[27] A. Dobreva, I. Gutzow, Activity of substrates in the catalyzed nucleation of glass-forming melts. II. Experimental evidence, J. Non. Cryst. Solids. 162 (1993) 13–25.
[28] Y. Zhang, J.S. Parent, M. Kontopoulou, C.B. Park, Foaming of reactively modified polypropylene: Effects of rheology and coagent type, J. Cell. Plast. 51 (2015) 505–522.
[29] M. Nofar, Y. Guo, C.B. Park, Double crystal melting peak generation for expanded polypropylene bead foam manufacturing, Ind. Eng. Chem. Res. 52 (2013) 2297–2303.
[30] M. Nofar, W. Zhu, C.B. Park, Effect of dissolved CO2 on the crystallization behavior of linear and branched PLA, Polymer. 53 (2012) 3341–3353.
[31] G.J. Nam, J.H. Yoo, J.W. Lee, Effect of long-chain branches of polypropylene on rheological properties and foam-extrusion performances, J. Appl. Polym. Sci. 96 (2005) 1793–1800.
[32] H.E. Naguib, C.B. Park, N. Reichelt, Fundamental foaming mechanisms governing the volume expansion of extrudedpolypropylene foams, J. Appl. Polym. Sci. 91 (2004) 2661–2668.
[33] Y. Otsuki, T. Kanai, Numerical simulation of bubble growth in viscoelastic fluid with diffusion of dissolved foaming agent, Polym. Eng. Sci. 45 (2005) 1277–1287.
[34] K. Taki, D. Kitano, M. Ohshima, Effect of growing crystalline phase on bubble nucleation in poly(L -lactide)/CO2 batch foaming, Ind. Eng. Chem. Res. 50 (2011) 3247–3252.
[35] A.M. Kraynik, Foam Flows, Annu. Rev. Fluis Mech. 20 (1988) 325–327.
[36] M. Nofar, A. Tabatabaei, C.B. Park, Effects of nano- / micro-sized additives on the crystallization behaviors of PLA and PLA / CO_2 mixtures, Polymer . 54 (2013) 2382–2391.
[37] S. Khandavalli, J. Hendricks, C. Clasen, J.P. Rothstein, A comparison of linear and branched wormlike micelles using large amplitude oscillatory shear and orthogonal superposition rheology, J. Rheol. 60 (2016) 1331–1346.
[38] C. Wang, S.N. Leung, M. Bussmann, W.T. Zhai, C.B. Park, Numerical investigation of nucleating-agent-enhanced heterogeneous nucleation, Ind. Eng. Chem. Res. 49 (2010) 12783–12792.
[39] L. Wang, D. Wan, J. Qiu, T. Tang, Effects of long chain branches on the crystallization and foaming behaviors of polypropylene-g-poly(ethylene-co-1-butene) graft copolymers with well-defined molecular structures, Polymer. 53 (2012) 4737–4757.
[40] S. lin Yang, Z.H. Wu, W. Yang, M.B. Yang, Thermal and mechanical properties of chemical crosslinked polylactide (PLA), Polym. Test. 27 (2008) 957–963.
[41] J. You, L. Lou, W. Yu, C. Zhou, The preparation and crystallization of long chain branching polylactide made by melt radicals reaction, J. Appl. Polym. Sci. 129 (2013) 1959–1970.
[42] K. El Mabrouk, J.S. Parent, B.I. Chaudhary, R. Cong, Chemical modification of PP

architecture: Strategies for introducing long-chain branching, Polymer . 50 (2009) 5390–5397.
[43] T. Nemoto, J. Takagi, M. Ohshima, Nanocellular foams—cell structure difference between immiscible and miscible PEEK/PEI polymer blends, Polym. Eng. Sci. 50 (2010) 2408–2416.

Chapter 8
Discussion, Conclusions, Significant Contributions and Recommendation for Future Work

8.1 Discussion

This research implemented a practical and industrially relevant reactive processing technique to upgrade the properties of two important commodity thermoplastics, PP and PLA, thus making them more applicable in common processing techniques such as injection molding, which require fine-tuned rheological and thermal properties. The solution proposed in this work is a one-pot approach to produce controlled rheology and/or branched nucleated PP and PLA formulations with mechanical properties that match closely those of materials of much higher molecular weight.

Reactive extrusion of linear isotactic polypropylene in the melt state in the presence of peroxide and coagents produced materials that had lower viscosity and molar mass, narrower molar mass distribution and presence of chain branching when compared to neat PP, depending on the type and amount of coagent. Furthermore it was demonstrated that a separate phase, consisting of cross-linked sub-micron sized particles formed within coagent-modified PP. This separate phase acted as efficient nucleating agent for crystallization, resulting in significantly higher onset crystallization temperatures, faster crystallization kinetics and a finer spherulitic structure. These cross-linked nanoparticles also served as heterogeneous nucleation sites for gas phase formation during batch foaming. Therefore, the performance of these coagent modified foamed materials is dictated not only by the rheological properties brought about by chemical modification, but also through the enhanced nucleation generated by the dispersed solid phase. The altered crystallization kinetics of these materials resulted in the disappearance of the distinctive core-skin layer in injection molded specimens, and consequently a significant enhancement in their mechanical properties.

This peroxide mediated reactive extrusion approach was also applied to a thermoplastic biopolyester, PLA, which is used extensively in commodity applications. Reactive extrusion of PLA in the presence of peroxide and coagent yielded branched formulations having broad molecular weight tails, depending upon the concentration of peroxide and coagent. One of the allylic coagent, TAM was found to be particularly effective in producing long chain branched structures, having increased viscosity, elasticity, as well as strain hardening characteristics. Based on the rheological and GPC characterization, we infer that modified PLA consisted of mixtures of linear, and long-chain branched chains, depending upon the amount of the peroxide and coagent.

The propensity of acrylic (TMPTA, TMPTMA, and PETA) to oligomerize resulted in poor efficiency for LCB generation.

In addition to improved strain hardening characteristics, the reactively-modified PLA formulations displayed altered thermal properties, including capability to crystallize upon cooling, higher crystallinity, and a finer and denser spherulitic structure. The altered chain architecture did not compromise the capacity of the material to degrade hydrolytically. The mechanical properties of the base material were maintained, whereas impact strength was improved. This thesis also demonstrated the beneficial effects of branching and crystallization on the cellular structure of PLA foams, prepared through a batch foaming process in the presence of a supercritical gas.

The branched PLAs generated microcellular foams with high VERs and very high cell densities. This work demonstrated that reactive extrusion of PP, and PLA in the presence of peroxide and coagent provides a simple method to produce materials with improved melt strength and crystallization kinetics, while having beneficial mechanical properties. Additionally these modifications did not compromise the hydrolytic degradation profile of PLA, suggesting that a completely biobased and biodegradable compounds can be prepared following this technique.

8.2 Conclusions

Reactive extrusion in the presence of peroxide and tri-functional coagents provides an effective and industrially applicable means to introduce branching in linear polymers, such as PP and PLA. Depending upon the amount of peroxide and coagent, the branched polymers exhibited increases in their molar mass, high molecular weight tails, increases in the linear viscoelastic properties, and enhanced extensional strain hardening. The allylic-based coagent, TAM was most effective in introducing LCB, whereas the acrylate coagents were not efficient in introducing branches, alluding to the prevalence of an oligomerization side-reaction, which consumes the free-radicals added to the system.

PP is prone to chain scission in the presence of peroxide, therefore the results of chemical modification with TAM were mixtures of linear and degraded chains, together with small amounts of hyperbranched materials. However there was no evidence of degradation in PLA, therefore a mixture of linear and long-chain branched chains is a more suitable conceptual model to characterize the coagent-modified materials.

In addition to the positive effects of branching on the rheological properties, coagent-modified materials experience significantly higher onset crystallization temperatures, faster crystallization kinetics and a finer spherulitic structure. Whereas it is known that LCB can promote nucleation in

polymer melts, these effects were significantly more pronounced than the ones obtained simply by branched polymers. It was suggested therefore that a separate phase consisting of oligomerized or cross-linked coagent, that form in situ during the reactive extrusion process may have served as heterogeneous nucleation sites for crystallization from the melt. The altered crystallization kinetics of coagent-modified PP resulted in the disappearance of the distinctive core-skin layer in injection molded specimens, and consequently resulted in significant enhancement of their mechanical properties.

On the other hand TAM-modification influenced positively the impact strength of the material, whereas the rest of the properties remained unaffected. It is noteworthy that these modifications did not affect the capacity of the material to degrade, during short term degradation experiments.

The separate phase formed during reactive extrusion also facilitated gas phase formation during batch foaming in the presence of supercritical nitrogen. Microcellular foams were prepared, having cell densities of the order of 10^{11} cells/cm^3 when coagent modified PLA was foamed at temperatures close to the crystallization point.

Despite the thermal property enhancements achieved in PLA-TAM, the mechanical properties such as modulus and strength which are influenced by improved crystallization kinetics and crystallinity were retained in PLA-TAM owing to quick cooling achieved in injection molding process. The Izod impact strength of PLA-TAM was found to increase when compared to neat PLA which could be related to increase in the molecular mass of PLA modified with TAM.

In addition, the hydrolytic degradation was found to be unhindered with coagent modification of PLA.

8.3 Significant Contributions

This thesis implemented an easy to implement, industrially relevant one-pot approach to produce branched and nucleated PP and PLA. The coagent modified materials had substantially improved melt and solid state properties that can prove beneficial in a range of polymer processing operations.

It was demonstrated that the allylic coagent – TAM was discovered to be was extremely effective, compared to the more commonly used acrylate coagents in modifying the melt and solid state properties of PP and PLA. It should be therefore the material of choice in these processes.

One of the major findings of this work is that besides long-chain branching, coagent modification results in significant improvements in thermal properties. Specifically for PP these were: Shifts in the crystallization peak of PP to higher temperature, significant acceleration of the

crystallization kinetics, and finer spherulitic structure. The enhanced crystallization kinetics improved significantly the mechanical properties of specimens prepared by injection molding.

In PLA the observations include appearance of crystallization peak, disappearance of cold crystallization peak, and enhanced crystallinity when compared to neat PLA. It is the first time that PLA is transformed to exhibit ability to crystallize upon cooling within the timeframe allowed during typical polymer processing applications. This should have significant implications in processes such as injection molding.

Finally sub-micron sized foams of PLA were demonstrated for the first time, without the need to add external nucleating agents. The ranges of material property values that are most conducive to the production of micro- and sub-micron sized PLA foams were identified.

8.4 Recommendations for Future Work

I. An interesting contribution would be to study the effect of various peroxide types in the presence of a coagent on the chain branching of PLA and PP. One of the approaches can be to select a particular processing temperature to have a comparative analysis of the efficiency of peroxides and peroxide types. The interaction between processing temperature and peroxide degradation will result in various amounts of chain grafts.

II. Scale-up to industrial scale foam processing machine will enhance the foam production and yield more uniform cell sizes. This prospect opens up significant opportunities where the various foam properties like thermal and mechanical properties can be measured. The sub-micron size foams obtained from coagent modified PLA are expected perform better when compared to PLA.

III. Further detailed investigation of the improvements in crystallization and mechanical properties in the presence of coagents should be carried out. The effect of cooling rates on the crystallization of injection molded specimen should be investigated. The different crystallization rate is expected to have significant effect on mechanical properties, if conducted under well controlled conditions.

IV. The environmental effect of coagent modification on PLA can be explored through various degradation studies. A long term hydrolytic degradation will highlight the degraded products and outline the degradation mechanism.

V. After studying hydrolytic degradation, degradation under composting condition presents a lot of opportunities. This step will help in completing the assessment of coagent modified PLA in various applications as a sustainable material for replacement of fossil fuel based polymer.

Appendix A – PP foams

In this appendix foams prepared by batch foaming of the various PP formulations discussed in Chapter 4 are examined.

A.1 Batch foaming methodology

Compression molded sheets 0.75 mm - thick were prepared at 180 °C for 2 min in a Carver hydraulic press. These sheets were cut into small specimens (0.5 X 0.5 cm^2) and loaded into a high pressure cylindrical chamber (radius: 1 cm, length: 8 cm). A schematic of the batch foaming setup is shown in Fig. A.1(a). The chamber was heated to saturation temperature of 180 ˚C through a heat gun. The samples were saturated at 180°C with N_2 at 2,000 psi for 30 min. These conditions were chosen following a series of preliminary experiments.

The pressure cell was cooled with a spray of water. Once the desired foaming temperature was reached (within 5 sec, as monitored by a thermocouple), the pressure was released to allow the samples to foam. The samples were then quenched to room temperature to freeze in the foam morphology. A detailed schematic of the processing conditions is shown in **Figure A.1(b)**

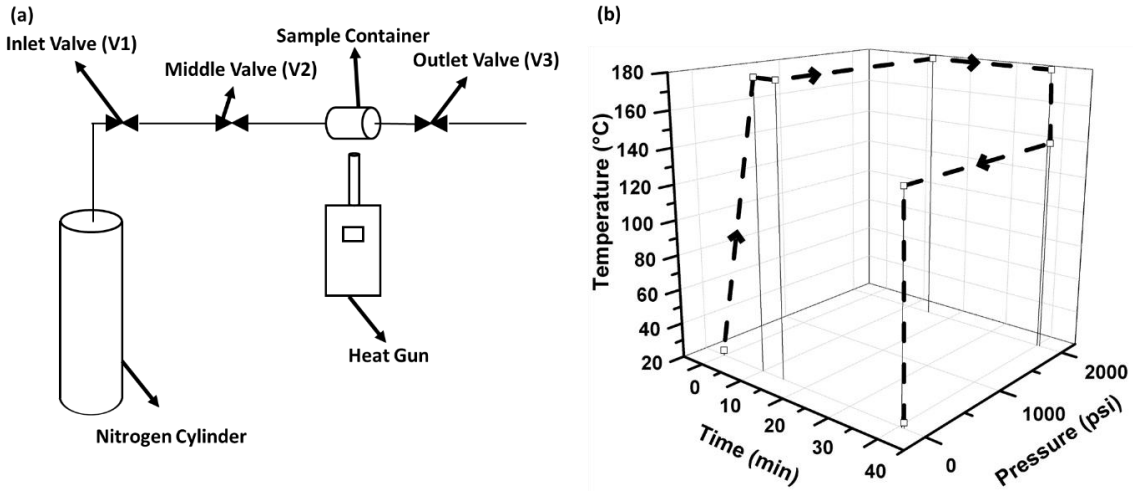

Figure A.1 a) Schematic of setup used for batch foaming, (b) Schematic of the processing conditions used for batch foaming at a representative foaming temperature of 140°C; the dashed black line represent the process; arrows are used to guide the eye.

A.2 Foams of PPs

The SEM Images for the different poly (Propylene) (PP6532, chapter 4) foams for a foaming time of 30 minutes are shown in **Fig.A.2**. It can be clearly seen that the cellular structure for the neat PP foams was not significantly influenced by the decrease of foaming temperature. Expanded closed-cells were obtained for the neat PP foam at each foaming temperature. The addition of 0.1 wt.% of DCP in the polymer blend showed some positive impact on the cell morphology of the foam. For the foaming temperature of 140°C and 150°C, the cell size seems to get reduced as compared to that for the neat PP foam. A significant increase in the cell density was observed for the DCP modified PP foam at the foaming temperature of 140°C. The addition of 6 wt.% of TMPTMA in the polymer blend dramatically reduced the cell size and increased the cell density for the foam obtained at 150°C temperature. At foaming temperatures of 160 °C and 180 °C, the addition of TMPTMA caused the cell morphology to become irregular in shape, while at 140 °C, no foam was obtained. For the TAM modified PP foam, the cellular structure was irregular at a foaming temperature of 160°C and 180°C, while at 150°C, the cell morphology was observed to become quite regular with hexagonal closed-cells. The cell size was reduced considerably at the foaming temperature of 140°C with a dramatic increase in the cell density.

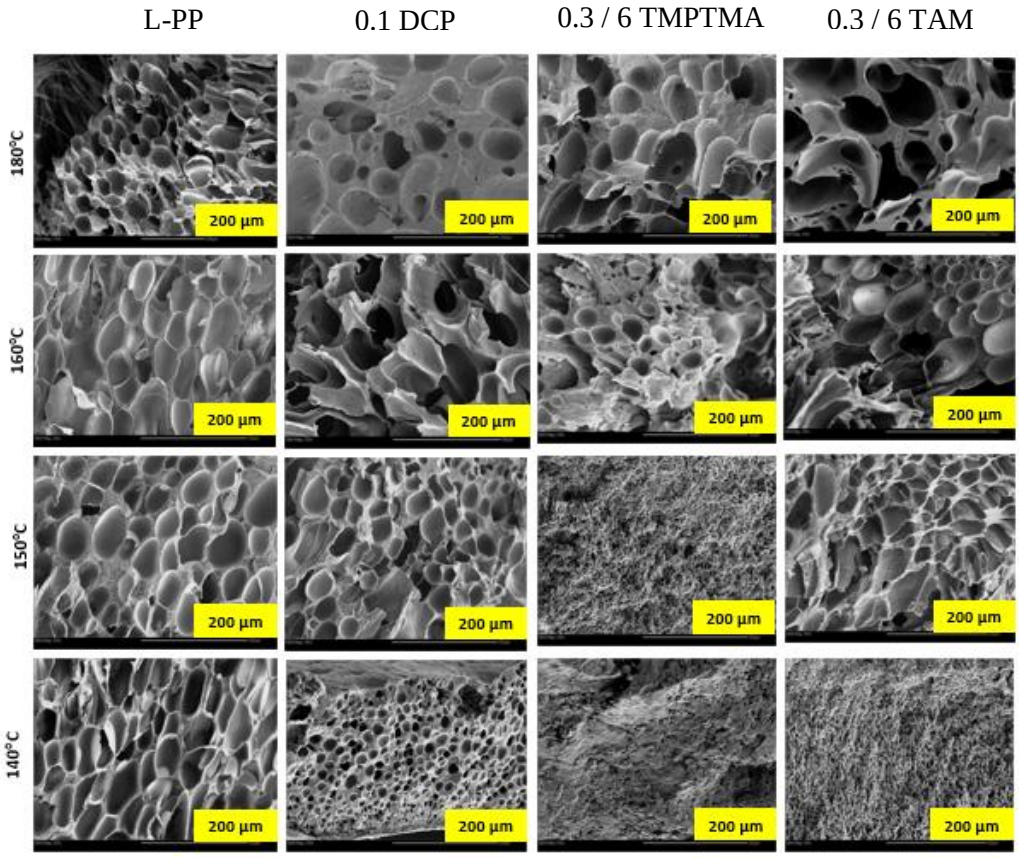

Figure A.2 SEM Image comparison of different poly (propylene) foams for 30 min foaming time (Scale given in yellow boxes)

A histogram is presented in Fig.A.3 which clearly compares the average cell diameter of the neat and modified PP foams with respect to the foaming temperatures for a foaming time of 30 minutes. A downward trend was observed for the average cell diameter when the foaming temperature was decreased from 180°C to 140°C respectively. The modified PP foams showed reduced cell diameter as compared to that for the neat PP foams for each foaming temperature except for 160°C, for which the average cell size was lower for neat PP foams. The maximum cell size reduction of approximately 89% was observed for TAM modified PP foam at 140°C temperature, with an average cell diameter value of 3.1 µm as compared to that of neat PP foam. The TMPTMA modified PP foam also showed reduced average cell size of 3.4 µm at a foaming temperature of 150°C, with approximately 88% cell size reduction as compared to the neat PP foam. No foam was obtained at 140°C for the TMPTMA modified PP which reflects towards the occurrence of the crystallization of the polymer at this temperature. The increase in viscosity and

the strain hardening effect might also be a reason due to which the polymer samples were not foamed at the respective foaming temperature.

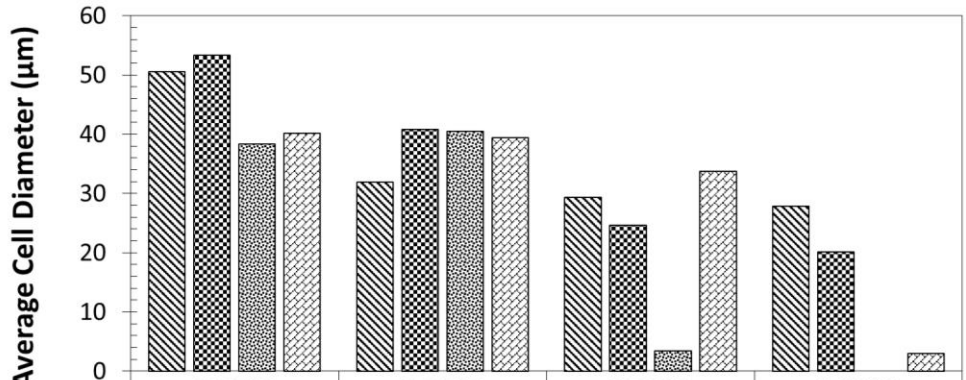

	180°C	160°C	150°C	140°C
L-PP	51	32	29	28
0.1 DCP	53	41	25	20
0.3/6 TMPTMA	38	41	3	0
0.3/6 TAM	40	39	34	3

Foaming Temperature (°C)

Figure A.3 Cell Size comparison of different poly (propylene) foams for 30 min foaming time.

The results show that the careful choice of foaming temperature as well as formulation plays a critical role in controlling the cell size of PP foams.